A Computational Approach for the Design of Epidural Electrical Spinal Cord Stimulation Strategies to Enable Locomotion after Spinal Cord Injury

THÈSE N^O 9076 (2018)

PRÉSENTÉE LE 6 DÉCEMBRE 2018
À LA FACULTÉ DES SCIENCES ET TECHNIQUES DE L'INGÉNIEUR
CHAIRE FONDATION BERTARELLI EN NEURO-INGÉNIERIE TRANSLATIONNELLE
PROGRAMME DOCTORAL EN GÉNIE ÉLECTRIQUE

ÉCOLE POLYTECHNIQUE FÉDÉRALE DE LAUSANNE

POUR L'OBTENTION DU GRADE DE DOCTEUR ÈS SCIENCES

PAR

Emanuele FORMENTO

acceptée sur proposition du jury:

Prof. D. Floreano, président du jury
Prof. S. Micera, Prof. G. Courtine, directeurs de thèse
Dr E. Neufeld, rapporteur
Prof. A. Prochazka, rapporteur
Prof. D. Ghezzi, rapporteur

EPFL

ÉCOLE POLYTECHNIQUE
FÉDÉRALE DE LAUSANNE

Suisse
2018

"A man can surely do what he wills to do,
but he cannot determine what he wills."
— Arthur Schopenhauer

Acknowledgements

Firstly, I would like to express my most heartfelt gratitude to Prof. Silvestro Micera for giving me the opportunity of performing this PhD thesis in his amazing lab and for his supervision during these four years. I really appreciated the freedom he gave me in exploring every side project I was interested in, even if these were not always the most fruitful.

Equally, I would like to express my sincerest gratitude to Prof. Grégoire Courtine for allowing me to conduct my research in his lab and for his guidance during my PhD project. His passion and commitment for science were extremely motivating.

A big thanks also to Marco, who wasn't only a great supervisor but also a valuable friend, always ready to help in the toughest moments of these years.

My genuine thanks to Karen, for his essential inputs on this work, for sharing his encyclopedic knowledge, and of course for having introduced me to femoral nerve stimulation.

To my colleague and friend Edoardo, thank you for all the hours (days) we spent laughing, discussing science, and philosophizing or arguing about no-matter what.

A great thanks to all the members of Silvestro's and Grégoire's labs, it was great to share this experience with you.

My warmest thanks also to Stephanie, for supporting me during the last months of my PhD, for helping me editing this thesis, and for always being so encouraging.

And finally, last but by no means least, I would like to thank my parents, Elisabetta and Edoardo, and my brother Filippo for their unconditional support and love.

Lausanne, 19 September 2018   E. F.

Abstract

Spinal cord injury (SCI) is a major cause of paralysis with currently no effective treatment. Epidural electrical stimulation (EES) of the lumbar spinal cord has been shown to restore locomotion in animal models of SCI, but has not yet reached the same level of efficacy in humans. The mechanisms through which EES promotes locomotion, and the causes underlying these inter-species differences remain largely unknown, although essential to fully exploit the therapeutic potential of this neuromodulation strategy. Here, we addressed these questions using a deductive approach based on computer simulations and hypothesis-driven experiments, and proposed complementary strategies to enhance the current efficacy of EES-based therapies.

In the first part of this thesis, we studied the mechanisms through which EES enables locomotion in rat models of SCI. Performing simulations and behavioral experiments, we provided evidence that EES modulates proprioceptive afferents activity, without interfering with the ongoing sensory signals. We showed that this synergistic interaction allows muscle spindle feedback circuits to steer the unspecific excitation delivered by EES to functionally relevant pathways, thus allowing the formation of locomotor patterns. By leveraging this understanding, we developed a stimulation strategy that allowed adjusting lesion-specific gait deficits, hence increasing the therapeutic efficacy of EES.

In the second part of this thesis, we evaluated the influence of trunk posture on proprioceptive feedback circuits during locomotion, and thus on the effect of EES, in rat models of SCI. By combining modeling and experiments, we showed that trunk orientation regulates leg proprioceptive signals, as well as the motor patterns produced during EES-induced stepping. We exploited these results to develop a control policy that by automatically regulating trunk orientation significantly enhanced locomotor performance.

In the last part of this thesis, we investigated the causes underlying species-specific effects of EES. Hypothesis-driven simulations suggested that in humans continuous EES blocks the proprioceptive signals traveling along the recruited fibers. We corroborated this prediction by performing experiments in rats and people with SCI. In particular, we showed that EES disrupts the conscious perception of leg movements, as well as the afferent modulation of sensorimotor circuits in humans, but not in rats. We provide evidence that in humans, due to this phenomenon, continuous EES can only facilitate locomotion to a limited extent. This was insufficient to provide clinically relevant improvements in the tested participants. Finally, we proposed two sensory-compliant stimulation strategies that might overcome these limitations, and thus augment the therapeutic efficacy of EES.

In this thesis we elucidated key mechanisms through which EES promotes locomotion, we exposed critical limitations of continuous EES strategies when applied to humans, and we introduced complementary strategies to maximize the efficacy of EES therapies. These findings have far-reaching implications in the development of future strategies and technologies supporting the recovery of locomotion in people with SCI using EES.

Keywords

Sommario

La lesione del midollo spinale (LMS) è una delle principali cause di paralisi con attualmente nessun trattamento efficace. È stato dimostrato che la stimolazione elettrica epidurale (SEE) del midollo spinale ripristina la locomozione in modelli animali di LMS, ma non ha ancora raggiunto lo stesso livello di efficacia nell'uomo. I meccanismi attraverso cui SEE promuove la locomozione e le cause alla base di queste differenze tra specie rimangono in gran parte sconosciute, sebbene siano essenziali per sfruttare appieno il potenziale terapeutico di questa strategia. Qui, abbiamo affrontato queste problematiche utilizzando un metodo deduttivo basato su simulazioni al computer ed esperimenti, e proposto strategie complementari per migliorare l'attuale efficacia terapeutica di SEE.

Nella prima parte di questa tesi, abbiamo studiato i meccanismi attraverso i quali SEE promuove la locomozione in ratti con LMS. Eseguendo simulazioni ed esperimenti, abbiamo presentato prove che SEE modula l'attività afferente propriocettiva, senza interferire con i segnali sensoriali. Abbiamo mostrato che questa interazione sinergica consente i circuiti propriocettivi di trasformare l'eccitazione erogata da SEE in pattern locomotori. Sfruttando questi risultati, abbiamo sviluppato una strategia di stimolazione che ha permesso di trattare deficit motori lesione-specifici, aumentando così l'efficacia terapeutica di SEE.

Nella seconda parte di questa tesi, abbiamo valutato l'influenza della postura del tronco sui circuiti propriocettivi durante la locomozione, e quindi sull'effetto di SEE, in ratti con LMS. Combinando simulazioni ed esperimenti, abbiamo dimostrato che l'orientamento del tronco regola i segnali propriocettivi delle gambe, così come i pattern motori prodotti durante la locomozione indotta da SEE. Abbiamo sfruttato questi risultati per sviluppare un paradigma di controllo che regolando automaticamente l'orientamento del tronco ha migliorato significativamente le prestazioni locomotorie.

Nell'ultima parte di questa tesi, abbiamo studiato le cause alla base degli effetti specie-specifici di SEE. Simulazioni hanno suggerito che negli esseri umani SEE blocca i segnali propriocettivi che viaggiano lungo le fibre stimolate. Abbiamo validato questa previsione eseguendo esperimenti su ratti e persone con LMS. In particolare, abbiamo dimostrato che SEE interrompe la percezione cosciente dei movimenti delle gambe, così come la modulazione afferente dei circuiti sensomotori negli esseri umani, ma non nei ratti. Abbiamo mostrato che negli esseri umani, a causa di questo fenomeno, l'uso continuo di SEE può solo agevolare la locomozione in misura limitata. Infine, abbiamo proposto due strategie di stimolazione che potrebbero superare questi limiti e quindi aumentare l'efficacia terapeutica di SEE.

In questa tesi abbiamo chiarito meccanismi chiave attraverso cui SEE promuove la locomozione, abbiamo rivelato delle limitazioni critiche delle strategie SEE-continue, e abbiamo introdotto strategie complementari per massimizzare l'efficacia delle terapie basate su SEE. Queste scoperte hanno implicazioni di vasta portata nello sviluppo di strategie e tecnologie future per promuovere il recupero della locomozione nelle persone con LMS tramite SEE.

Abstract

Paroli chiave

Lesione del midollo spinale, stimolazione elettrica epidurale, neuroprotesi, locomozione, riabilitazione, circuiti spinali sensomotori, propriocezione, neuroscienze computazionali, spiking neural networks, modelli neuromuscoloscheletrici.

Contents

Contents

List of Figures

List of Tables

1 Introduction

Spinal cord injury (SCI) is one of the leading cause of paralysis, and affects approximately 1.5 millions of people in the United States (Armour et al., 2016). Depending on its level and severity, a SCI leads to different symptoms, with roughly 65% of SCIs resulting in either partial or complete paraplegia and the remaining 35% in either partial or complete tetraplegia (Wyndaele & Wyndaele, 2006).

Currently, viable clinical therapies for restoring the lost functions are lacking. Physiotherapy is performed when the injury is stabilized to train the remaining voluntary motor functions and to encourage the spontaneous recovery of the lost abilities. Typically, the amount of recovery is inversely proportional to the severity of the injury. People with a clinically complete lesion experience a limited recovery, which is generally restrained to the areas with preserved functionalities. Instead, people with an incomplete lesion tend to experience more substantial and variable recoveries (Fawcett et al., 2007). However, given the limited capability of the nervous system to regenerate, in most of the cases a SCI leads to permanent disabilities and dysfunctions. These are not limited to the loss of sensory and motor abilities, but they also include other disorders, such as neurogenic bladder, spasticity, and cardiovascular problems (Nas et al., 2015). As such, the impact of a SCI on the quality of life of the affected people and the cost associated to the healthcare of these individuals is extremely high.

Rehabilitation priorities strongly depend on the residual functions. For paraplegic patients, the recovery of locomotion is one of the most urgent concerns (Anderson, 2004). Restoring walking in these cases would not only improve patients' independence, but it would also reduce the side effects caused by immobilization, such as an increased spasticity and a low cardiovascular endurance (Nash et al., 1997; Guest et al., 1997). For this reason, multiple research efforts, including this thesis, aim at promoting the recovery of this particular function.

Diverse therapeutic strategies have been proposed in order to restore locomotion after SCI (Courtine et al., 2009; Hofstoetter, Krenn, et al., 2015; O'Shea et al., 2017). Among these, epidural electrical stimulation (EES) of the spinal cord has been shown to provide the most impressive results in animal models of SCI (Van den Brand et al., 2012; Capogrosso et al., 2016; Asboth et al., 2018). However, this therapy has yet to provide similar level of efficacy in people with SCI. To foster clinical translation, in this thesis we investigated the mechanisms through

which EES facilitates locomotion, and used the acquired knowledge to develop hypothesis-driven strategies for enhancing the efficacy of this therapy. For this, we used a deductive approach based on computational modeling and experiments in rats and people with SCI.

In the next sections, I first review how the intact nervous system controls locomotion. The aim of this section is to provide the theoretical background necessary to understand how EES can interact with the central and peripheral nervous systems in order to promote locomotion after SCI. Then, I describe how a SCI interferes with the normal functioning of locomotor circuits, and illustrate current technologies and promising strategies for promoting the recovery of locomotion. I highlight the accomplishments and limitations of current EES therapies, and emphasize how a deductive approach is essential to steer the design of more effective strategies. Then, I introduce the computational tools that we used to investigate the mechanisms of EES. Finally, I provide the outline of the work carried out in this thesis.

1.1   Neural control of locomotion

Locomotion, consisting of walking, running, swimming, flying or any other variety of movements animals perform to move from one place to another, is one of the most fundamental skill in the animal kingdom. Being able to interact and move within the surrounding environment is indeed a prerequisite for a multitude of basic behaviors, such as searching for food and escaping from predators. From a control point of view, locomotion is an extremely complex task that involves the coordinated activation of numerous muscles, spanning different joints and limbs. Despite this complexity, control of locomotion seems effortless, almost automatic. This automaticity is the result of millions of years of evolution that, in vertebrates, led to the development of dedicated neural circuitries located in the spinal cord that are responsible for generating the pattern of muscle activations underlying this function (**Figure 1.1**, Rossignol & Frigon, 2011; Kiehn, 2016). Supraspinal centers act on these spinal circuitries to initiate locomotion, to control the speed and balance, and to adjust limb trajectories (Shik & Orlovsky, 1976; Takakusaki, 2013). In parallel, sensory signals regulate the activity of spinal neural networks and provide supraspinal centers with an essential source of control (Kiehn, 2016). These three components embody the decentralized structure of the neural control of locomotion in vertebrates.

In the following sections I briefly review the current understanding of these components in mammals. A particular focus is given to the role of the spinal cord and of peripheral sensory signals.

1.1.1   Spinal locomotor network

The role of the spinal cord in controlling locomotion was first studied in cats more than a hundred years ago (Sherrington, 1910; T. G. Brown, 1911). Since then, a lot of experimental evidence has been gathered and it is now established that mammalian spinal neural networks play a critical role in generating the rhythm and the pattern of muscle activations underlying locomotion. Nevertheless, the precise organization of the spinal locomotor network is still a mater of debate, and particularly in humans, where only indirect studies are possible, the
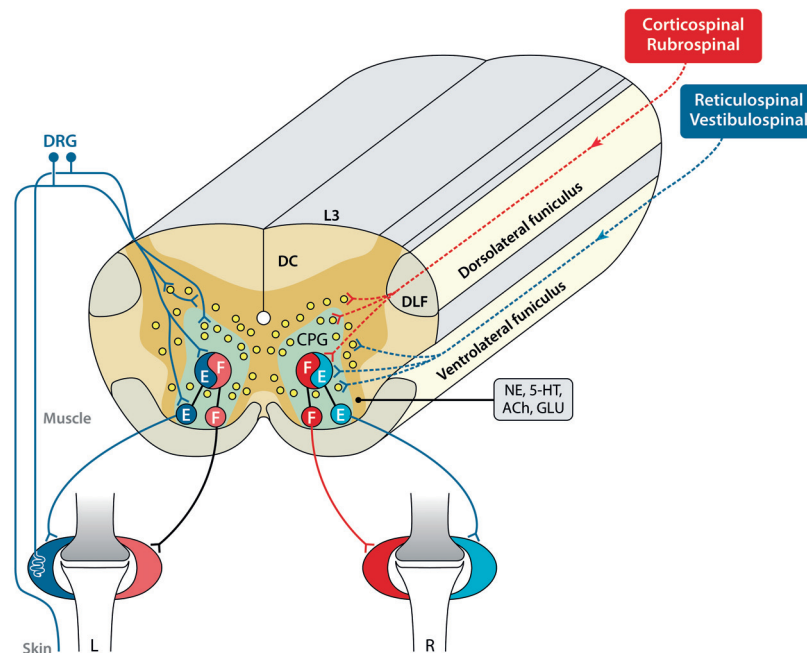
Figure 1.1 | Framework of neural control of locomotion. The spinal cord central pattern generator (CPG) produces the basic rhythm underlying locomotion. Spinal sensorimotor circuits integrate sensory signals arising from receptors located in muscles, tendons and skin to supervise the motor pattern formation. Supraspinal signals descending from the cortex and the brainstem regulate the speed, onset and balance. Figure taken with permission from (Rossignol & Frigon, 2011).

structure and the specific role of different spinal networks are still not clear (Dietz, 2003). Several observations, however, suggest that the neural circuits controlling locomotion are broadly conserved across mammals (Nadeau et al., 2010; Dominici et al., 2011; Grillner, 2011; Danner et al., 2015). Therefore, even if most of the current knowledge on the organization of the spinal locomotor network in mammals is derived from experiments in cats and rodents, it is reasonable to assume that the human spinal locomotor network is similarly organized.

The ability of the spinal cord to produce the rhythm underlying locomotion was first uncovered by Brown, in experiments where deafferented cats with a complete transection of the spinal cord were shown to produce rhythmic alternating activity of the flexor and extensor muscles of the ankle (T. G. Brown, 1911, 1912). This observation led Brown to hypothesize that neural networks within the spinal cord, successively termed central pattern generators (CPGs), have the intrinsic ability to generate the pattern of muscle activations underlying locomotion (T. G. Brown, 1914). Over the years, Brown's experiments have been replicated and his observations have been strengthened by several other investigations, with the strongest evidences supporting the hypothesis of CPGs being provided by experiments on fictive locomotion (see Duysens & Van de Crommert, 1998 for a review). In these experiments, preparations of cat and rodent spinal cords, completely deprived of any supraspinal and sensory signals, were shown to produce motoneuronal activations remarkably similar to those generated during real locomotion (see Grillner & Zangger, 1979; Chandler et al., 1984; Orsal et al., 1990; Barrière et al., 2004; Christie & Whelan, 2005 for examples). It is imperative to

point out, however, that while the isolated spinal cord can generate locomotor patterns in the absence of any sensory input, in intact animals sensory signals strongly interacts with CPG circuits in order to elaborate functional motor patterns (see section 1.1.2 at page 6).

The current understanding is that the spinal locomotor network is composed of modular and functionally confined neuronal circuits. In this view, different circuits can be defined depending on their role in the control of locomotion; namely, circuits that produce the rhythm underlying locomotion, circuits that ensure bilateral coordination, and circuits that control the alternation of antagonistic muscles (Kiehn, 2016). In addition to these circuits, a network of sensorimotor pathways integrates sensory inputs within the spinal locomotor network.

Circuits producing the rhythm underlying locomotion

The spinal locomotor network is driven by a group of spinal interneurons that can initiate and control the speed of locomotion. Studies in rodents and cats demonstrated that these neurons are excitatory, uniquely glutamatergic in most species, and project ipsilaterally (see Goulding, 2009; Kiehn, 2016 for extensive reviews). Among the several observations that support this conclusion, optogenetic studies in mice have provided the most compelling set of evidence (Hägglund, Borgius, Dougherty, & Kiehn, 2010; Hägglund et al., 2013). In these experiments, optogenetic activation of spinal glutamatergic neurons was shown to elicit locomotor activity, while inhibition of these neurons prevented this activity from emerging. Therefore, glutamatergic neurons within the spinal cord — at least in mice — are both sufficient and necessary for rhythm generation. Interestingly, when optogenetic stimulation of these neurons was restricted to a specific region of the spinal cord, rhythmic flexor-extensor activity only emerged in the muscles innervated by the motoneurons confined to the stimulated segment (Hägglund et al., 2013). As such, the rhythm generating circuit is composed of multiple modules that are organized in close association with the motoneuron pools on which they act.

While the general phenotype of rhythm generating neurons is determined, it is still largely unclear which subpopulation of glutamatergic interneurons is responsible for this function and how rhythmicity is generated (Kiehn, 2016).

Circuits ensuring bilateral coordination

Coordination between muscles on the left and right side of body is critical during locomotion. This function relies on commissural neurons (CNs) that, with axons crossing the midline of the spinal cord, link contralateral networks (Shevtsova et al., 2015; Kiehn, 2016). Experiments in rodents and cats revealed that both excitatory and inhibitory pathways are involved in this function (Jankowska et al., 2005; Jankowska, 2008; Butt & Kiehn, 2003; Quinlan & Kiehn, 2007). Cross inhibition was shown to be carried out by two different populations of CNs. The first pathway involves ($V0_D$) inhibitory CNs that directly act on contralateral motoneurons. The second one, instead, involves ($V0_V$) excitatory CNs that provide cross inhibition by acting on inhibitory premotor interneurons (Butt & Kiehn, 2003; Quinlan & Kiehn, 2007). Ablation studies in mice showed that both these pathways are necessary for left-right alternation. Indeed,

suppression of even one of these circuits leads to a synchronous, hopping-like, contralateral activity (Talpalar et al., 2013). Contrary to inhibitory pathways, cross excitation supports left-right synchronization. This pathway relies on the ($V0_3$) excitatory CNs, which synapse on contralateral motoneurons and interneurons (Y. Zhang et al., 2008).

Despite the different subpopulations of CNs that are known, the precise architecture of the network involved in coordinating right and left movements is still unclear. Interestingly, however, a recent computational study proposed a circuit organization that can explain several experimental observations (Shevtsova et al., 2015). Further studies will be necessary to confirm the proposed organization.

Circuits controlling the alternation of antagonistic muscles

During locomotion, motoneurons innervating flexor and extensor muscles are activated in a sequential and alternating pattern. This pattern divides locomotion in stance and swing phases, during which the leg is extended to propel the body forward and subsequently flexed to clear the leg from the ground and to allow the progression. This alternating activity originates both from inhibitory and from excitatory inputs that reach the flexor and extensor motoneuron pools out of phase (Hochman & Schmidt, 1998; Endo & Kiehn, 2008). The network generating this alternating activity is believed to be divided in circuits directly coupled to the motoneuron pools, and in circuits that interact with rhythm generating modules (Kiehn, 2016).

The Ia-inhibitory interneurons are a group of last-order interneurons that have been proposed to provide the main source of rhythmic inhibition to flexor and extensor motoneuron pools during locomotion (Pratt & Jordan, 1987; Geertsen et al., 2011). These interneurons receive excitatory synapses from the group Ia afferents of one muscle and inhibit the motoneuron pool of the antagonist muscle. At the same time, pools of Ia-inhibitory interneurons, innervating pools of antagonistic motoneurons, mutually inhibit each other and are inhibited by Renshaw cells (Hultborn et al., 1971; Hultborn, 1976; Kiehn, 2016). Multiple studies have shown that these cells are rhythmically active during locomotion, and for this reason it was suggested that these neurons were involved in controlling flexor and extensor alternation (Pratt & Jordan, 1987; Geertsen et al., 2011). Subsequently, studies in mice provided further evidence supporting this hypothesis. In particular, Talpalar and colleagues showed that the reciprocal Ia inhibitory pathway is sufficient to coordinate the alternating activity between flexor and extensor motoneurons, and that, in the absence of excitatory pathways, this circuit can also produce the rhythmic activity underlying locomotion (Talpalar et al., 2011). A complementary study, also demonstrated that blocking the synaptic output of V1 and V2b spinal neurons — neural populations that together account for all Ia-inhibitory interneurons — the flexor-extensor alternation is disrupted, with motoneurons innervating antagonistic muscles bursting in synchrony (J. Zhang et al., 2014). These combined results provide compelling evidence that the Ia inhibitory network contributes extensively to the control of agonist-antagonist muscle pairs.

How excitatory rhythm generating circuits are coupled to motoneurons and to Ia inhibitory interneurons is still unclear. However, excitatory pathways linking the rhythm gener-

ating circuits to the motoneurons are certainly present, given the observation of synchronized bursts of activity in the absence of V1 and V2b neurons. In addition, the rhythm generating circuits are believed to be directly coupled also to the Ia-inhibitory interneurons to drive their activity together with the group Ia afferents (Kiehn, 2016).

Sensorimotor circuits

The discussed circuits are an integral part of the spinal CPG and, isolated, can produce locomotor activity in the absence of descending and peripheral sensory signals. Nevertheless, the locomotor network relies on peripheral sensory inputs in order to elaborate functionally relevant movements. Thus, the spinal locomotor network includes numerous other sensorimotor circuits that by interacting with sensory activity steer and modulate the central pattern generated by the described circuits, as discussed in the next section.

1.1.2 Spinal sensorimotor interactions

Sensory afferents innervating receptors located in the skin, joint and muscles provide the spinal cord with a dynamic representation of the limbs during locomotion. The spinal locomotor network uses this information to elaborate the locomotor pattern itself, as well as to produce state-dependent adaptive motor responses necessary to rapidly adjust the motor output for different stepping speeds, levels of load imposed during stepping and unpredictable perturbations (Rossignol et al., 2006; Kiehn, 2016). Therefore, even though the isolated spinal CPG can generate the rhythm underlying locomotion, it critically depends on sensory signals in order to generate functional motor behaviors.

In the next sections, I expand on the role of cutaneous and proprioceptive signals in the control of locomotion, as these two sensory modalities are the most relevant for walking.

Cutaneous sensory feedback

Cutaneous information originates from a multitude of mechanoreceptors located in the skin, and it is broadcast to the spinal cord by different types of afferent fibers. Ascending sensory pathways bring this information to the brain, while spinal sensorimotor circuits use this information to regulate locomotor movements. Cutaneous inputs play a key role in the precise positioning of the foot and in correcting gait to overcome possible obstacles. In addition, they can reinforce extensor muscles activity during stance and even initiate or block locomotion (Rossignol et al., 2006). After a brief overview on the cutaneous sensory organs, the following paragraphs briefly analyze how cutaneous signals serve the functions above.

The sensory organs

The perception of touch emerges from mechanosensory neurons located in the skin (see (Abraira & Ginty, 2013) for a comprehensive review). Two families of mechanoreceptors can be distinguished: light-threshold mechanoreceptors (LTMRs) and high-threshold mechanoreceptors (HTMRs). LTMRs are responsible for sensing innocuous mechanical stimuli, and include Merkel cells, Ruffini organs, Meissner corpuscles, Pacinian corpuscles, and longitudinal lanceolate endings. A part from the longitudinal lanceolate endings that are innervated by type $A\delta$

and C afferents, these cells are all innervated by type $A\beta$ afferents. Contrarily, LMRs sense harmful stimuli and mainly consist of free nerve endings. The activity of both LTMRs and HTMRs strongly interacts with the spinal locomotor circuitry.

Cutaneous sensory inputs drive precise foot positioning
After cutaneous deafferentation of the hindpaw, otherwise intact cats have been shown to completely lose the ability to walk over an horizontal ladder but to have only minor deficits during treadmill locomotion (Bouyer & Rossignol, 2003a). These observations suggest that cutaneous sensory signals are involved in the fine control of the feet during locomotion. Interestingly however, within a few weeks of denervation cats largely recovered the lost functions, presenting close-to-normal locomotion behaviors both over a treadmill and on a horizontal ladder (Bouyer & Rossignol, 2003a). Therefore, it appears that the CNS can learn to compensate, at least partially, for the lack of cutaneous sensory inputs with other sensory modalities, such as vision or proprioception.

Cutaneous sensory inputs adapt the motor output in response to external perturbations
Cutaneous sensory inputs have also been shown to play a key role in generating adaptive behaviors when unexpected stimuli are presented during locomotion. Experiments on humans and cats where cutaneous stimuli were applied to the feet during locomotion revealed complex reflex responses that varied significantly depending on the task, the phase of gait during which the stimulus was applied, and the precise location of the stimuli (see Rossignol et al., 2006 for an extensive review).

Cutaneous sensory inputs can initiate and block locomotion
Finally, cutaneous sensory signals can initiate or block the spinal locomotor network activity. In particular, a continuous non-specific cutaneous stimulation of the perineal region has been shown to elicit or strengthen locomotor activity in spinal cats (Sherrington, 1910; Rossignol et al., 2000). Similarly, continuous electrical stimulation of the foot dorsum in rabbits, or of the sural nerve in cats, were shown to entrain fictive locomotion (Fleshman et al., 1984; Viala & Buser, 1969). On the other hand, stimulation of certain lumbar dermatomes in rabbits can instantaneously block locomotion (Viala & Buser, 1974). While the mechanisms underlying these responses are still not clear, these results highlight how cutaneous sensory signals are broadly integrated in the spinal locomotor circuitry.

Proprioceptive sensory feedback

Proprioceptive signals generated from muscle spindles and Golgi tendon organs (GTOs) contribute to different aspects of the control of locomotion. First, they reinforce and adapt the activity of alpha motoneurons. Second, they contribute to the formation of motor patterns by regulating the timing of locomotor movements. Finally, they can initiate and block locomotion. After a quick overview of the transducing properties of muscle spindles and GTOs, the following paragraphs briefly analyze how these signals contribute to the above functions.

The sensory organs
Muscle spindles are sensory organs located in the muscle belly that sense the changes in length of the muscles. These sensory organs are composed of a small group of intrafusal muscle

fibers, attached at their endings to neighboring extrafusal fibers. Each intrafusal fibers consist of a central non-contractile element and two contractile elements on the extremities. The non-contractile element is innervated by primary (Ia) and secondary (II) spindle afferents. Both primary and secondary axonal endings are sensitive to stretch, and they thus transduce muscle length information into neural activity. In particular, while secondary endings discharge proportionally to the stretch of the non-contractile elements, primary endings are more responsive to the stretch velocity (Prochazka, 1996). The contractile elements, instead, are innervated by fusimotor neurons (γ and β motoneurons), and allow a dynamic adjustment of the muscle spindles sensitivity (Prochazka, 2015).

Golgi tendon organs are located in the musculotendinous junctions and transduce information about the force generated by a muscle. Contrarily to muscle spindles, GTOs have no mechanisms to adjust their sensitivity. Ib afferents innervating these organs fire proportionally to the force that is actively generated by the group of motor units they are linked to. Consequently, the average firing rate of the Ib afferents innervating a muscle is closely linked to the force produced by the whole muscle (Prochazka & Gorassini, 1998a).

Proprioceptive signals reinforce and adapt motoneurons activity

Proprioceptive circuits significantly contribute to the production of the motor output during locomotion. For example, experiments in humans and cats demonstrated that, during the stance phase, between 30% and 60% of activity of the ankle extensor muscles is produced by afferent signals associated with stretch (Sinkjær et al., 2004; Donelan & Pearson, 2004). The proprioceptive sensorimotor pathways involved in shaping the motor output are multiple. The most studied is the excitatory monosynaptic Ia pathway that directly links muscle spindles to the motoneurons innervating the homonymous muscle and, to a lower extent, other synergistic muscles. More complex di- and polysynaptic pathways involve the group Ia, group II and Ib afferents and are responsible for diverse sensory feedback control mechanisms. The contribution of each of these pathways largely depends on the muscle considered and on the performed movement. Indeed, depending on the performed task, the strength of the sensorimotor input associated with different muscles is strongly modulated by spinal and supraspinal circuits through presynaptic inhibition and the fusimotor system (Rossignol et al., 2006). Therefore, while all motoneuronal pools may be innervated by similar sensorimotor pathways, a functional reorganization during locomotion adjusts the contribution of the different pathways in a muscle-specific manner.

Overall, sensorimotor pathways controlling extensor muscles appear to be similarly reorganized (Rossignol et al., 2006). Group Ia and Ib afferents that are active during stance contribute to the activation of extensor muscles, possibly to assist during the propulsion phase of stance and to compensate for terrain irregularities. In particular, Ib afferents are suggested to be involved in a positive force feedback loop that may play a key role in weight-bearing during locomotion (Dietz & Duysens, 2000). Notably, in a non-locomotor state the Ib afferent pathway is inhibitory. Group II afferents pathways innervating extensor motoneurons also appear to be reorganized. While group II afferents are normally associated with an excitatory pathways of the homonymous muscle, group II afferents originating from the ankle and knee

extensor muscles were shown to evoke a flexion reflex in spinal cats (Schomburg et al., 1998; Rossignol et al., 2006). Whether this reorganization is still present during intact locomotion is unknown. The reorganization of sensorimotor pathways involving the flexor muscles is less marked and might be more muscle specific. However, as for the extensor muscles, the overall effect induced by a recruitment of these pathways largely consists in an excitation of the flexor motoneurons. In this case, group Ia and group II afferents are the main actors. These afferents are active at the end of stance, because of stretch, and during swing, because of gamma drive (Rossignol et al., 2006). They are thus believed to contribute to the initiation of the swing phase and to sustain the activity of the flexor muscles during swing (Rossignol et al., 2006).

Proprioceptive signals regulate the timing of locomotor movements
Cats and rats with a complete thoracic transection of the spinal cord above the hindlimb locomotor areas can be trained to walk over a treadmill belt. Interestingly, when the treadmill speed is increased, stance and swing phases adapts as in healthy animals. The stance phase gets shorter with the increase in speed, while the swing phase remains approximately constant (e.g., Forssberg et al., 1980; Grillner & Zangger, 1984; Barbeau & Rossignol, 1987; Courtine et al., 2009). Moreover, when reversing the direction of the treadmill belt, spinal rats were shown to generate backward locomotion, a task requiring a significant reorganization of the pattern of muscle activities (Courtine et al., 2009). This ensemble of observations suggests that sensory signals reaching the spinal cord can modulate central programs and regulate the timing of locomotor movements. In particular, the adaptation of the stance phase at different treadmill speeds is a key evidence that the transition between stance and swing is largely controlled by sensory signals. Specifically, this transition is believed to be controlled by proprioceptive signals related to hip extension and to the unloading of the ankle extensor muscles (Pearson, 2008). Multiple evidence suggest that also swing-to-stance transition is regulated by proprioceptive signals, yet to a lower extent compared to the stance-to-swing transition (McVea et al., 2005; Pearson, 2008; Akay et al., 2014; Takeoka et al., 2014).

Proprioceptive signals can initiate and block locomotion
Numerous experiments in cats showed that locomotor patterns can be initiated and terminated by proprioceptive signals, and in particular those generated in proximal muscles (Rossignol et al., 2006). For instance, passive hip extension in spinal cats has been shown to initiate air stepping or treadmill locomotion, while a passive flexion to stop it (Sherrington, 1910; Grillner & Rossignol, 1978). Similarly, passive limb manipulations were shown to block fictive locomotion evoked by MLR stimulation (Orlovskii & Fel'dman, 1973). In addition, when delaying or anticipating hip movements during intact locomotion the activity of more distal muscles was also modified. These results further highlight how proprioceptive signals, and especially those those generated at the hip joint, are strongly integrated in the spinal locomotor network and act at a multi-joint level.

1.1.3 Supraspinal control

While the spinal cord is responsible for the generation of the patterns of muscle activity underlying locomotion, supraspinal centers are essential for initiating and adjusting locomotor

movements (see **Figure 1.2** for an overview). Initiation of locomotion involves different brain areas, and can arise both as a voluntary process or as an automatic reaction in response to external stimuli. Voluntary initiation and adjustments of locomotion involve cortical areas. Automatic reactions, instead, originate from the limbic system. To control the onset or other high-level features of locomotion (e.g. speed, termination) both the cortex and the limbic system largely rely on the brainstem, which can regulate the activity of spinal circuits through different descending pathways. To mediate fine voluntary adjustments, instead, the cerebral cortex directly projects to spinal neurons through the corticospinal tract. Numerous other subcortical structures are also involved in controlling locomotion, including the cerebellum and the basal ganglia (Jordan et al., 2008; Le Ray et al., 2011; Takakusaki, 2013; Drew & Marigold, 2015).

In the next sections I briefly review the current picture of the role of the main supraspinal centers involved in the control of locomotion. A special emphasis is given to the role of the brainstem.

The brainstem

The brainstem includes structures that are specifically dedicated to the control of posture and locomotion, namely: the mesencephalic locomotor region (MLR), the subthalamic locomotor region (SLR), and the cerebellar locomotor region (CLR) (Takakusaki, 2013).

The MLR is probably the most important of these structures. Pioneering experiments in decerebrated cats showed that electrical stimulation of this brain area can trigger full weight-bearing treadmill locomotion (Shik et al., 1969). Moreover, by modifying the intensity of the stimulation, different locomotor patterns were shown to be elicited, including walking, trotting, and galloping. It is now established that the MLR plays a key role in initiating and controlling the speed of locomotion (Jordan et al., 2008; Le Ray et al., 2011; Takakusaki, 2013; Takakusaki et
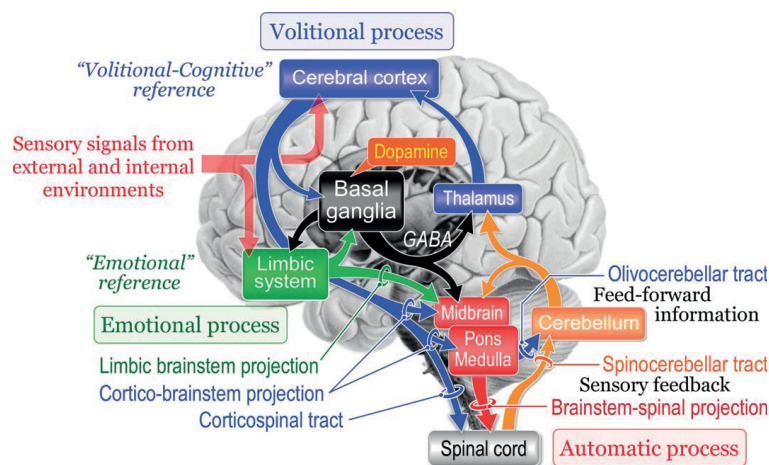
Figure 1.2 | Overview of the supraspinal control of locomotion. The cerebral cortex is involved in the voluntary control and fine adjustments of locomotion. The limbic system leads to automatic, emotional, reactions. The midbrain projects to the spinal locomotor network and receives projections from the basal ganglia, the limbic system, the cortex and the cerebellum. Figure taken with permission from (Takakusaki, 2013).

al., 2016), with some evidence also in humans (Masdeu et al., 1994; Jahn et al., 2008). This brain area is part of the cuneiform nucleus and of the pedunculopontine tegmental nucleus (PPN). It receives inputs from numerous brain structures, including the premotor cortex, the limbic system and the basal ganglia (Sinnamon, 1993; Matsuyama & Drew, 1997; Takakusaki, 2013). The MLR indirectly acts on the spinal cord through reticulospinal neurons in the ventromedial medullary reticular formation (vMRF), as well as through monoaminergic pathways, such as the coerulospinal and raphespinal tracts (Takakusaki, 2013). The reticulospinal tract is considered to have a dual function. First, it activates the rhythm generating circuits within the spinal locomotor network, thus initiating locomotion. Second, it contributes to the control of postural muscles. On the other hand, monoaminergic pathways, because of their widespread projections to the spinal cord (Basbaum & Fields, 1984), have been suggested to regulate the sensitivity of the spinal locomotor network to other descending commands or incoming sensory signals (Takakusaki, 2013). Specifically, serotonergic neurons have been shown to play a key role in promoting rhythm generation during locomotion (Sławińska et al., 2012, 2013). Both the SLR and CLR are also believed to regulate locomotion through the reticulospinal neurons in the vMRF, either with direct projections or indirectly through the MLR (Takakusaki, 2013; Sinnamon, 1993; Rossignol et al., 2006). The SLR is part of the hypothalamus and for this reason is supposed to be involved in emotional motor behaviors, such as the fight-or-flight reaction. The CLR is associated with the hooked bundle of Russell which originates in the fastigial nuclei of the cerebellum and projects to the vestibular nuclei in the brainstem. It is implicated in the feedforward control of locomotion (Mori et al., 1999).

A part from these locomotor regions, other structures of the brainstem are implicated in the control of balance and locomotion. One of these regions is located in the PPN. Cholinergic neurons within this area have been shown to be at the origin of an inhibitory pathway reaching the spinal locomotor network through reticulospinal neurons in the dorsomedial medullary reticular formation (dMRF, Takakusaki, Saitoh, et al., 2004; Takakusaki, Habaguchi, et al., 2004; Takakusaki et al., 2006). This pathway inhibits both flexor and extensor motoneurons, as well as interneurons controlling sensorimotor circuits (Takakusaki, 2013). This system is thus believed to be involved in controlling both the activity of postural muscles and in adjusting rhythm generation. The descending vestibulospinal and rubrospinal tracts also originate in the brainstem and are strongly involved in the control of locomotion. The vestibulospinal tract relays motor commands originating from the vestibular nucleus to control balance and posture (Takakusaki, 2013). The rubrospinal tract, instead, has been suggested to convey fine motor commands necessary for voluntary gait modifications. This tract is particularly involved in the visually guided control of flexor muscles necessary for foot clearance when passing an obstacle (Rho et al., 1999).

Cortical and subcortical areas

Planning, fine tuning, and the execution of precise locomotor movements requires the cooperation of different cortical and subcortical areas, including the posterior parietal cortex (PPC), the motor cortex, the premotor cortex, the cerebellum and the basal ganglia (Drew & Marigold, 2015).

The PPC plays a key role in the visuomotor integration necessary when a precise foot placement is required (Drew & Marigold, 2015). In particular, an increasing amount of evidence suggests that neurons within the PPC contribute to the estimation of the position of external objects with respect to the body, and in planning possible corrective motor actions. This structure thus appears to be deeply involved when navigating in complex environments or when stepping over an obstacle (McVea et al., 2009; Sato et al., 2010; Marigold & Drew, 2011; Harvey et al., 2012). To this aim, the PPC integrates sensory inputs from sensorimotor cortex, the visual cortex, and efference copy signals arising from different brain structures. Motor programs are then supposedly forwarded to the motor cortex.

The motor cortex is implicated in the execution of planned motor actions and gait adjustments. Pyramidal tract neurons (PTNs) within the motor cortex project to spinal neurons — both directly through the corticospinal tract and indirectly through the brainstem — and are responsible for regulating locomotor movements (Drew & Marigold, 2015). Evidence of this is that PTNs are strongly modulated during gait modifications (Amos et al., 1990; Beloozerova & Sirota, 1993), and their inactivation was shown to impair limb kinematic during gait adjustments (Drew et al., 1996, 2002; Friel et al., 2007). It is still not clear, however, how PTNs interact with the ongoing locomotor activity, and especially whether the PTNs control single muscle activations, as in the case of discrete movements, or more high-level parameters, such as the step height. The leading hypothesis is that, during locomotion, PTNs act on the motoneurons through the spinal locomotor network, thus ensuring smooth changes in muscle activity and enabling a direct control over the locomotor rhythm (Drew & Marigold, 2015).

Both the PPC and the motor cortex are part of an extended network that is also implicated in planning and executing locomotor movements. In particular, the premotor cortex, the cerebellum and the basal ganglia are all structures implicated in the control of voluntary movements and are heavily interconnected with both the PPC and the motor cortex. However, the contribution of these structures, and especially of the premotor cortex and of the basal ganglia, remains largely unknown (Drew & Marigold, 2015). The current view is that the premotor area, projecting to the brainstem reticulospinal neurons (Matsuyama & Drew, 1997; Keizer & Kuypers, 1989), plays a crucial role in initiating locomotion and possibly in coordinating postural changes that anticipates gait initiation (Bartels & Leenders, 2008; Takakusaki, 2013). At the same time, direct connections between the premotor area and the motor cortex may relay precise motor intentions to the spinal cord through the corticospinal tract. The cerebellum and the basal ganglia, instead, may be involved, together with other cortical areas, in the constant adaptation of muscle activity required to navigate in complex terrains — a process requiring both predictive and cognitive functions (Middleton & Strick, 2000).

1.2 Restoring locomotion after spinal cord injury

After SCI, descending spinal tracts are damaged and thus the ability to control the limbs is lost or profoundly impaired. However, in most of the cases, the spinal locomotor network remains intact, and peripheral sensory information continues to flow into the spinal cord. The spinal cord retains the ability to generate locomotor movements, but because of the lack of

supraspinal excitation it declines in an altered state (Rossignol & Frigon, 2011).

Rehabilitation strategies aim at restoring the functional state of the spinal cord and at recreating a link between the brain and the spinal neural network controlling locomotion. In the next sections, we briefly describe current and promising rehabilitation strategies to promote locomotion after SCI. In particular, we first present locomotor training as the key to promote functional recovery through activity-dependent plasticity mechanisms. Then, we describe pharmacological and electrical neuromodulation strategies to facilitate locomotion, and thus to promote functional recovery through training. We discuss the limited efficacy of pharmacological treatments in humans and the promising results of epidural electrical stimulation (EES). Finally, we emphasize the need of a deeper understanding of how EES interacts with the recruited circuits to promote the translation of this strategy into a viable clinical application.

1.2.1   Locomotor training

Early studies on spinal cats demonstrated that treadmill training, enabled by body weight support systems, is sufficient to restore full weight-bearing locomotion (e.g., Barbeau & Rossignol, 1987; Belanger et al., 1996). Several observations suggested that this recovery is mediated by the sensory signals generated during stepping, which, by steering the activity of spinal sensorimotor circuits, promote their reorganization through activity-dependent plasticity mechanisms (Edgerton et al., 2008; Rossignol & Frigon, 2011). Accordingly, even a partial ablation of peripheral sensory pathways severely affects the recovery of locomotion (Carrier et al., 1997; Bouyer & Rossignol, 2003b; Rossignol & Frigon, 2011). For instance, cutaneous deafferentation of the hind paw before spinalization was shown to hinder the recovery of proper foot placement during stepping (Bouyer & Rossignol, 2003b). Similarly, cats and mice models of incomplete SCI have been shown to spontaneously recover locomotion only when intact sensory feedback circuits are preserved — particularly those associated with muscle spindles (Goldberger, 1977; Takeoka et al., 2014). These observations indicate that after SCI sensory signals play a key role in reorganizing spinal circuits to allow spinal locomotor behaviors, as well as to promote the rearrangement of descending pathways necessary to reestablish voluntary control.

These observations in animal experiments led to the development of gait rehabilitation strategies based on body-weight-supported treadmill training. In people with incomplete SCI, this gait rehabilitation strategy was shown to be considerably effective, in some cases even promoting the recovery of independent overground locomotion in previously wheelchair-bound patients (Wernig & Müller, 1992; Wernig et al., 1995). However, when this strategy was tested in people with clinically complete lesions, only limited improvements have been observed (Dietz et al., 1995; Wirz et al., 2001). These consisted of an increased weight bearing during standing and of an enhanced extensor muscle activity generated during treadmill locomotion. Nevertheless, no facilitation of voluntary overground locomotion was observed (Wirz et al., 2001).

These results show that locomotor training can promote a reorganization of the spared

pathways and allow a functional recovery of the lost functions, even in humans. However, complementary, neuromodulation strategies are essential in order to promote the recovery of locomotion in people with severe lesions.

1.2.2 Pharmacological neuromodulation strategies

After SCI, the excitability of spinal circuits is largely depressed (Rossignol & Frigon, 2011). This altered state of the spinal cord results from the loss of excitatory inputs descending from the brain and from increased levels of inhibitory neurotransmitters within the spinal cord (Tillakaratne et al., 2000; Hultborn, 2003). The return of a physiological level of neural excitability is necessary to enable motor control. While this recovery can occur spontaneously, impaired regulatory mechanisms might lead to aberrant excitability of motoneurons and cause spasticity (Rossignol & Frigon, 2011). In this context, pharmacological neuromodulation strategies have been proposed to artificially regulate spinal excitability. In particular, multiple pharmacological agents, including alpha-2 agonists, glycinergic agonists, serotonergic agonists, and GABAergic antagonists, have been shown to promote locomotion in animal models of SCI (Forssberg & Grillner, 1973; Robinson & Goldberger, 1985; Barbeau & Rossignol, 1990; Chau et al., 1998; de Leon et al., 1999; Edgerton et al., 2008; Rossignol & Frigon, 2011). While their cellular mechanisms are poorly understood, these drugs appear to modulate the excitability of the spinal sensorimotor circuits to a level that allows the sensory information generated during movement to control motor pattern formation (Edgerton et al., 2008).

Following the success of these strategies in spinal animals, pharmacological agents were also tested in people with SCI. However, these strategies failed to significantly enhance locomotor functions (Rossignol & Frigon, 2011). In fact, the alpha-2 agonist, Clonidine, was even shown to suppress muscle activity during treadmill locomotion in people with complete SCI (Dietz et al., 1995).

A deeper knowledge of the neurophysiology of the spinal cord after injury and of the role of different neurotransmitters in controlling locomotion in humans will be essential to develop effective pharmacological treatments. To date, however, other neuromodulation strategies are needed to promote locomotion after SCI.

1.2.3 Epidural electrical stimulation of the spinal cord

Epidural electrical stimulation (EES) of the lumbar spinal cord has been shown to provide a viable strategy to increase spinal excitability, and to facilitate locomotion in both animal models and humans with SCI (C. Angeli et al., 2018; Gill et al., 2018; Courtine et al., 2009; Asboth et al., 2018). As such, it is currently the most promising neuromodulation strategy to be used in combination with locomotor training.

EES has been tested in humans for several decades (Waltz et al., 1981; Dimitrijevic et al., 1998; Grahn et al., 2017). This neuromodulation strategy promoted full weight-bearing standing (Harkema, Gerasimenko, et al., 2011), and elicited locomotor-like movements in people with clinically complete SCI (Dimitrijevic et al., 1998; Minassian et al., 2004). Moreover, the combination of intensive training and EES enabled independent stepping (C. Angeli et al.,
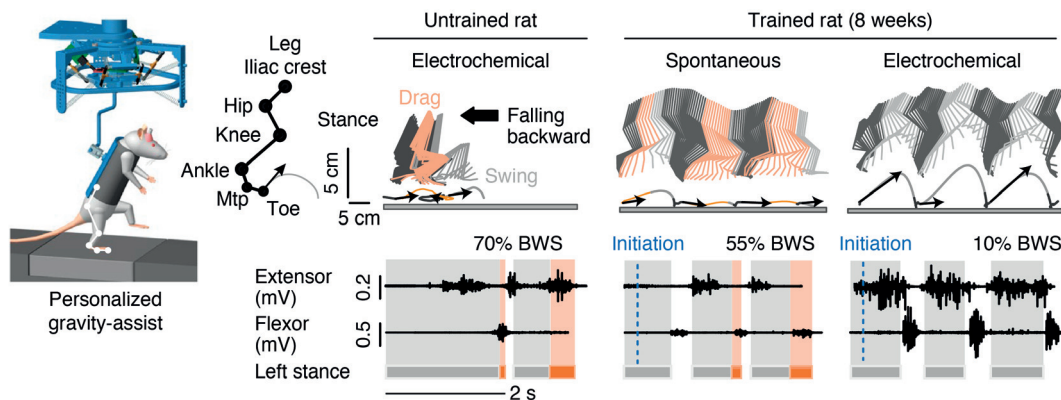
Figure 1.3 | EES-based locomotor training restores overground locomotion in rat models of severe SCI. EES combined with overground locomotor training and pharmacological neuromodulation allowed the recovery of voluntary locomotion in rat models of severe SCI. Figure taken with permission from (Asboth et al., 2018).

2018; Gill et al., 2018), and restored voluntary control over paralyzed muscles in people with clinically complete SCI (Harkema, Gerasimenko, et al., 2011; C. A. Angeli et al., 2014; Grahn et al., 2017). Despite these promising results, EES has yet to provide a similar facilitation of locomotion as that reported in rodent and non-human primate models of paralysis (Courtine et al., 2009; Capogrosso et al., 2016; Asboth et al., 2018). In particular, in rats, the combination of EES with locomotor training and pharmacological neuromodulation was shown to promote the recovery of full weight-bearing treadmill locomotion after complete SCI (Courtine et al., 2009), and of voluntary overground walking after severe SCI (Van den Brand et al., 2012; Asboth et al., 2018, **Figure 1.3**). In addition, in animal models, a modulation of the stimulation parameters allows for a precise control over the motor output produced during gait (Wenger et al., 2014; Capogrosso et al., 2016). This feature is essential to adapt the level of motor facilitation delivered by EES depending on the residual motor functions. However, it has never been reported in clinical studies. Indeed, only a limited range of EES parameters appears to provide a therapeutic effect in humans (Harkema, Gerasimenko, et al., 2011; C. A. Angeli et al., 2014).

To date, the reasons underlying these different effects of EES on humans and animal models remain largely unknown. Computational and experimental studies, performed both in animals and humans, suggested that EES primarily recruits large-diameter proprioceptive afferents (Rattay et al., 2000; Gerasimenko et al., 2006; Minassian et al., 2007; Capogrosso et al., 2013). The current understanding is that the recruitment of these fibers activates motoneurons through mono- and disynaptic pathways, and increases the excitability of the whole spinal locomotor network through the broad integration of these afferents in the spinal cord (C. A. Angeli et al., 2014; Danner et al., 2015). In turn, this increased in excitability augments spinal circuits sensitivity to sensory feedback signals and residual descending inputs, presumably allowing the emergence of locomotor behaviors (Edgerton et al., 2008). However, the mechanisms through which the recruitment of proprioceptive afferents leads motor pattern formation remain mostly unclear. In addition, this conceptual view implies

that proprioceptive afferents are both responsible for conveying the excitation provided by EES and for carrying the sensory drive that controls locomotion. Yet, it is enigmatic whether the electrical recruitment of these fibers might interfere with the propagation of the ongoing sensory signals.

Because of this lack of understanding, the development of EES strategies has been mainly supported by behavioral experiments where different stimulation parameters were tested on a trial-and-error basis. This intrinsically suboptimal approach limited the delivery of EES as a non-modulated waveform continuously applied to rhythmogenic centers of the lumbar spinal cord (Minassian et al., 2007; Courtine et al., 2009). These protocols are based on the conceptual view that EES increases spinal excitability to allow sensory signals and residual descending commands to control locomotion. However, current technologies allows delivering complex stimulation patterns that have the potential to even enhance these control signals in order to promote locomotion. Nevertheless, modulated stimulation patterns have rarely been tested, as their development necessitates a deductive approach based on a deeper understanding of how EES interacts with the recruited circuits, and of how different stimulation parameters alter this interaction.

In this thesis, we aimed at addressing this problem using a computational approach, with the goal of promoting the development of hypothesis-driven strategies that might augment the therapeutic efficacy of EES therapies.

1.3   Modeling for neuroprosthetics and locomotion

Computational modeling provides a unique tool to study the behavior of complex neural systems, as well as the effect of neuromodulation therapies. In particular, when electrical stimulation is studied, modeling is essential to investigate the high-dimensional space of the stimulation parameters, and thus to guide the design of hypothesis-driven strategies that can optimize the therapeutic efficacy of a given stimulation paradigm. In the context of this thesis, modeling is used to evaluate how epidural electrical stimulation interacts with the ongoing spinal neuronal activity to enable locomotion after SCI. For this, two main problems need to be addressed: evaluating which neural circuits are recruited by EES, and assessing how the induced neural activity interacts with the underlying circuits to enable locomotion. These problems can be tackled combining two modeling techniques, namely, multiscale finite element methods modeling, and neuromusculoskeletal modeling.

In the next sections, I will briefly describe these two modeling approaches, their current applications, and how they can be used together to investigate how EES interacts with spinal circuits to promote locomotion.

1.3.1   Multiscale finite element methods modeling

Multiscale finite element methods models allow estimating the neural circuits recruited by a given electrical stimulation setting, by solving two problems: computing the electric potential generated by the stimulation, and evaluating the impact of the generated electrical potential on the neighboring neural circuits.

Considering a point source electrode and an homogeneous infinite medium, the induced electrical potential at a given distance from the electrode can be computed using **Equation 1.1**, where ρ_{medium} is the resistivity of the medium and $I_{injected}$ is the current injected by the electrode. In realistic scenarios, however, the medium is far from being infinite and homogeneous, and the electrode is not a point source. Therefore, it is necessary to make use of finite element methods (FEM) modeling. This technique consists in developing a realistic volume conductor 3D model of the studied anatomical structures, and of the electrode used to deliver the stimulation. Then, the 3D model is discretized in finite elements with homogeneous conductivity properties to compute the electrical potential generated by the considered current source, solving the quasi-static approximation of the Maxwell equations (see Rattay et al., 2000; Capogrosso et al., 2013 for examples).

$$V = \frac{\rho_{medium} \cdot I_{injected}}{4\pi r} \qquad \text{(\textbf{Equation 1.1})}$$

The next step is to understand how the generated electric potential affects the neighboring neural circuits. For this, it is necessary to build geometrically and biophysically realistic models of the neurons located in the studied anatomical structures. The neural membrane can be represented as an electrical circuit composed of a capacitor, representing the lipid bilayer, with in parallel a series of nonlinear conductances, representing the ion channels (**Figure 1.4A**). Using this scheme, geometrically realistic axons and neurons, can be modeled as a series of circuits connected together — as shown in **Figure 1.4B** in the case of an axon cable model (McNeal, 1976; Rattay, 1986; McIntyre & Grill, 2002). Subsequently, modeling the biophysics of a neuron consists in formulating the system of differential equations describing the dynamics of the ion channels specific to the considered neuron. Interestingly, current models describing ion channels dynamics are still largely based on the pioneering works carried out by Hodgkin and Huxley, where they described the membrane dynamics of giant squid axons using a system of four nonlinear differential equations (Hodgkin & Huxley, 1952). In brief, these models allows simulating the neural response to a given external potential. Therefore, by combining FEM modeling and biophysical and geometrically realistic neural models it is possible to evaluate which neural circuits are recruited by a given stimulation setup.

Multiscale FEM models have been successfully used in the field of neuroprosthetics in order to steer the design of different electrical neuromodulation therapies. For example, in the case of deep brain stimulation, these models have been shown to be fundamental to tune the stimulation settings necessary to optimize the benefits of the stimulation (Frankemolle et al., 2010; McIntyre & Foutz, 2013). Regarding EES, multiscale FEM models have been used to investigate which neural structures are recruited during the stimulation (i.e., the large-diameter afferents entering into the spinal cord from the dorsal roots) (Rattay et al., 2000; Capogrosso et al., 2013), as well as to optimize stimulation parameters to target specific segments of the spinal cord (Wenger et al., 2016).
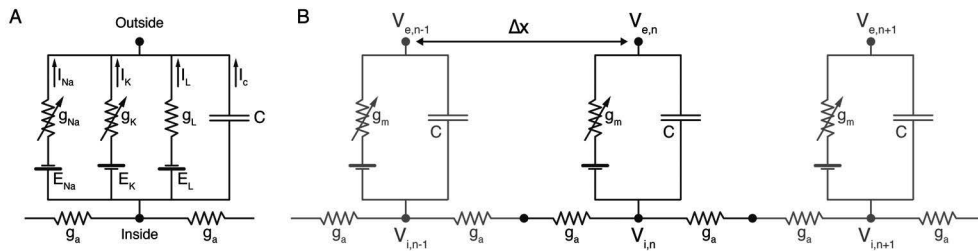
Figure 1.4 | The electric circuit equivalent of the neuron membrane. A Electric circuit equivalent of the neuron membrane as in (Hodgkin & Huxley, 1952). The sodium and potassium conductances (g_{Na}, g_{Na}) are described by the a set of non-linear differential equations, both as a function of time and membrane potential. g_l models the leak channels. **B**, axon-cable model. g_m indicates the ionic nonlinear conductances, and g_a the axoplasmic conductance.

1.3.2 Neuromusculoskeletal modeling

Neuromusculoskeletal modeling allows evaluating the interplay between neural circuits and the musculoskeletal system, and thus provides a unique tool to study locomotion. A neuromusculoskeletal model can be divided in three main components: a model of the neural circuits, a model of the musculoskeletal system, and a link connecting these two models.

Depending on the phenomenon to investigate, neuronal circuits can be modeled with different levels of abstractions. Generally, spiking neural networks are used for analyzing the dynamic behavior of complex neural systems. In this case, single neurons can be modeled with either biophysically realistic models (Wallen et al., 1992), or with phenomenological models, such as integrate-and-fire neurons (Burkitt, 2006; Stienen et al., 2007). Biophysically realistic models are necessary when investigating the effect of neuromodulatory drugs on the network behavior, while phenomenological models are often sufficient to simulate the spiking neural dynamics in response to synaptic inputs. On the other hand, entire populations of neurons can be approximated by a simple system of differential equations when their dynamic behavior is already known. For example, the behavior of salamander central pattern generators has been shown to be precisely captured by phase oscillators (Ijspeert et al., 2007).

Modeling the musculoskeletal system involves the development of the skeletal system and of the coupled muscles. The skeletal system is usually modeled as rigid body segments, with defined inertial and mass properties, connected together by a set of constraints modeling the joints. When muscle activations are known, muscle models are used to compute the moment acting on these joints by modeling the muscle contraction dynamics (see Buchanan et al., 2004 for a review). Then, using the equations of motion, joint moments can be transformed into joint movements. Conversely, joint movements can be used to compute the moments acting on the different joints, and thus the muscle activations underlying a given movement.

Neural circuit and musculoskeletal models can be used independently to study motor control. For instance, modeling studies on spinal neural circuits are providing crucial insights on the organization of the spinal locomotor network (Wallen et al., 1992; Rybak et al., 2006; Shevtsova et al., 2015), while musculoskeletal models have been widely used to back-engineer possible neural control strategies underlying locomotion (Berniker et al., 2009; Sartori et al.,

2013). However, only when these models are used together, is it possible to investigate the functional role of different circuits in controlling locomotion. Coupling neuronal circuits and musculoskeletal models can be performed at different levels. Specifically, the neural circuits can be used to compute the muscle activations of the modeled muscles, while the musculoskeletal models can be used to steer the neural network with sensory signals. Feedforward simulations can be performed by only coupling one model to the other, while closed loop simulations requires both models to be reciprocally coupled. An example on how closed-loop models can be used to study locomotion is provided by the works of Geyer and colleagues, in which they emphasized the ability of feedback circuits in generating multiple locomotor behavior in the absence of central pattern generating networks (Geyer & Herr, 2010; Song & Geyer, 2015).

1.3.3 Combining multiscale FEM and neuromusculoskeletal modeling

Multiscale FEM models can provide an estimate of the neural circuits recruited by a single pulse of EES. However, since these models are intrinsically static, they cannot evaluate how a given stimulation protocol results in a functional locomotor behavior. Moreover, since EES mainly recruits proprioceptive afferents, there is no direct link between the delivery of an EES pulse to a motor response. Indeed, each single EES pulse will produce remarkably different motoneuron responses depending on the phase of the gait (see section 1.1.2). On the other hand, neuromusculoskeletal models can be used to evaluate the dynamics of spinal neural networks during locomotion, as well as how these dynamics are modified by the recruitment of a given subset of neurons during electrical stimulation. Therefore, in order to estimate the effect of a given stimulation protocol on the motor output, in this thesis we will combine multiscale FEM models with neuromusculoskeletal models.

1.4   Thesis outline

In this introduction, we provided the theoretical background underlying this work, thereby highlighting current achievements and limitations of EES strategies to enable locomotion after SCI. In particular, we emphasized the translational gap between animal experiments and clinical studies, and the lack of understanding that limits the development of these strategies. As such, **the aim of this thesis was to investigate the mechanisms through which EES facilitates locomotion and the causes of its limited efficacy in humans, and to exploit the acquired knowledge to develop hypotheses-driven strategies to improve EES therapies**. For this, we used a deductive approach based on computational modeling and experiments in rats and people with SCI.

In **Chapter 2**, we investigated how EES dynamically interacts with the recruited proprioceptive feedback circuits in order to promote locomotion in rat models of SCI. Combining simulations and behavioral experiments, we provided evidence that in rats EES modulates proprioceptive afferent fibers, without interfering with the ongoing sensory signals. We proposed that this synergistic interaction allows muscle spindle feedback circuits to gate the unspecific excitation delivered by EES towards functionally relevant pathways, thus promoting the formation of motor patterns. Finally, we developed an EES protocol that can correct bilateral gait deficits, and thus ameliorate the therapeutic efficacy of EES, by exploiting muscle spindle circuits natural modulation.

These results emphasized the critical role of proprioceptive signals in both controlling locomotion after SCI, and in mediating the therapeutic effect of EES. Consequently, we reasoned that acting on these signals by adjusting trunk posture might allow refining the locomotor output produced by EES. In **Chapter 3**, we investigated this possibility by performing simulations and by engineering a robotic interface that allowed controlling trunk posture in realtime during EES-enabled treadmill locomotion, in rat models of SCI. We found a remarkable impact of trunk orientation on leg proprioceptive signals and muscle activity produced by EES. By leveraging these results, we developed a trunk posture control scheme that optimized the locomotor performance during EES.

In **Chapter 4**, we investigated the mechanisms underlying the limited efficacy of EES in humans compared to animal models. Hypothesis-driven simulations suggested that in humans, as opposed to rats, EES blocks the sensory signals traveling along the recruited fibers. We validated this prediction performing a series of experiments in rats and people with SCI. In particular, we found that continuous EES disrupts the conscious perception of leg movements, as well as the afferent modulation of spinal sensorimotor circuits in humans, but not in rats. Then, by performing both computer simulations and behavioral experiments we showed that in humans, because of this phenomenon, only a limited range of EES parameters can be used to facilitate locomotion. This translated into limited walking improvements. Lastly, we propose two novel stimulation protocols that might improve the efficacy of EES therapies by minimizing the interference of the stimulation with the ongoing sensory signals.

In the last chapter (**Chapter 5**), we discussed the potential of the proposed strategies, as well as the current technological limitations that impedes their direct application in clinical

studies. Finally, we highlighted future research directions that will bring us closer to develop a viable therapy to restore locomotion in people with SCI.

2 Proprioceptive circuits mediate the effect of epidural spinal cord stimulation

Locomotor rehabilitation combined with epidural electrical stimulation (EES) of the spinal cord has been shown to promote the recovery of locomotion in animal models of spinal cord injury (SCI) (Courtine et al., 2009; Asboth et al., 2018). To date, however, this therapy has not mediated similar effects on human patients. Due to a lack of a mechanistic understanding of how EES facilitates locomotion, the development of current EES strategies has been mainly supported by empirical observations. This inductive approach is intrinsically suboptimal given the enormous number of variables that can influence the effect of EES. Consequently, a deeper understanding of how EES interacts with the recruited spinal sensorimotor circuits is essential to promote the design of effective, hypothesis-driven EES strategies. In this chapter, we addressed this question by combining computational modeling and behavioral experiments in rat models of SCI.

Related publication and personal contributions

The content of this chapter is adapted — with permission of the co-authors and journal — form the following publication: E. Moraud[*], M. Capogrosso[*], **E. Formento**, N. Wenger, J. DiGiovanna, G. Courtine[†], and S. Micera[†], *"Mechanisms Underlying the Neuromodulation of Spinal Circuits for Correcting Gait and Balance Deficits after Spinal Cord Injury"*, Neuron (2016).

Personal contributions: developed the computational model, computer simulations, data analysis, figures preparation, manuscript editing.

2.1 Abstract

Epidural electrical stimulation of lumbar segments facilitates standing and walking in animal models and humans with spinal cord injury. However, the mechanisms through which this neuromodulation therapy engages spinal circuits remain enigmatic. Using computer simulations and behavioral experiments, we provide evidence that epidural electrical stimulation interacts with muscle spindle feedback circuits to modulate muscle activity during locomotion. Hypothesis-driven strategies emerging from simulations steered the design of stimulation protocols that adjust bilateral hindlimb kinematics throughout gait execution. These stimulation strategies corrected subject-specific gait and balance deficits in rats with incomplete and complete spinal cord injury. The conservation of muscle spindle feedback circuits across mammals suggests that the same mechanisms may facilitate motor control in humans. These results provide a conceptual framework to improve stimulation protocols for clinical applications.

2.2 Introduction

Severe spinal cord injury (SCI) disrupts the communication between supraspinal centers and spinal circuits producing leg movement. The interruption of descending pathways abolishes the sources of modulation and excitation that are essential to enable functional states of spinal circuits (Orlovskiĭ et al., 1999; Courtine et al., 2009; Kiehn, 2006). Albeit intact, denervated lumbar circuits remain in a state that is not permissive for standing and walking. Electrical epidural stimulation (EES) of lumbar segments provides a strategy to reactivate these circuits (Carhart et al., 2004; C. A. Angeli et al., 2014; Hofstoetter, Danner, et al., 2015). For example, individuals with a chronic, functionally complete SCI immediately regained the ability to stand and produce voluntary movements during continuous EES of lumbar segments (C. A. Angeli et al., 2014).

These preliminary results have triggered the deployment of clinical studies that evaluate the potential of EES to improve motor recovery after SCI. However, the mechanisms through which EES enables the production of motor patterns remain enigmatic, even though this understanding is pivotal in the translation of this paradigm into a viable clinical application. Computer simulations (Rattay et al., 2000; Capogrosso et al., 2013) and experimental studies (Gerasimenko et al., 2006; Hofstoetter, Danner, et al., 2015) provided evidence that EES primarily engages large myelinated fibers associated with proprioceptive and cutaneous feedback circuits. The prevailing view is that the recruitment of these fibers raises the excitability of spinal circuits and modulates central pattern generator networks (C. A. Angeli et al., 2014; Danner et al., 2015). This conceptual framework has restricted the clinical application of EES to continuous, non-modulated stimulation patterns (Carhart et al., 2004; C. A. Angeli et al., 2014; Hofstoetter, Danner, et al., 2015). However, this strategy fails to address subject-specific deficits of gait and balance throughout movement execution, which is essential to maximize the outcome of rehabilitation protocols (Barbeau et al., 1999; Edgerton et al., 2008).

In this study, we hypothesized that EES paradigms exploiting the dynamic properties of spinal circuits in real time provide the opportunity to target subject-specific motor deficits,

mediating superior therapeutic effects compared to tonic stimulation. We previously showed that closed-loop control of EES is capable of modulating gait features during locomotion in rats with complete SCI (Wenger et al., 2014). However, the design of EES paradigms that ecologically interact with spinal circuit dynamics is contingent on a mechanistic understanding of how the recruitment of large myelinated fibers translates into modulation of muscle activity (Courtine & Bloch, 2015).

Computational models have played an important role in guiding the application of neuromodulation therapies to alleviate motor deficits in Parkinson's disease (McIntyre & Foutz, 2013) and neuropathic pain (T. C. Zhang et al., 2014). Here, we developed a computational model that predicts the interactions between EES and spinal circuit dynamics. Simulations uncovered the mechanisms through which EES interacts with muscle spindle feedback circuits to modulate standing and walking in the absence of supraspinal contribution. We found that spinal circuits filter the modulating effects of EES toward functionally relevant pathways. This finding steered the design of stimulation protocols that reestablished gait symmetry and corrected balance deficits in rats with incomplete and complete SCI. These results establish a computational framework for the development of neuromodulation therapies that harness spinal circuit dynamics to facilitate rehabilitation and recovery in patients with SCI.

2.3 Results

2.3.1 Dynamic model combining realistic neuronal networks coupled to hindlimb biomechanics

To study the mechanisms through which EES leads to motor pattern formation, we elaborated a dynamic model wherein muscle spindle feedback circuits receive natural sensory input from realistic hindlimb neurobiomechanics.

First, we modeled muscle spindle feedback pathways and integrated these circuits within the minimal neuronal network that is responsible for the reciprocal recruitment of agonist muscles. This neural network, inspired from experimental (Jankowska, 1992; Talpalar et al., 2011) and computational studies (Stienen et al., 2007), embeds realistic alpha motoneurons (**Figures 2.1D** and **2.12**) (Booth et al., 1997; Jones & Bawa, 1997; McIntyre & Grill, 2002), Ia-inhibitory interneurons, group-II excitatory interneurons, and group-Ia and group-II afferents (**Figure 2.1A**). To simulate serotonin-mediated modulation of motoneuron membrane dynamics that is required to enable locomotion in rats with SCI (Courtine et al., 2009), we reduced the conductance of potassium-calcium gated ion channels in the model (Booth et al., 1997).

Second, we estimated the time profiles of firing rates of groupIa and group-II afferent fibers during gait using a muscle spindle model (Prochazka & Gorassini, 1998a, 1998b) and a validated biomechanical model of the rat hindlimb (Johnson et al., 2011). We recorded joint trajectories during locomotion in healthy rats and estimated muscle stretch profiles of flexor (tibialis anterior) and extensor (gastrocnemius medialis) muscles of the ankle through inverse kinematics (**Figure 2.1B**).

Third, we modeled the interactions between the natural firing rate of efferent and afferent
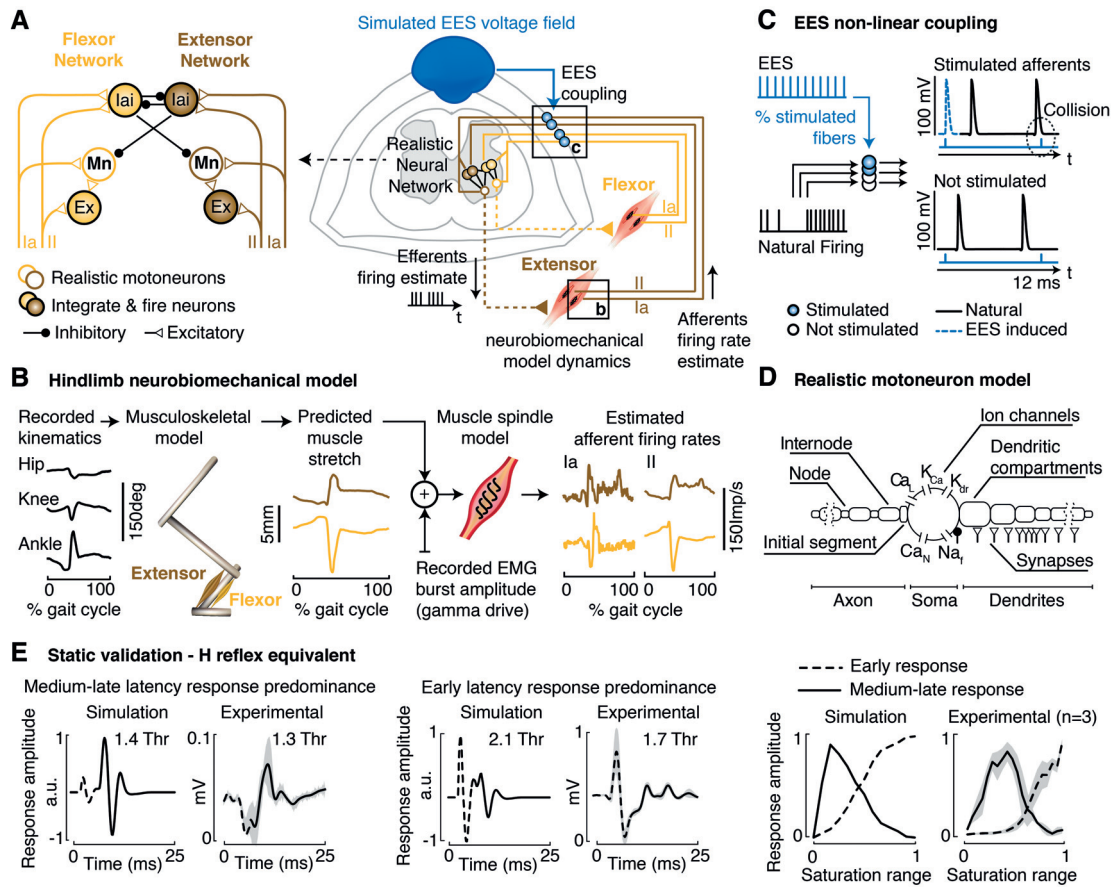
Figure 2.1 | Computational model of muscle spindle feedback circuits. **A**, Biologically realistic neural network of muscle spindle feedback circuits for two antagonist muscles, including reciprocal inhibition. **B**, Musculoskeletal model of the rat hindlimb, prediction of the muscle stretch during locomotion for antagonist ankle muscles, and resulting firing rates using a muscle spindle model. **C**, Modeling of nonlinear interactions between natural firing rates along afferent fibers and depolarization induced by EES. **D**, Realistic motoneuron model. **E**, Motor responses evoked in ankle muscles when delivering a single pulse of EES at various intensities expressed with respect to the motor threshold (Thr) in the model and experimentally. Plots report the modulation (±SEM) of motor responses with increasing EES intensities, expressed as percent of the saturation level.

fibers and the depolarization elicited by EES pulses. These interactions are non-linear, since EES induced depolarization may fail to elicit action potentials if the stimulation collides with ongoing depolarization or refractory state (**Figure 2.1C**). To account for this non-linearity, we computed the membrane summation of natural and EES induced depolarization for each simulated fiber. Estimates of the percentage of recruited fibers were derived from our validated finite element model of EES (Capogrosso et al., 2013).

Fourth, we converted efferent firing rates into electromyographic (EMG) activity by convolving wavelets of Gaussian distributed amplitudes and durations with population of action potentials (**Figure 2.13C**).

2.3.2 Validation of the muscle spindle feedback circuit model

To validate the predicted interactions between EES and the neuronal network, we assessed whether the model was able to qualitatively replicate the spinal reflex recruitment curves elicited by EES (Gerasimenko et al., 2006). We simulated the recruitment of afferent and efferent fibers in response to single EES pulses of increasing intensity and computed motor responses evoked in ankle muscles. We then compared simulations with experimental recordings in rats (n = 3). Until half the saturation range, EES only elicited medium and late-latency motor responses through the recruitment of afferent fibers (92% energy of medium responses in simulations; 96% ± 2% in experiments). The shape, latency, and modulation of these responses exhibited qualitative similarities in the model and in vivo (**Figure 2.1E**). At higher intensities, EES additionally recruited efferent fibers, which led to the progressive decrease and eventual suppression of medium and late-latency motor responses, both in the model and in vivo (66% energy of early responses in simulations; 67% ± 20% in experiments).

2.3.3 Impact of EES on efferent and afferent fibers

We then exploited the computational model to study the impact of EES frequency and amplitude on the firing rate of afferent and efferent fibers during locomotion.

We found that increments in frequency ranging from 10 to 100 Hz led to a linear increase in the mean firing rate of groupIa and group-II afferents (**Figure 2.2A**; R^2 = 0.99 for extensors and flexor). A comparable modulation was observed when increasing EES amplitude from 0.8 to 2 times the motor threshold, although the responses rapidly reached saturation due to the recruitment of all fibers. In all conditions, however, the temporal profiles of afferent firing rates were preserved, indicating that EES does not interfere with the natural encoding of locomotor-related information.

The integration of afferent firing rates into the neuronal network led to reciprocal activation of extensor and flexor motoneurons during specific phases of gait (**Figures 2.2B** and **2.3**). Increments in EES frequency mediated a linear increase in the firing rates of both extensor (R^2 = 0.99) and flexor (R^2 = 0.93) motoneurons. Due to reciprocal inhibitory networks, this modulation only occurred during the phase corresponding to the natural recruitment of motoneurons (**Figure 2.3**), regardless of EES frequency. In contrast, increasing EES amplitude recruited the axons of motoneurons, including during the inactive phase, which disrupted the natural alternation between extensor and flexor (**Figure 2.2B**).

2.3.4 Dynamic validation of the computational model

We tested whether the model was able to predict the modulation of muscle activity mediated by varying EES frequencies and amplitudes during gait, and under different conditions of standing and walking. For stimulation values normally used during experimental recordings (40 Hz frequency, 1.2 muscle response threshold amplitude), the model generated reciprocal bursts of modulated electromyographic activity in extensor and flexor muscles that matched experimental observations in rats with complete SCI (r = 0.86 and 0.85 for extensors and flexors; **Figure 2.2C**). These bursts were composed of modulated medium and late-latency re-
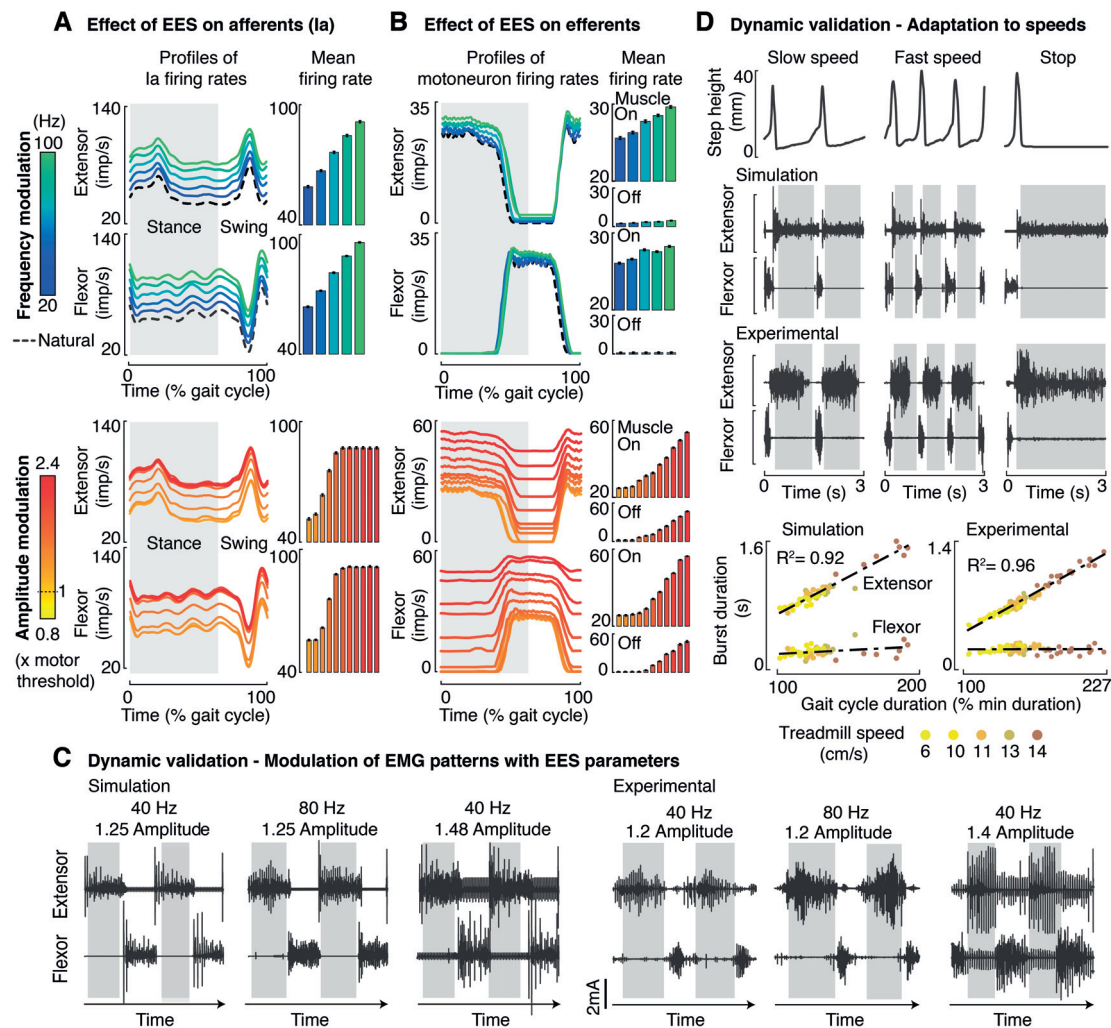
Figure 2.2 | Interactions between EES and spinal circuit dynamics during locomotion. A, Estimated firing rate along group-Ia fibers over the gait cycle under different EES frequencies (top) and amplitudes (bottom). Shaded areas indicate phases of extensor activity (stance). Bar plots report the mean (±SEM) firing rates computed over ten simulated gait cycles. **B**, Estimated firing rate along efferent axons under the same conditions as in **A**. Bar plots report the mean (±SEM) firing rates over ten simulated gait cycles for each motor pool. The ON/OFF phases of each muscle were defined as the time period when motoneuron activity was higher/lower than one SD from the maximum. **C**, Simulated and experimental muscle activity patterns during locomotion under different EES frequencies and amplitudes. **D**, Simulated and experimental muscle activity patterns during locomotion under different treadmill speeds and during the transition from stepping to standing. Plots report the relationships between gait cycle duration and burst duration of flexor and extensor muscles derived from simulations and experimental recordings.

sponses that were locked to each pulse of EES (**Figure 2.4A**). A 2-fold increase in EES frequency induced a higher density of responses, which augmented the overall muscle activity (25% ± 8% for extensors and 27% ± 7% for flexors in the model versus 29% ± 15% for extensors and 33% ± 16% for flexors in vivo, n = 55 steps; **Figure 2.4B**). However, the reciprocal activation between antagonist muscles remained unaffected, both in the model and in vivo (**Figure 2.2C**). Increasing EES amplitude led to co-activation of extensor and flexor muscles, as observed in
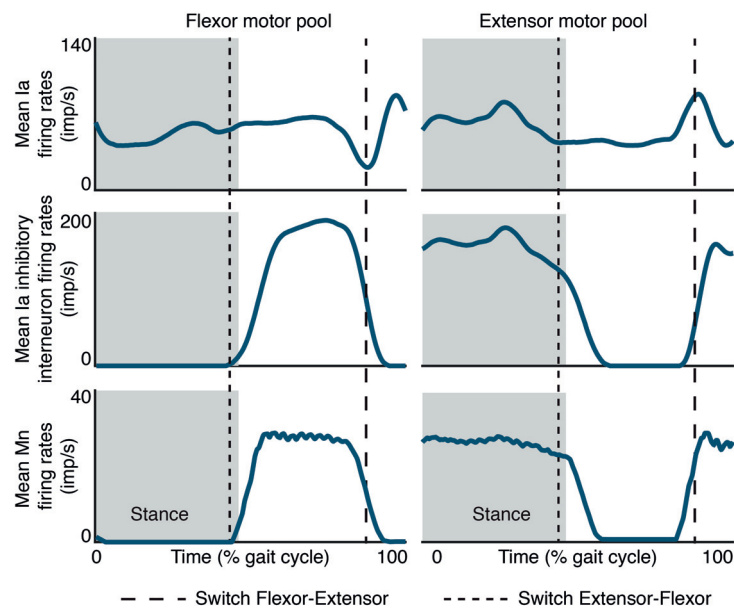
Figure 2.3 | Cellular mechanisms underling the alternation between flexor and extensor motoneurons during locomotion enabled by EES in the model. Firing rate profiles of group-Ia afferent fibers (top), group-Ia inhibitory interneurons (middle), and motoneurons (bottom) associated with flexor (left) versus extensor (right) motor pools. The change in firing rates is displayed over a complete gait cycle. During the first half of the stance phase, group-Ia afferents innervating extensor muscles display a larger firing rate than those innervating flexor muscles. This imbalance reinforces the activity of group-Ia inhibitory interneurons associated with extensor muscles, which results in the complete inhibition of both motoneurons and antagonist group-Ia inhibitory interneurons associated with flexor muscles. Towards the end of stance, the balance between the firing rates of extensor versus flexor group-Ia afferents reverses, which results in a rapid switch from extension to flexion. The same switch occurs during the second half of the swing phase. The emergence of a peak in the firing rates of group-Ia afferents from extensor muscles coincides with a concurrent drop in the firing rate of group-Ia afferents from flexor muscles afferents. This opposing changes trigger a sudden inhibition of flexor motoneurons and a sharp excitation of extensor motoneurons.

simulations.

EES enables spinal circuits isolated from supraspinal inputs to use sensory information as a source of control to produce motor patterns for standing and walking at different speeds (Courtine et al., 2009). The model reproduced the differential modulation of burst durations in extensor and flexor muscles with increasing treadmill velocities and during transitions from walking to standing (**Figure 2.2D**). These combined results support the validity of our model and suggest that EES modulates muscle spindle feedback circuits to facilitate the alternating recruitment of antagonist motor pools in the absence of supraspinal input.

2.3.5 Exploiting spinal circuit dynamics to target distinct muscle spindle feedback circuits with EES

Simulations show that reciprocal inhibition restricts the effects of EES to the phase during which motoneurons are recruited (**Figures 2.2B** and **2.4**). This result suggests that phase-dependent modulation of muscle spindle feedback circuits filters the effects of EES toward functionally relevant pathways. We hypothesized that this property may be exploited to
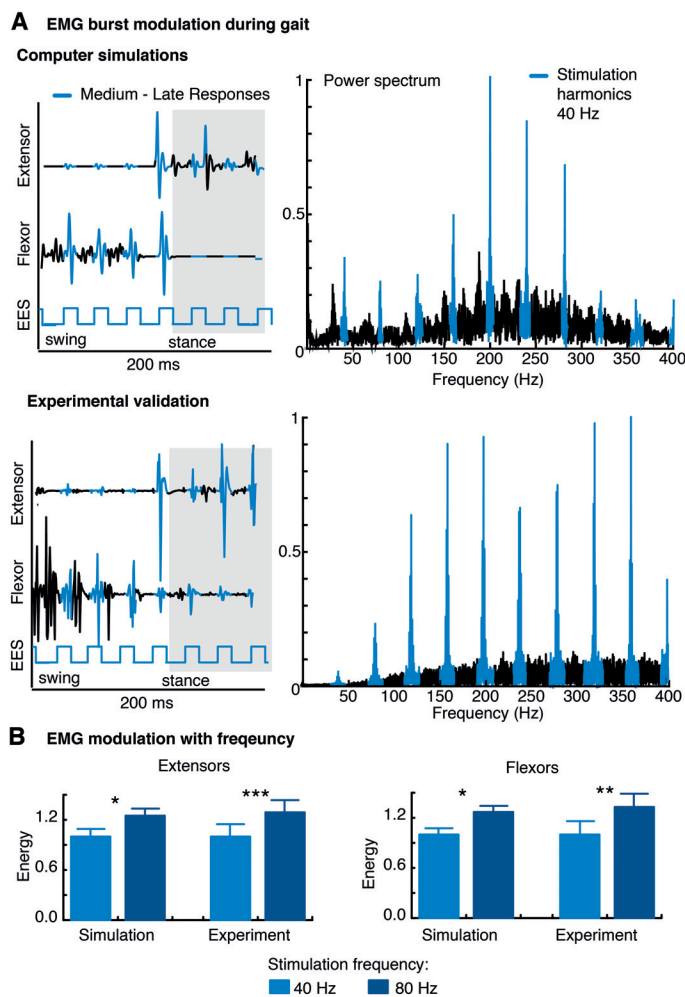
Figure 2.4 | Modulation of muscle activity during locomotion under different EES frequencies. **A**, Simulated and experimental recordings of muscle activity during EES delivered at 40 Hz. The lower trace indicates the occurrence of EES pulses, which triggered mono- and poly-synaptic motor responses, represented in color. The bursts of EMG activity are composed of a succession of motor responses elicited by each EES pulse. The intrinsic dynamics of muscle spindle feedback circuits modulates the amplitude of these responses over the course of the gait cycle, which result in modulated and alternating bursts of EMG activity in flexor and extensor muscles. The plots show the power spectrum of simulated and experimental EMG signals, which reveals that muscle activity is built from components of EES frequency harmonics, both in simulations and experiments. **B**, Bar plots reporting mean (±SEM, n = 55 steps) energy of extensor and flexor EMG bursts during locomotion under 40 versus 60 Hz EES frequencies in simulations and experimentally. ***, $p < 0.001$; **, $p < 0.01$; *, $p < 0.05$

selectively modulate flexor versus extensor muscles through phase-specific adjustment of EES. We performed simulations in which EES frequency was independently tuned during stance versus swing phases. These simulations revealed that phase-specific EES gradually and specifically modulates the activity of extensor versus flexor muscles (**Figures 2.5A** and **2.6A**).

We tested whether the same specificity was obtained in rats with complete SCI. The combination of a serotonin replacement therapy and midline EES enabled locomotion in all rats (Courtine et al., 2009). We expanded our real-time stimulation platform (Wenger et al., 2014) to enable closed-loop adjustment of EES parameters based on bilateral hindlimb kinematics.
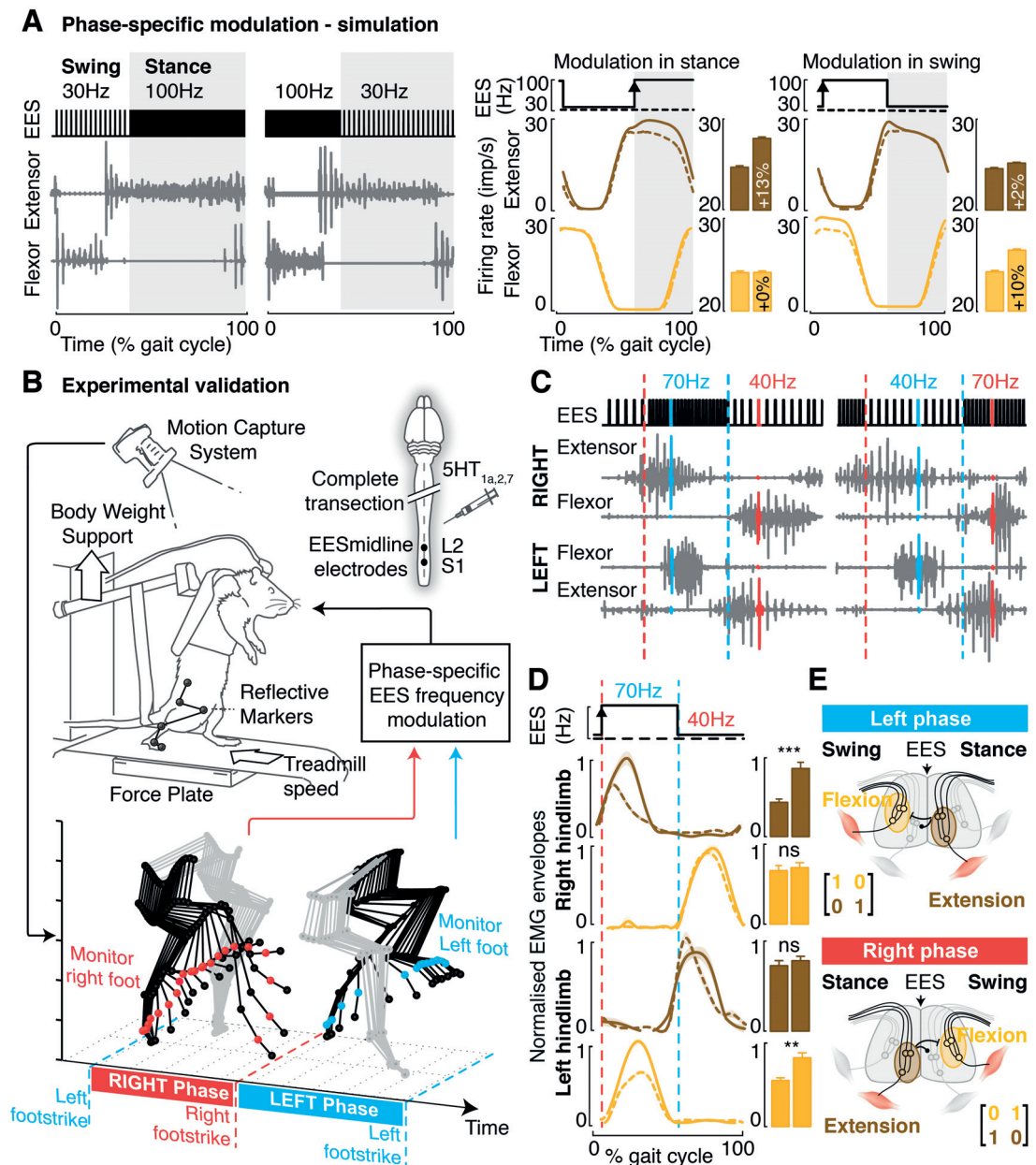
Figure 2.5 | Phase-specific modulation of EES frequency during gait. A, Simulated EMG patterns and estimated firing rates along efferents during locomotion while EES frequency varies during stance or swing. Conventions are the same as in **Figure 2.2**. Bar plots report the mean (±SEM) firing rates over ten gait cycles for each motor pool. **B**, Experimental platform for phase-specific modulation of EES frequency based on movement feedback in rats with complete SCI. Real-time monitoring of hindlimb kinematics automatically detected left and right foot strikes, which segmented gait cycles in two phases. **C**, Muscle activity patterns during stepping under phase-specific EES, together with train of stimulation pulses. **D**, Rectified muscle activity (continuous lines) recorded during locomotion with phase-specific modulation of EES frequency, compared to continuous EES (40 Hz, dashed lines). Bar plots report the mean (±SEM) activity of each muscle during continuous (left) versus phase-specific (right) EES (n = 4 rats). **E**, Scheme and matrix formulation illustrating the natural gating of muscle spindle feedback circuits during locomotion, which filter the effects of EES toward active muscles (2 × 2 matrices, input stimulation spatial specificity, and output functional specificity).
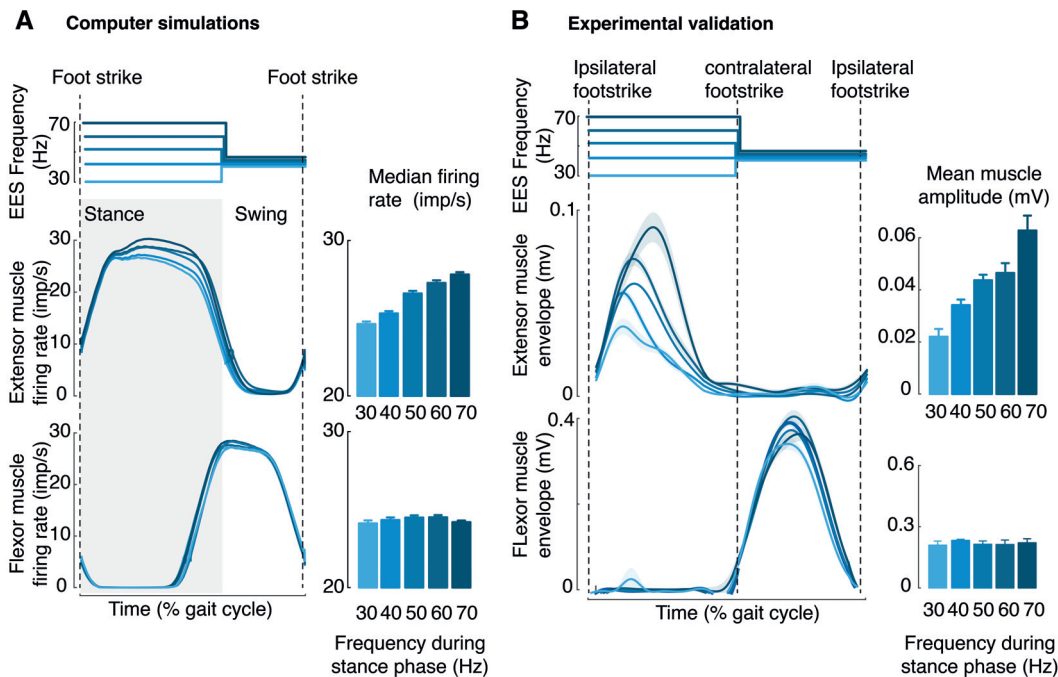
Figure 2.6 | Modulation of motoneuron output during phase-specific changes in EES frequency. A, Averaged (n = 10 gait cycles) modulation of firing rates along efferent axons of extensor and flexor motor pools during simulated locomotion under EES frequency ranging from 30 to 70 Hz during the stance phase, and remaining constant at 40 Hz during the swing phase. Firing rates of flexor motoneurons were not affected by phase-specific EES frequency restricted to the stance phase. Bar plots report mean firing rate (± SEM) measured over 10 gait cycles under different EES frequencies. **B**, Similar representations and quantifications are shown during locomotion in rats with complete SCI, except that bar plots report the mean muscle activity recorded over more than 10 gait cycles per EES frequency. Phase-specific changes in EES frequency supported the specific modulation of extensor versus flexor muscles during locomotion through the introduction of a temporal structure in EES profiles.

Automated detections of foot strikes divided gait into interleaved left and right phases (**Figure 2.5B**). During stepping, extensor muscles of one hindlimb are active at the same time as flexor muscles of the other hindlimb (**Figure 2.5C**). Consequently, model predictions suggested that changes in EES frequency during the left-stance phase would simultaneously modulate left extensor and right flexor muscles and inversely for the right-stance phase. Experimental recordings validated these predictions. We found a linear relationship between EES frequency and the amplitude of ipsilateral extensor and contralateral flexor muscles (**Figures 2.5C**, **2.5D**, and **2.6B**). These effects were restricted to the period during which muscles were active, confirming the ability of phase-specific EES to modulate distinct spinal circuits during gait.

2.3.6 Model-derived control policies modulate bilateral hindlimb movements during locomotion

We next sought to leverage these properties to develop control policies that actively tune left versus right hindlimb movements during locomotion. We conducted a comprehensive

mapping of changes in left and right step heights for pairs of EES frequencies ranging from 20 to 80 Hz, which we represented in a 3D space (n > 300 steps per rat; **Figure 2.7B** and **Supplementary FigureA.1** in the appendix). Each hindlimb displayed a linear relationship between step height and phase-specific EES frequency, which was independent of the contralateral hindlimb. Consequently, the modulation for each hindlimb laid on a planar surface (**Figure 2.7B**). These planes quantified the degree of asymmetry between the left and right steps, while their intersection defined the pairs of EES frequency that are theoretically appropriate to correct these idiosyncratic deficits (**Figure 2.7C**).

To test this possibility, we embedded a control structure within the real-time stimulation platform, composed of two controllers interleaved in time. Each controller monitored the foot trajectory of one hindlimb and adjusted EES frequency during its swing phase to target a desired step height, regardless of the other limb (**Figure 2.8A**). We thus capitalized on phase-dependent modulation of spinal circuits to control a single-input multiple-output (SIMO) system out of two independent controllers operating in parallel. To evaluate the performance of this control structure, we applied sudden changes in the desired step height for each hindlimb independently (**Figure 2.8B** and **Supplementary Figure A.2B** in the appendix). For each task, the controllers successfully adjusted phase-specific EES frequencies to target the desired step height of each hindlimb with high precision (error <5 mm), even when imposing references reaching the physiological limits of motion (**Supplementary Figure A.2B** in the appendix). More complex feed-forward predictive models that implicitly account for time and interlimb effects required longer convergence times and failed to improve performance (**Supplementary Figure A.2C** in the appendix).

2.3.7 Model-Derived control policies restore symmetry and improve balance

We next tested whether closed-loop control of phase-specific EES frequencies is able to correct idiosyncratic deficits of gait and balance. Each injured rat exhibited a distinct degree of asymmetry that altered inter-limb coordination and balance, primarily due to discrepancies in the recruitment of extensor muscles (**Figure 2.9A**). We configured the controller to maintain left and right steps at the same height. Corrections in EES frequency during the stance phase of the weaker hindlimb augmented extensor muscle activity and promoted whole-limb extension. This tuning reestablished symmetry and distributed vertical ground reaction forces equally in all tested rats ($p < 0.001$ for each rat; **Figure 2.9A**). The controller converged toward EES frequency pairs that scattered along the symmetry line defined by the intersection of the correlation planes (**Figure 2.9B**). These adaptions also restored balance. During controlled conditions, the center of pressure displayed oscillations centered on the body midline, which contrasted with the pronounced lateral shifts underlying non-controlled steps ($p < 0.001$; **Figure 2.9C**). Moreover, the distribution of ground reaction forces was less variable during controlled compared to non-controlled steps ($p < 0.001$).
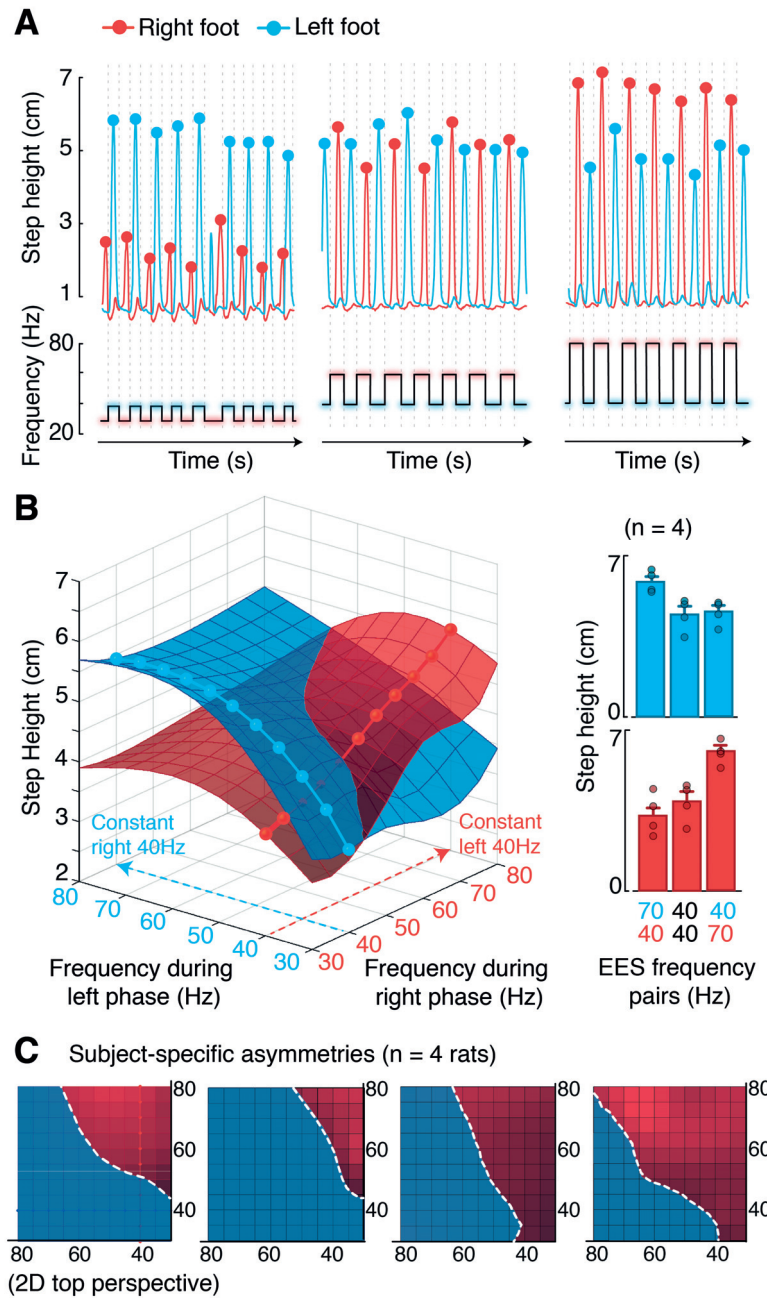
Figure 2.7 | Phase-specific adjustment of EES frequency independently modulates bilateral foot trajectories in rats with complete SCI. A, Vertical displacements of the left and right feet during locomotion under three patterns of phase-specific EES frequencies. EES frequency was adjusted during the right phase (30 Hz, 60 Hz, and 80 Hz), while EES remained unchanged on the left phase for all three protocols. The dots and dashed vertical lines highlight maximum foot heights and foot strike events, respectively. **B**, 3D plot showing the relationships between maximum left and right step heights and phase-specific EES frequencies (>850 step cycles covering the entire input space). Bar plots highlight side-specific modulations across animals (n = 4). **C**, 2D projections of the same representation as in (**B**) for each tested rat. The white dotted line indicate the intersection between both surfaces, highlighting the pairs of phase-specific EES frequencies that would theoretically induce symmetry for each rat.
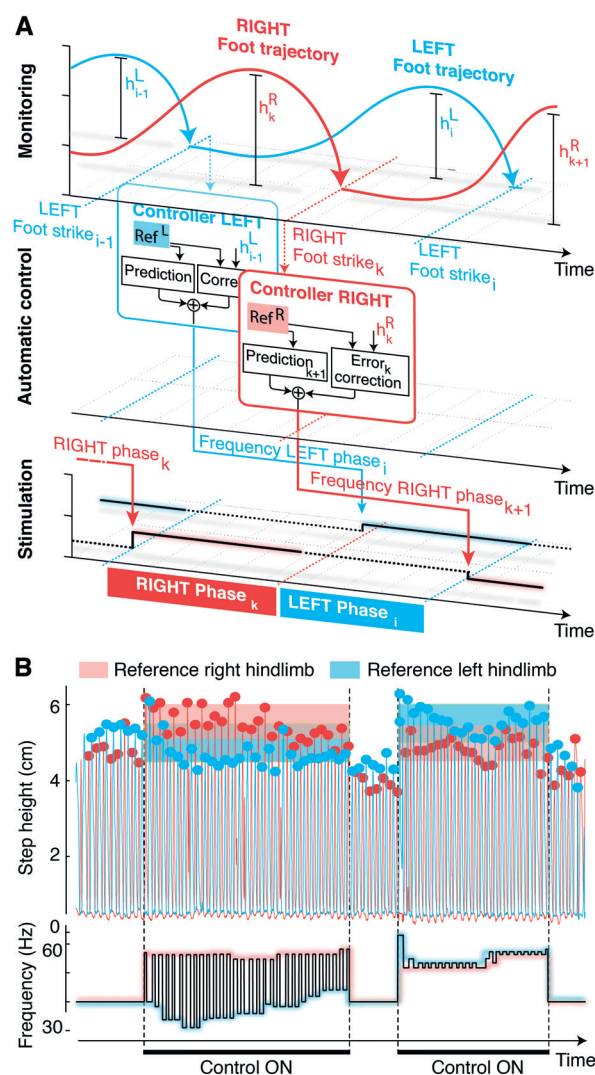
Figure 2.8 | Real-time control of bilateral step height during locomotion in rats with complete SCI.
A, Closed-loop control structure composed of two independent controllers, one for each hindlimb, operating in parallel. Each controller combines a forward model and a proportional integral controller that calculate corrections of EES frequency during the phase k in order to maintain the maximum step height (h_k^R and h_k^L for right and left hindlimbs) within a predefined reference band (Ref^L and Ref^R). Corrections in EES frequency are applied at the next iteration of the same phase (k + 1). **B**, Continuous sequence showing the controllability of step heights for the left and right hindlimbs with phase-specific EES frequencies. The left and right controllers target step height reference bands (shaded areas) that were inverted between the first and second controlled periods.

2.3.8 Model-derived control policies improve locomotor performance

We then evaluated whether the controller was able to maintain gait performance while increasing weight-bearing levels and speeds, two behavioral conditions that involve enhanced physical effort. During non-controlled steps, reduction of bodyweight support led to a decrease in step height and extension, together with increased variability (**Figure 2.10A**). The controller adjusted EES frequency to preserve left and right foot elevation. Tuning of EES frequency reinforced the activity of extensor muscles, which resulted in larger vertical ground

35
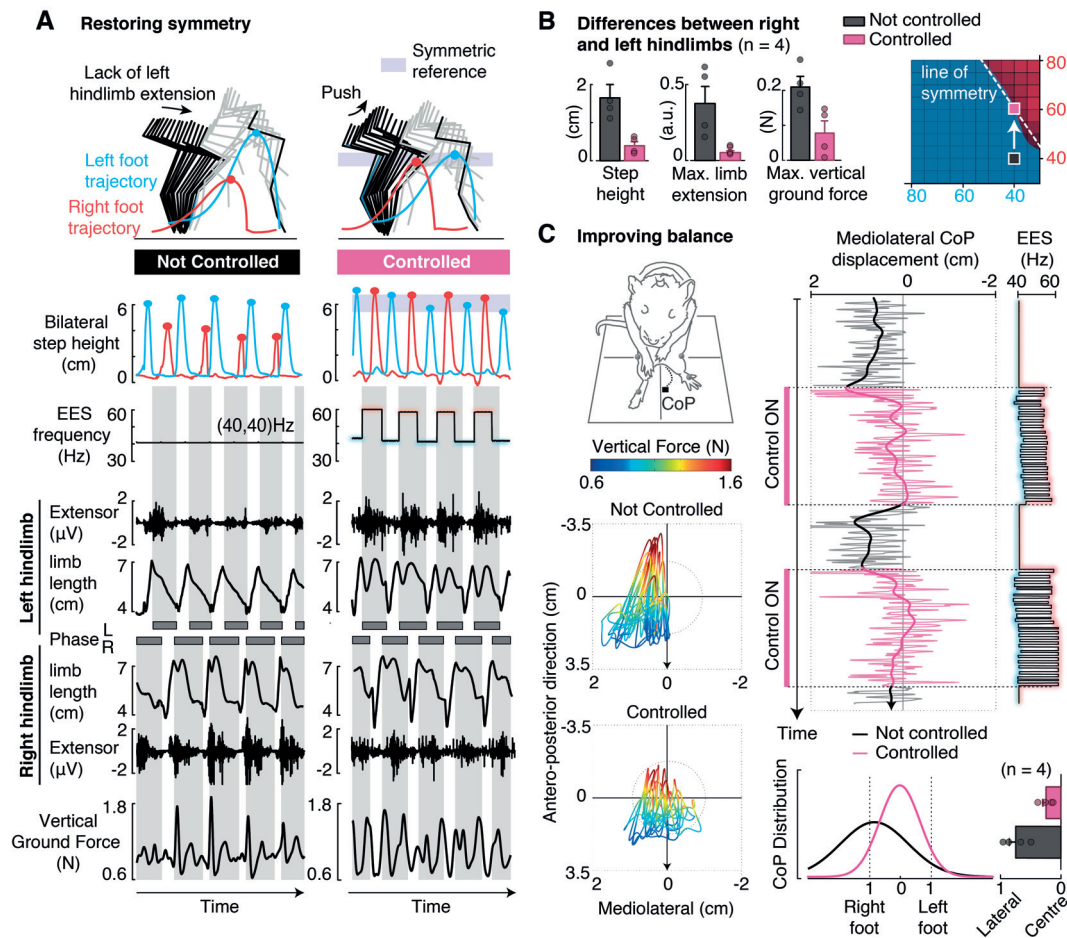
Figure 2.9 | Closed-loop control of phase-specific EES frequency restores symmetry and balance in rats with complete SCI. A, Decomposition of left hindlimb kinematics and trajectories of the left and right feet under non-controlled and controlled conditions. The vertical displacements of both feet are displayed together with concurrent changes in EES frequency, EMG activity of left and right extensor muscles, and bilateral hindlimb length during a non-controlled and controlled sequence. Boxes indicate left (L) and right (R) stance phases. **B**, Bar plots reporting mean differences (±SEM) between the left and right hindlimbs for relevant gait features during non-controlled and controlled conditions. Single dots refer to individual rats. The controller selected pairs of EES frequencies that converged toward the theoretical line of symmetry. **C**, Center of pressure (CoP) displacement and color-coded vertical ground reaction forces during locomotion. The origin indicates the equidistant position of the CoP between both feet during standing. Continuous changes in mediolateral CoP displacements are shown together with phase-specific EES frequencies during a sequence alternating non-controlled and controlled conditions.

reaction forces that enabled the rats to sustain increased loads equivalent to 15% of their body weight (**Figure 2.10A**).

During transitions from normal to high speeds, injured rats exhibited an increase in backward foot movements during stance and pronounced dragging during swing, which reflected their difficulties to meet task requirements (**Figure 2.10B**). The controller adjusted EES frequencies to alleviate these deficits ($p < 0.01$ for each rat).
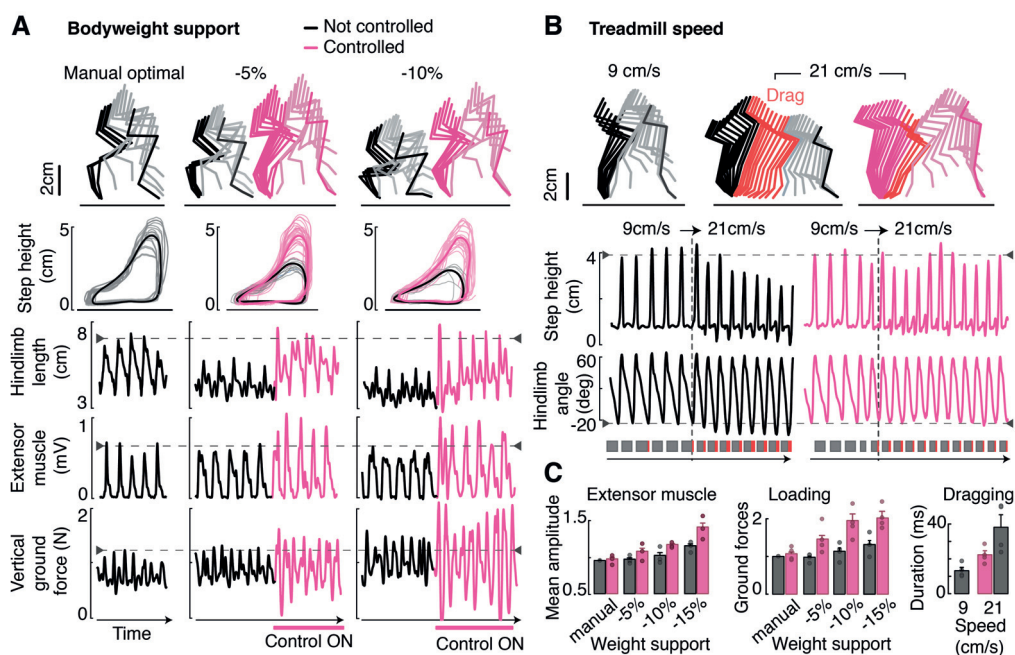
Figure 2.10 | Closed-loop control of phase-specific EES frequency preserves stepping performance during tasks requiring enhanced physical effort. Rats with complete SCI were tested in two challenging tasks under non-controlled versus controlled conditions. **A**, Decomposition of hindlimb kinematics, foot trajectories, and continuous changes in hindlimb length, extensor muscle activity, and vertical ground reaction forces during locomotion under progressive decrease in body-weight support. **B**, Decomposition of hindlimb kinematics and continuous changes in vertical foot displacement and hindlimb angle during locomotion during the transition from slow to fast stepping. The controller progressively reinforced the amplitude of muscle activity, which enhanced weight-bearing levels while maintaining stepping consistency and minimizing dragging. **C**, Bar plots report mean values (±SEM, n = 4 rats) of relevant gait parameters during decrease in body-weight support and increase in speed. Single dots refer to individual rats.

2.3.9 Model-derived control policies in clinically relevant rodent models

Finally, we sought to evaluate the translational potential of phase-specific EES protocols. SCI in humans primarily results from contusion injuries, which lead to variable damage. Consequently, these lesions induce a broad spectrum of asymmetries in gait deficits (Friedli et al., 2015). Moreover, the severity and specificity of the SCI is likely to determine the appropriate level of serotoninergic replacement therapies to facilitate gait.

To address these issues, we first studied whether the modulation of muscle activity with EES frequency was preserved in the absence of serotoninergic replacement therapies. We withdrew serotonin-mediated modulation of motoneuron membrane dynamics in the model (**Figure 2.11A**). Simulations showed that the absence of serotonin reduced muscle burst amplitude, but did not affect the alternation between extensor and flexor muscles. Moreover, the modulation of muscle activity during changes in EES frequency was preserved, which compensated for the withdrawal of serotonin (**Figure 2.11A**). To validate these results, we placed a lateralized contusion SCI that induced different degrees of gait asymmetry and deficits (**Figures 2.11B** and **2.11C**). Without serotonin, EES promoted locomotion in all tested rats despite a significant decrease in muscle activity ($p < 0.05$; **Figure 2.11B**). As observed
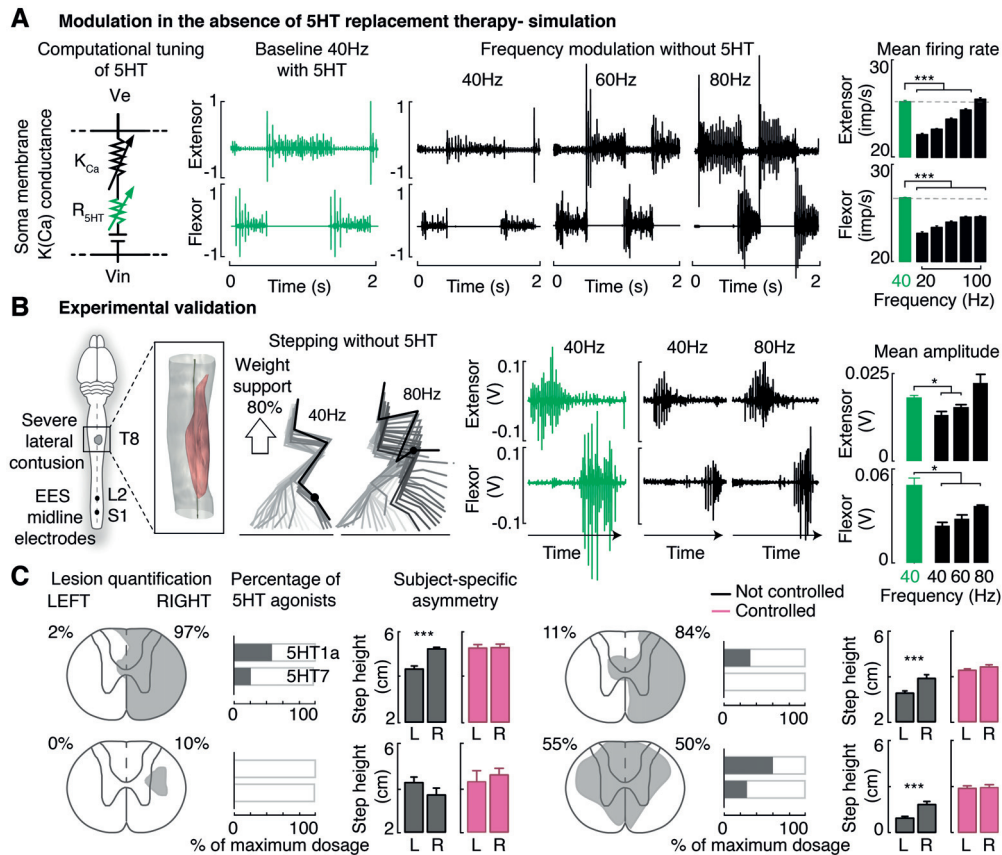
Figure 2.11 | Phase-specific EES frequency in rats with clinically relevant SCI under minimal serotonin replacement therapy. A, Model of 5-HT mediated tuning of motoneuron soma membrane conductance. Simulated muscle activity patterns during locomotion with 5-HT and without 5-HT under different EES frequencies. Bar plots report mean firing rates along efferent axons computed over 10 gait cycles per EES frequency. Increase in EES frequency compensated for the lack of 5-HT. **B**, 3D reconstruction of a lateralized contusion SCI. Decomposition of hindlimb kinematics under two distinct EES frequencies. Muscle activity patterns recorded in a rat with a contusion SCI under the same conditions as in **A**, including quantifications of muscle activity across the four tested rats. **C**, Reconstruction of damaged tissue (shaded area, including percent) on each hemicord for each rat. Horizontal bar plots report the optimal 5-HT agonist dosage for each rat, expressed in percent of the maximum dosage necessary for rats with complete SCI. Bar plots report mean values (±SEM) of left (L) and right (R) step heights under non-controlled and controlled conditions for each rat. ***, $p < 0.001$, unpaired t test. The controller restored symmetry in all the rats, regardless of idiosyncratic motor deficits and the level of 5-HT agonist concentration.

in the model, the tuning of muscle activity and hindlimb kinematics was conserved during changes in EES frequency, which robustly modulated hindlimb movements.

We then personalized the serotoninergic replacement therapy for each rat and tested whether phase-specific EES frequency was able to correct gait asymmetry and subject-specific deficits. While rats exhibited markedly different alterations, phase-specific EES frequency restored symmetry and improved hindlimb kinematics in all tested rats ($p < 0.001$; **Figure 2.11C**).

2.4 Materials and methods

2.4.1 Computational model

Realistic neural network

The neural network is implemented in NEURON (Hines & Carnevale, 1997) using a parallel multi-threaded structure. Afferent fibers are modeled as Poisson point processes with average firing rates estimated from a spindle model and 20% noise level. The latency between action potentials and elicited excitatory postsynaptic potentials (EPSPs) to the target cell follows a normal distribution (mean = 2 ms, variance = 0.3 ms) accounting for the variability in afferents diameter. A total of 60 Ia and group-II fibers are implemented for each motor pool (Segev et al., 1990). Each group-Ia fiber forms excitatory synapses to all motoneurons of the homonymous motor pool (Segev et al., 1990), while group-II fibers establish excitatory synapses onto each group-II interneuron (Stienen et al., 2007).

Each motor pool comprises 169 alpha motoneurons (**Figure 2.12**)) (Jones & Bawa, 1997; McIntyre & Richardson, 2002; Stienen et al., 2007; Capogrosso et al., 2013). The membrane potential of each cell is described as a modified Hodgkin-Huxley model comprising sodium, potassium, calcium, and potassium-calcium gated ion channels (McIntyre & Richardson, 2002). To model the effect of 5-HT agonists, which is used with EES to enable locomotion, we lowered the potassium-calcium gated ion channels conductance by 40% (Booth et al., 1997).

Motoneuron morphology consists of a 32 ±10 mm diameter spherical soma connected to an electronic-equivalent dendritic tree of mammalian S type alpha motoneurons (Fleshman et al., 1988; Jones & Bawa, 1997), dendritic sizes adapted to match soma diameter, from cell S-type cell 35/4. The initial segment and efferent axon are implemented with dedicated membrane dynamics (Capogrosso et al., 2013; McIntyre & Richardson, 2002). Inhibitory synapses innervate the soma and behave as alpha functions with a reversal potential E_{syn} = -75 mV, a rise time constant σ = 1.5 ms, and a decay time constant τ = 2 ms. The resulting inhibitory postsynaptic potential (IPSP) at the soma reaches an amplitude of -3 mV (Pratt & Jordan, 1987; McIntyre & Grill, 2002) (**Figure 2.13A**). Group-II interneuron excitatory synapses are located along the dendritic tree with a Poisson distribution (Jones & Bawa, 1997). Excitatory synapses are modeled by an exponential function with reversal potential E_{syn} = 0 mV and decay time constant τ = 0.5 ms. The conductance of excitatory synapses from group-Ia fibers was tuned to a mean EPSP amplitude = 212 μV (Harrison & Taylor, 1981), increased by 28% to mimic the heteronymous contribution of synergistic innervations (Scott & Mendell, 1976) (**Figure 2.13B**). The conductance of group-II interneuron synapses was set to one-third the size of group-Ia fiber EPSPs to mimic the smaller impact of group-II fibers on motoneurons (Munson et al., 1980).

Excitatory and inhibitory interneurons were modeled as Integrate and fire cells with membrane time constant τ_m = 30 ms. Due to the absence of experimental measurements, we tuned the strength of the reciprocal inhibition by comparing the energy of the simulated and experimental EMG signals. We computed a fitness score to measure the amount of alternation in bursting activity of antagonist motor pools during gait (**Equation 2.1**).

$$Alternation = mean(1 - (\textbf{EMGenvelope}_{flex} \odot \textbf{EMGenvelope}_{ext}))$$

$$EnergyRatio = \frac{EnergyEMGenvelope_{flex}}{EnergyEMGenvelope_{ext}} \times \frac{EnergyExperimentalEMGenvelope_{ext}}{EnergyExperimentalEMGenvelope_{flex}}$$

$$FitnessScore = Alternation \times EnergyRatio \qquad \textbf{(Equation 2.1)}$$

Synaptic strengths were set to match recordings in healthy rats during stepping (**Equation 2.1** equal to 1). We performed a robustness test over the chosen value. A variation of 40% in IPSP conductance of Ia-interneurons induced a 37% change in fitness, compared to a total possible maximum change of 1,400% ranging from tonic activation to complete suppression of the motor pool activity. A variation of 56% in EPSP strength resulted in a 10% change in fitness score, showing that the chosen parameters are robust and preserve results over a wide range of values (**Figure 2.13D**).

Muscle spindles model

Instantaneous firing rates of group-Ia and group-II afferents fibers were computed using a spindle model (Prochazka & Gorassini, 1998a, 1998b). Fibers stretch and stretch velocity were linked to the envelope of EMG bursts to mimic the alpha-gamma linkage. The firing rates of the different fibers were computed using **Equation 2.2** and **Equation 2.3**.

$$
\begin{aligned}
IaFiringRate = {} & 50 + 2 \times stretch \\
& + 4.3 \times sign(stretchVelocity) \times |stretchVelocity|^{0.6} \quad \textbf{(Equation 2.2)} \\
& + 50 \times EMG_{env}
\end{aligned}
$$

$$IIFiringRate = 80 + 13.5 \times stretch + 20 \times EMG_{env} \qquad \textbf{(Equation 2.3)}$$

Biomechanical model

Estimation of the muscle fiber stretch during gait was derived from a realistic musculoskeletal model of the rat hindlimb implemented in OpenSim (Delp et al., 2007) and validated experimentally (Johnson et al., 2008, 2011). We fed OpenSim with crest, hip, knee, ankle, and metatarsophalangeal joint positions recorded in healthy rats (n = 10 steps) to calculate the corresponding muscle stretch profile of muscles of the ankle (**Figure 2.1B**).

Coupling with EES

The number of fibers recruited by EES was computed using a validated finite element model of EES (Capogrosso et al., 2013) with the same geometry and parameters. The coupling between

Realistic motoneuron model

Equations in figure:

$$I_{ex} = w_{ex}e^{(-t/\tau)}(V_m - V_{ex})$$
$$I_{in} = w_{in}(e^{(-t/\tau)} - e^{(-t/\sigma)})(V_m - V_{in})$$

Parameters of the axon model

Parameter	Value	
Electrical parameters		
Membrane capacitance	2	$\mu F/cm^2$
Axoplasmic resistivity	70	Ω cm
Nodes parameters		
Max fast Na$^+$ conductance	3	S/cm^2
Max slow K$^+$ conductance	0.08	S/cm^2
Leakage conductance	0.007	S/cm^2
Na$^+$ Nernst potential	60	mV
K$^+$ Nernst potential	-80	mV
Leakage reverse potential	-80	mV
Internode parameters		
Myelin conductance/lamella	0.1	$\mu F/cm^2$
Myelin capacitance/lamella	0.001	S/cm^2

Parameters from Capogrosso et al. 2013, McIntyre et al. 2002

Parameters of the motorneuron model

Parameter	Value	
Electrical parameters		
Membrane capacitance	2	$\mu F/cm^2$
Axoplasmic resistivity	200	Ω cm
Soma parameters		
Max fast Na$^+$ conductance	0.05	S/cm^2
Max rectifier K$^+$ conductance	0.3	S/cm^2
Max Ca^{2+}/K$^+$ conductance	0.3	S/cm^2
Max N-Ca^{2+} conductance	0.05	S/cm^2
Max L-Ca^{2+} conductance	0.0001	S/cm^2
Leakage conductance	0.002	S/cm^2
Na$^+$ Nernst potential	50	mV
K$^+$ Nernst potential	-80	mV
Leakage reverse potential	-70	mV
Dendrite parameters		
Passive conductance	7.7e^{-6}	S/cm^2
Initial segment parameters		
Max fast Na$^+$ conductance	0.5	S/cm^2
Max rectifier K$^+$ conductance	0.1	S/cm^2
Leakage conductance	0.01	S/cm^2

Parameters from Capogrosso et al. 2013, McIntyre et al. 2002 and Fleshman et al. 1998

Figure 2.12 | Realistic alpha motoneuron model. The morphology of the cells consists of a spherical soma that is connected to an electronic equivalent representation of the dendritic tree of a real mammalian S type alpha motoneuron. The soma, initial segment and efferent axon are implemented with dedicated active membrane dynamics (Capogrosso et al., 2013; McIntyre & Richardson, 2002). Inhibitory synapses were placed at the soma and modeled as alpha functions with a reversal potential Esyn of -75 mV, a rise time constant σ of 1.5 ms, and a decay time constant τ of 2 ms. Excitatory synapses were distributed along the dendritic tree with a Poisson distribution estimated from experimental measurements of the location of synaptic on mammalian S motoneurons. Excitatory synapses were represented by a simple exponential function with reversal potential Esyn of 0 mV and decay time constant τ of 0.5 ms. The tables report the properties of the motoneuron in the model.

EES and the natural firing rate of afferent fibers is nonlinear. If a depolarization event occurs when the nodes of Ranvier are producing an action potential or during its refractory period, EES may fail to elicit a depolarization, or it may occur at higher thresholds. We modeled afferents fibers as integrate and fire cells with a membrane time constant τ = 30 ms. EES and natural firing rates were provided as suprathreshold synaptic inputs to each fiber. Firing rates were calculated from the sum of EES frequency and natural firing rate on the cell membrane (**Figure 2.1C**).

EMG model

Alpha motoneuron action potentials occurring at the last node of Ranvier were convolved with representative motor unit action potentials (MUAPs), modeled as damped sinusoidal waves with normally distributed amplitude (1 ± 0.2 a.u.) and duration (7.5 ± 2 ms) (**Figure 2.13C**). A latency of 2 ms between each event and the corresponding MUAP was implemented to account for the traveling time of an action potential from the spinal cord to the rat triceps surae (Gerasimenko et al., 2006).

2.4.2   Animals and Animal Care

All procedures and surgeries were approved by the Veterinarian Office Vaud, Switzerland. The experiments were conducted on 13 adult female Lewis rats (200 g body weight, Centre d'Elevage R. Janvier). Hindlimb kinematic and muscle activity during stepping were obtained in two healthy rats. Electrophysiology recordings were conducted in three rats. Behavioral experiments in eight rats with SCI. Rats were housed individually on a 12-hr light/dark cycle, with access to food and water ad libitum.

Surgical Procedures and Post-surgical Care

Surgical Procedures and Post-surgical Care Procedures have been described in detail previously (Courtine et al., 2009; van den Brand et al., 2012). All interventions were performed under general anesthesia and aseptic conditions. Briefly, EMG electrodes were created by removing a small part (~1 mm notch) of insulation from a pair of Teflon-coated stainless steel wires inserted into the gastrocnemius medialis and tibialis anterior muscles of both hindlimbs. Stimulation electrodes (same type as EMG) were secured at the midline of the spinal cord at spinal levels L2 and S1 by suturing over the dura mater above and below the electrode. A common ground wire was inserted subcutaneously over the right shoulder. In the same surgery, the rats received a complete thoracic (T7) SCI (n = 4) or a lateralized contusion (250–300 KDyn) using the Infinite Horizon Impactor (n = 4). The extent and location of the lesions was verified postmortem on 20 equally spaced 40-μm-thick transverse sections incubated in serum containing anti-GFAP (1:1,000, Z033429, Dako) antibodies. Contusion SCIs were reconstructed in 3D and the lesion extent expressed as a percentage of damaged tissue for each hemicord.

Locomotor Training and Recording

Rats were trained to step bipedally on a treadmill supported by a robotic body-weight support system (Robomedica). Training occurred every other day, for 20 min per session, for 4 weeks, starting 8 days post-SCI. 5HT1A/7 (8-OHDPAT, 0.05–0.1 mg/kg body weight) and 5HT-2A/C (quipazine, 0.2–0.3 mg per kg body weight) agonists were administered 10 min prior to training, and EES was delivered throughout the session at S1 and L2 (cathodes vs. common ground at intracostal muscles). EES amplitude was selected to maximize locomotor performance. Drug dosage for rats with contusion SCI was adjusted over a few successive days in order to obtain the most stable walking conditions. Optimal body-weight support was defined as the minimum support level that they could sustain while maintaining appropriate extension and swing excursions without dragging (55%–65% of body weight). To evaluate the effect of body-weight support, we gradually decreased the level of support by fixed decrements of 5%.

Hindlimb kinematics was recorded using 12 infrared motion capture cameras (200 Hz; Vicon). Reflective markers were attached to anatomical landmarks of both hindlimbs (**Figure 2.5B**). Nexus (Vicon) was used to obtain 3D coordinates of the markers. EMG signals (12.207 kHz) were amplified and filtered online (10–5,000-Hz bandpass, AM-System). Vertical ground reaction forces were measured using a biomechanical force plate (2 kHz; HE6X6, AMTI) located

below the treadmill belt. Video recordings (200 Hz) were obtained using two cameras (Basler Vision Technologies) oriented at 90° and 270° with respect to the direction of locomotion.

Processing of Kinematic, Ground Reaction Force, and Electromyographic Recordings

Data analysis and statistical procedures to process kinematic, ground reaction force and electromyographic have been described in detail previously (Courtine et al., 2009; Van den Brand et al., 2012; Wenger et al., 2014).

Real-Time Monitoring and Stimulation Platform

The real-time monitoring and stimulation infrastructure was implemented within a multi-threaded C++ code (Visual Studio 2010, Microsoft) running on a quad-core Microsoft Windows 7 computer. Stimulation patterns were applied via an RZ5 processing unit (Tucker Davis Technologies) connected to an MS16 stimulus isolator (TDT). Raw 3D positions of markers were imported into the C++ environment (200 Hz) using a Datastream SDK software (Vicon). We used custom algorithms for online filtering (least mean squares adaptive filtering), interpolation (triangulation) and re-labeling of each marker (Wenger et al., 2014). Left and right foot strikes were automatically detected using online kinematic classification of limb endpoint trajectories. These gait events triggered controller calculations and model updates.

Controller Structure

The controller expanded the structure previously described in (Wenger et al., 2014). The continuous flow of bilateral kinematic information was discretized at bilateral foot strikes, which acted as sampling times $K = [k_i^R, k_i^L, k_{i+1}^R...]$ and defined gait phases. Each separate hindlimb was then considered as a single-input single-output (SISO) system, independently of the other, and was controlled by separate controllers operating in parallel during one or the other gait phase. At each foot strike, the relevant controller evaluated the step height of the limb in swing (defined for the right phase as $h_i^R = max(h_t^R), t \in [k_{i-1}^L, k_i^R]$, and for the left phase as $h_i^L = max(h_t^L), t \in [k_{i-1}^R, k_i^L]$), and corrected EES frequency to track a predefined reference height (r_{i+1}^R and r_{i+1}^L for the right and left phases, respectively; **Supplementary Figure A.2** in the appendix). Corrections in EES frequency were obtained from a combination of feedback (PI control) and feedforward linear prediction (Wenger et al., 2014) but were only applied at the next iteration of the same phase.

2.4.3 Statistics

Experimental data and simulations were processed offline using MATLAB R2013b (Math-Works). All data are reported as mean values ± SD or SEM, as indicated. Normality of data was tested using a Kolmogorov-Smirnov test with 95% confidence interval (CI). A one-tailed t test with 95% CI was applied for comparison between conditions. Multi-group comparison was performed using a one-tailed ANOVA with 95% CI and Tukey-Kramer correction of the p value.
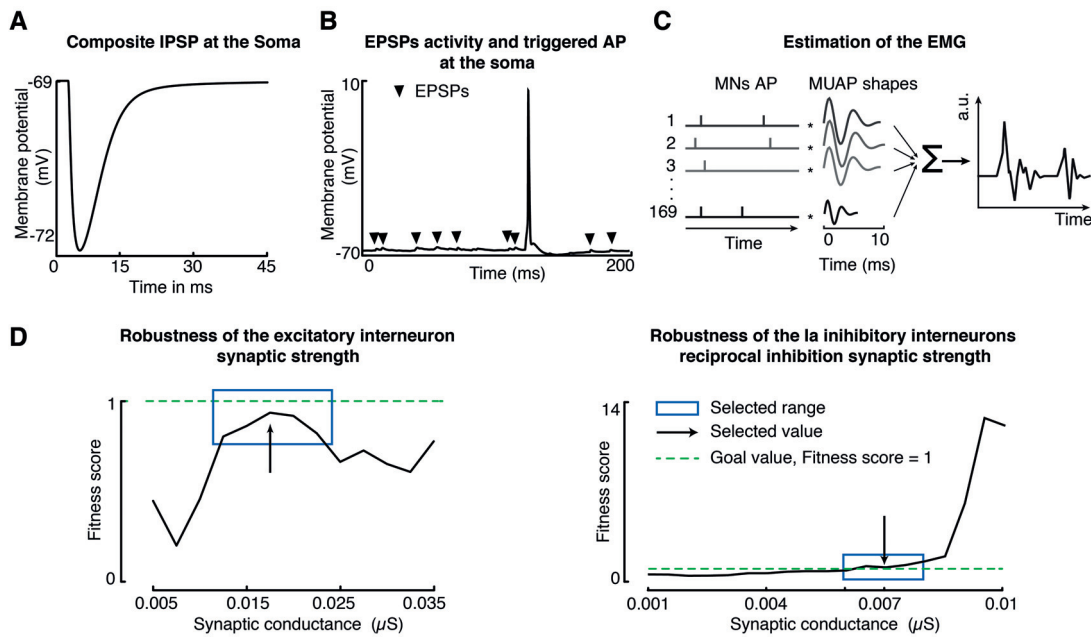
Figure 2.13 | Technical Implementation and robustness of the computational model. A, Resulting compound inhibitory post-synaptic potential (IPSP) on the membrane of motoneurons. **B**, Compound and single excitatory post-synaptic potentials (EPSP) on the membrane of motoneurons, including an example of action potential triggered by a supra-threshold event. **C**, EMG activity of modeled muscles was calculated from the combination of motoneuron action potentials (AP). Wavelets of motor unit action potential (MUAP) were convolved with random amplitude and latency distribution. **D**, Robustness of the strength of excitatory synapses from modeled interneurons. The range of synaptic conductance was selected based on a fitness index that ensured a variation lower than 10% between simulated and experimental EMG recordings. **E**, Robustness of the strength of Inhibitory synapses in the modeled reciprocal inhibition. The range of synaptic conductance was selected based on a fitness index that ensured a variation lower than 40% between simulated and experimental EMG recordings compared to a maximum variation of 1400%.

2.5 Discussion

EES of lumbar segments is undergoing a rapid transition from animal models to clinical applications. This transition requires a conceptual framework that guides the implementation and optimization of this intervention. Here, we derived stimulation protocols addressing subject-specific gait impairments from the identification of computational mechanisms underlying motor pattern formation during EES. This approach opens new perspectives for hypothesis-driven optimization of EES protocols. We discuss these findings with an emphasis on the computational mechanisms of EES, how this understanding can steer the design of ecological stimulation protocols, and their relevance for clinical applications.

2.5.1 Mechanisms underlying motor pattern formation during EES

Simulations (Rattay et al., 2000; Capogrosso et al., 2013) and experimental studies (Gerasimenko et al., 2006; Hofstoetter, Danner, et al., 2015) have provided evidence that EES primarily engages large-diameter afferent fibers. The prevailing view is that the recruitment of these afferents activates central-pattern generating networks (C. A. Angeli et al., 2014; Danner et al., 2015) and raises the excitability of spinal circuits to a level that enables sensory information

to become a source of motor control (Edgerton et al., 2008). Despite the wide acceptance of this interpretation, the principles from which the recruitment of afferents fibers translates into organized patterns of muscle activity has remained enigmatic. Here, we show that EES modulates muscle spindle feedback circuits and interacts with natural sensory information to elaborate and tune motor patterns for standing and walking at different speeds. Simulations integrating muscle spindle feedback circuits and reciprocal inhibitory networks were sufficient to reproduce a broad range of task-specific motor patterns that resembled those recorded experimentally in rats with SCI.

Dynamic simulations allowed us to probe the interactions between EES and each component of the modeled spinal circuits. We found that EES uniformly enhances the activity along muscle spindle feedback pathways throughout the duration of the gait cycle. Nevertheless, this global increase in afferent firing rates does not alter the natural information encoded in the temporal profile of muscle spindle firing. The interactions between EES and natural muscle spindle activity engage two synergistic mechanisms. First, the recruitment of muscle spindle feedback circuits provides a mono- and di-synaptic excitatory drive to motoneurons. Second, the strengthening of reciprocal inhibition between antagonist motor pools promotes the alternative recruitment of extensor and flexor muscles (Jankowska, 1992; Talpalar et al., 2011). In turn, the natural sensory input related to hindlimb movement modulates the balance between these two mechanisms, which gates the flow of information toward functionally relevant pathways (Tripodi, Stepien, & Arber, 2011). Thus, sensory information acts as the source of control that steers the production of versatile motor patterns without supraspinal input (Courtine et al., 2009; Edgerton et al., 2008). For example, changes in sensory information tuned extensor burst duration for different treadmill speeds while preserving flexor burst duration, as reported experimentally (Rossignol et al., 2006). Likewise, stopping the treadmill prolonged the activity of extensor muscles while inhibiting flexor muscles, which promoted an immediate transition from walking to standing (Quevedo, Fedirchuk, Gosgnach, & McCrea, 2000). Our computational model based on muscle spindle feedback circuits was sufficient to explain the production of these complex motor behaviors. While other mechanisms including central pattern generator networks may also contribute to the observed locomotor activities (Rybak et al., 2006), the present results reinforce current views on the predominant role of sensory information for the production of complex and adaptive motor behaviors in the absence of supraspinal drive in mammals (Ekeberg & Pearson, 2005; Song & Geyer, 2015).

2.5.2 Hypothesis-driven stimulation protocols manipulating circuit dynamics to improve gait

Computational models provide access to the detailed and global properties of circuit dynamics, supporting the formulation of novel hypothesis-driven neuromodulation therapies (McIntyre & Foutz, 2013). Our simulations led to the hypothesis that phase-specific adjustment of EES frequency would independently modulate the bilateral activity of active muscles during locomotion. We found that the filtering properties of spinal circuits ensure that frequency-mediated modulation of muscle activity is selectively directed toward functionally active muscles. Therefore, phase-specific EES frequency provides the opportunity to tune bilateral

motor patterns without disrupting the natural alternation between antagonist motor pool recruitment. The experimental implementation of this neuromodulation strategy corrected gait deficits and improved balance in rats with complete and incomplete SCIs. This bilateral modulation emerged from the natural gating of muscle spindle feedback circuits, which augmented extensor muscle activity on one hindlimb while concurrently enhancing flexor muscle activity on the other hindlimb. Phase-specific modulation of EES frequency thus harnesses the fundamental properties of spinal circuit dynamics to modulate bilateral leg movements. On the contrary, increases in EES amplitude additionally recruited efferent fibers directly, thus bypassing the filtering properties of spinal circuits and disrupting phase-dependent modulation of antagonist motoneurons. Phase-specific manipulation of EES parameters thus enables ecological interactions with the natural operations of spinal circuits (Courtine & Bloch, 2015).

This hypothesis-driven stimulation protocol steered the design of a minimal but effective closed-loop control policy that only necessitates a single input to trigger precise adjustments of bilateral movements. The controller monitored a single feature for each hindlimb, which was sufficient to capture changes in bilateral kinematics. This neuromodulation strategy required no manual tuning yet mediated robust adjustments of hindlimb movements and balance through personalized therapies targeting subject-specific motor deficits.

2.5.3 Conservation of Spindle Feedback Circuits across Mammals Supports Clinical Translation

Repetitive activation of motor circuits during rehabilitative training promotes activity-dependent plasticity of spinal circuits that improves functional recovery after SCI (Borton, Micera, Millán, & Courtine, 2013). Experiments in animal models and human patients showed that task-specific features such as weight-bearing levels, walking speed, gait symmetry, and balance play a key role in determining the kind and extent of motor improvements (Barbeau et al., 1999; Edgerton et al., 2008). Commonly, physical therapists seek to optimize these components through manual assistance (Dietz, Wirz, Curt, & Colombo, 1998). Our control strategy effectively targeted all these gait features. Closed-loop neuromodulation therapies automatically improved gait execution in rats with both complete and incomplete SCI, regardless of the amount of residual supraspinal control and/or levels of serotoninergic replacement therapy. These synergistic interactions were possible because our model-derived control strategies manipulate muscle spindle feedback circuits, which are the building blocks engaged by both sensory information and supraspinal commands to elaborate motor patterns (Arber, 2012; Levine et al., 2014). Electrophysiological evidence indicates that these ancestral components of the vertebrate motor infrastructure (Sherrington, 1910; Clarac, Cattaert, & Le Ray, 2000), which are remarkably conserved across mammals (Pierrot-Deseilligny, 1989), are also recruited by EES in humans (Sayenko, Angeli, Harkema, Edgerton, & Gerasimenko, 2014; Hofstoetter, Danner, et al., 2015). These results suggest that the manipulation of muscle spindle feedback circuits with EES has the potential to alleviate leg motor deficits in human patients with SCI.

2.5.4 Limitations and Future Perspectives

The electrophysiological signature of motor responses elicited in leg muscles after each pulse of EES suggested that this stimulation primarily engages large-diameter myelinated fibers, in particular muscle spindle feedback circuits (Capogrosso et al., 2013; Gerasimenko et al., 2006; Wenger et al., 2014). Therefore, we restricted our model to these pathways. However, gravity strongly influences the control and modulation of locomotion, especially in humans (Pearson, 1993; Cavagna, Willems, & Heglund, 2000; Lacquaniti, Ivanenko, & Zago, 2012). Golgi tendon organs and skin mechanoreceptors are the main sensory receptors providing gravity-related information to spinal circuits (Capaday, 2002). The inclusion of these pathways is thus a prerequisite to implement realistic forward biomechanics in our model. These pathways will also be critical to dissect the role of individual spinal circuits in the production of locomotion, including central pattern generating networks.

Here, we used our computational framework to develop a neuromodulation strategy that exploits temporal circuit properties to achieve functional specificity. Novel multi-electrode spinal implants (Minev et al., 2015) provide the opportunity to target subsets of muscle spindle feedback circuits, potentially supporting the development of spatially selective stimulation protocols. Thus, our computational model defines a framework to integrate spatial selectivity and temporal structure in neuromodulation therapies that would take full advantage of the distributed building blocks underlying motor pattern formation.

Despite scientific and technological challenges, we believe that the marriage between computational modeling and tailored neurotechnologies will foster the optimization of stimulation protocols that mediate therapeutic effects in individuals with SCI.

3 Controlling proprioceptive signals to enhance locomotor performance

In the previous chapter, we provided evidence that muscle spindle feedback circuits steer the excitation delivered by epidural electrical stimulation (EES), allowing the emergence of multiple locomotor behaviors. These results highlight the fundamental role of proprioceptive signals in both controlling locomotion after spinal cord injury (SCI), and in mediating the therapeutic effect of EES.

In this view, EES enhances the ability of proprioceptive signals to act as a source of control. Consequently, assistive technologies that control body kinematics, and thus dynamically act on the proprioceptive signals generated during gait, might provide a means of refining the locomotor output generated by EES.

Here, we combined computer simulations and behavioral experiments in rat models of SCI to investigate how adjusting trunk posture can influence the dynamics of spinal sensorimotor circuits during EES-enabled stepping, and thereby locomotor performance.

Related publication and personal contributions

The content of this chapter is adapted — with permission of the co-authors and journal — form the following publication: Eduardo Martin Moraud, Joachim von Zitzewitz, Jenifer Miehlbradt, Sophie Wurth, **Emanuele Formento**, Jack DiGiovanna, Marco Capogrosso, Grégoire Courtine, and Silvestro Micera, *"Closed-loop control of trunk posture improves locomotion through the regulation of leg proprioceptive feedback after spinal cord injury"*, Scientific Reports (2018).

Personal contributions: computer simulations, data analysis, figures preparation, manuscript editing.

3.1 Abstract

After spinal cord injury (SCI), sensory feedback circuits critically contribute to leg motor execution. Compelled by the importance to engage these circuits during gait rehabilitation, assistive robotics and training protocols have primarily focused on guiding leg movements to reinforce sensory feedback. Despite the importance of trunk postural dynamics on gait and balance, trunk assistance has comparatively received little attention. Typically, trunk movements are either constrained within bodyweight support systems, or manually adjusted by therapists. Here, we show that real-time control of trunk posture re-established dynamic balance amongst bilateral proprioceptive feedback circuits, and thereby restored left-right symmetry, loading and stepping consistency in rats with severe SCI during treadmill locomotion, enabled by epidural electrical spinal cord stimulation. We developed a robotic system that adjusts medio-lateral trunk posture during locomotion. This system revealed robust relationships between trunk orientation and the modulation of bilateral leg kinematics and muscle activity. Computer simulations suggested that these modulations emerged from corrections in the balance between flexor- and extensor-related proprioceptive feedback. We leveraged this knowledge to engineer a control policy that regulates trunk orientation in realtime. This dynamical postural interface immediately improved stepping quality in all rats regardless of broad differences in deficits. These results emphasize the importance of trunk regulation to optimize performance during rehabilitation.

3.2 Introduction

Leg sensory feedback circuits play an important role in the generation and regulation of leg movements (Orlovskiĭ et al., 1999; Rossignol et al., 2006; Kiehn, 2016). In healthy conditions, descending supraspinal commands continuously tune the dynamics of these circuits to ensure that movement-related afferent inputs adequately adjust gait patterns (Prochazka, 1996; Rossignol et al., 2006). After spinal cord injury (SCI), the descending sources of modulation are severely disrupted. Consequently, sensory feedback signals become the primary source of control to produce and regulate leg movements after SCI (Courtine et al., 2009; Akay et al., 2014; Gerasimenko et al., 2016).

The objective of gait rehabilitation therapies is to steer the functional reorganization of spared sensory pathways and residual descending projections through task-specific physical training in order to improve recovery (Dietz et al., 1998; Edgerton et al., 2008; Harkema, Behrman, & Barbeau, 2011). Repeated activation of sensory feedback circuits during standing and walking promotes activity-dependent reorganization of neural connections that ameliorates locomotor performance (Courtine et al., 2009; Van den Brand et al., 2012; Rossignol & Frigon, 2011). In particular, various studies showed that proprioceptive feedback circuits play a pivotal role in guiding motor execution and circuit reorganization after SCI. For example, epidural electrical stimulation of the lumbar spinal cord specifically modulates proprioceptive feedback circuits associated with extension and flexion of the legs, which enabled refined control of leg motor patterns during gait (Wenger et al., 2016; Moraud et al., 2016; Capogrosso et al., 2016). Moreover, we found that mice lacking muscle spindle feedback circuits fail to

display the activity-dependent reorganization of neural pathways that support recovery after SCI (Takeoka et al., 2014). These findings stress the importance of targeting proprioceptive feedback circuits in the design of rehabilitative strategies.

The critical role of movement-related sensory information to steer recovery has motivated the design of training protocols, robotic interfaces and neuroprosthetic systems that predominantly focus on reinforcing reproducible leg movements during rehabilitation (Riener et al., 2006; Borton et al., 2014). In these scenarios, the trunk is typically constrained within body-weight support systems providing vertically restricted forces, or exoskeletons that constrain pelvis movements. However, natural locomotion involves precisely-timed trunk movements in multiple directions (Thorstensson et al., 1984), which directly determine leg biomechanics, and consequently leg sensory feedback during locomotion (Veneman et al., 2008; Nott et al., 2010; Deliagina et al., 2012). Indeed, therapists commonly seek to adjust pelvis movements manually during rehabilitation. When possible, they also provide cues to the trunk in order to reinforce the interplay between trunk posture and leg biomechanics. However, the lack of technologies to assist these movements limits the spectrum of possibilities offered to therapists during rehabilitation. The development of rehabilitation protocols and robotic systems that actively regulate trunk posture during training relies on a deeper understanding of the interactions between trunk posture, proprioceptive feedback circuit modulations and leg motor pattern production during locomotion.

Here, we aimed to address these combined aspects in a well-controlled SCI rodent model of bipedal locomotion. First, we designed and fabricated a robotic postural interface that allows real-time control of mediolateral trunk orientation during locomotion in rats with severe spinal cord injury. This robotic system revealed robust relationships between mediolateral trunk orientation and the bilateral modulation of leg motor patterns during locomotion. We next used a neuro-biomechanical computational model of muscle spindle feedback circuits to study some of the mechanisms underlying these modulations. We found that mediolateral trunk orientation modulates the flow of information in muscle spindle feedback circuits. In turn, optimal locomotor performance emerged when mediolateral trunk orientation helped preserve the balance between muscle spindle feedback circuits associated with extensor and flexor muscles for both limbs. This knowledge guided the design of a control algorithm that regulated mediolateral trunk orientation in real-time based on subject-specific deficits. Compared to static trunk orientation, this targeted strategy improved locomotor performance across a broad spectrum of gait asymmetries and motor deficits. These results provide an important proof of concept that stresses the need to develop similar dynamic trunk assistance during gait rehabilitation in humans.

3.3 Results

3.3.1 A closed-loop robotic interface for controlling trunk posture

We developed a closed-loop robotic postural interface that supports the control of trunk orientation in the mediolateral direction during bipedal locomotion in rats (**Figure 3.1**). To enable the actuation of trunk orientation with minimal inertial effects, we developed a system
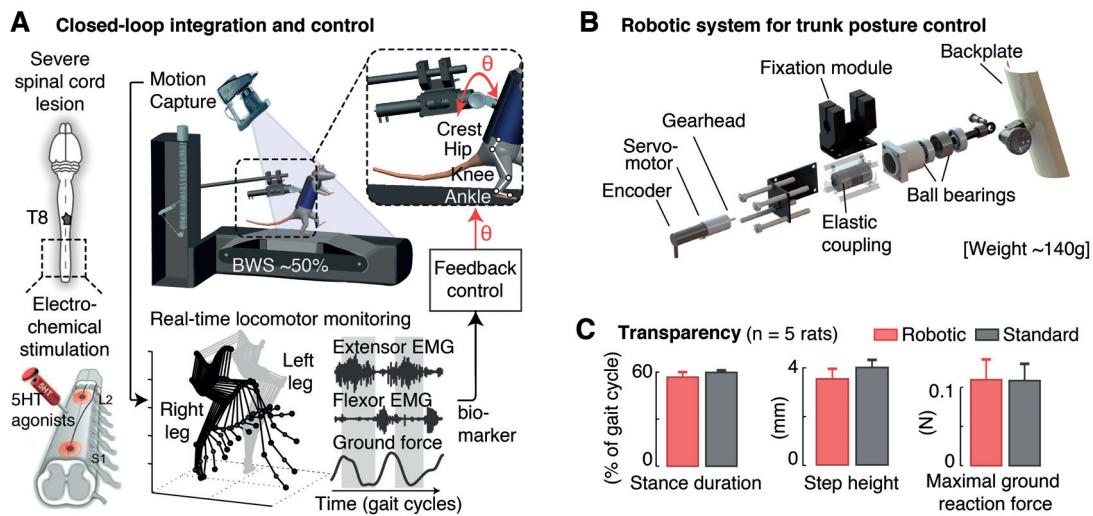
Figure 3.1 | Closed-loop robotic interface for online posture control. A, Integration of the robotic interface within a real-time monitoring platform for closed-loop postural control in paralyzed rats. Animals received a severe contusion of the spinal cord, and were trained to stand and step on a treadmill with body-weight support under electrical and pharmacological spinal cord neuromodulation. Bilateral kinematics, extensor (Medial Gastrocnemius) and flexor (Tibialis Anterior) electromyographic signals and ground reaction forces are recorded synchronously and available online (200 Hz) during continuous stepping. **B**, Attachment system and embedded components to provide mediolateral actuation with minimal inertial effects. **C**, Bar plots comparing various locomotor features using the robotic vs. standard non-actuated attachment systems. Data are mean ± SEM.

whose weight remained within the range of existing non-actuated attachment systems (<150 g). We designed a minimal lightweight frame structure and selected miniaturized components to provide sufficient torque in the coronal plane (47.8 mNm) (**Figure 3.1**), and we integrated this postural interface within a commercially available bodyweight support system (Robomedica Inc, USA). The attachment of the rats to the backplate and the control of the vertical support remained unchanged. We then incorporated the robotic postural interface onto a real-time platform that allows online control of trunk orientation based on bilateral leg kinematics, muscle activity and ground reaction forces (**Figure 3.1**).

To validate the transparency of the system during locomotion, we recorded gait patterns in rats when attached to the robotic postural interface and compared them to standard non-actuated conditions. Rats (n = 5) received a severe lesion of the spinal cord contusion that led to leg paralysis. To enable locomotion, we delivered an electrochemical neuromodulation therapy to the lumbar spinal cord according to methods described previously (**Figure 3.1B**). Detailed analyses of gait kinematics and kinetics did not reveal significant differences between both support conditions (p > 0.05 across conditions for each rat, Ranksum test, **Figure 3.1C**).

3.3.2 Adjustment of trunk posture corrects locomotor asymmetries after SCI

We then used this robotic postural interface to characterize the impact of trunk orientation on gait patterns. We mapped the relationships between trunk orientations (angles from -20 to +20 degrees, steps of +/-5 degrees) and the resulting changes in bilateral leg kinematics, muscle activity and ground reaction forces. Prior to stepping, we calibrated the attachment of each rat

to the backplate ensuring that both feet touched the treadmill belt symmetrically. This posture was defined as the baseline trunk orientation. During stepping, rats exhibited variable gait asymmetries that emerged from well-known differences in the performance of the left and right legs after severe spinal cord injury. For example, **Figure 3.2** shows the gait pattern from a rat whose right leg was weaker than the left. Due to this inter-limb asymmetry, the weak leg failed to provide enough support during stance and remained continuously over-flexed, while the stronger leg exhibited an over-extended configuration (**Figure 3.2A**). Changes in trunk posture induced gradual modulations in gait patterns, inversely proportional for the right and left legs, which compensated for these deficits. Concretely, rotations towards the stronger leg reinforced the loading on this leg during stance. Concomitantly, it reduced the load on the weak leg, which facilitated foot unloading and improved limb excursions during swing (**Figure 3.2A,B**). In doing so, trunk orientation naturally corrected the abduction angles for both legs. To capture this modulation, we extracted the angle of the whole limb (line connecting the hip to the foot) with respect to the direction of gravity in the mediolateral direction (**Figure 3.2A**). We found robust, monotonic relationships between trunk orientation and this angle for both limbs (**Figure 3.2B**). Together, these adjustments enhanced stepping consistency and gait symmetry (**Figure 3.2B**). In contrast, trunk rotations in the opposite direction exacerbated differences between the right and left legs, which increased gait deficits.

Comparisons across rats (n = 5) with different lesion severities confirmed these results (**Supplementary Figure A.3** in the appendix). Regardless of idiosyncratic gait deficits and varying levels of residual supra-spinal control, adjustments of trunk orientation promoted gradual, monotonic changes in whole-limb abduction angles for both legs. These adjustments decreased or increased differences in the limb length and step-height of the left and right legs. For each rat, the more symmetrical gait pattern emerged at a specific degree of trunk orientation in the mediolateral direction (black squares, **Supplementary Figure A.3** in the appendix).

3.3.3 Trunk posture modulates muscle spindle afferent dynamics during gait

We next sought to study the neural mechanisms that were likely to underlie the corrections induced by trunk posture on gait patterns. Due to the extensive loss of supra-spinal control, sensory afferent feedback signals were the primary source of control and modulation of leg movements. In particular, muscle spindle afferent feedback circuits are known to play a critical role in the production of locomotion after SCI. These afferents directly encode the changes in limb abduction during trunk rotations. We thus investigated the impact of mediolateral trunk orientation on muscle spindle afferents firing during gait.

For this purpose, we employed a dynamic computational model of muscle spindle feedback circuits (Moraud et al., 2016) to estimate the changes in afferent firing rates for multiple leg muscles. For each trunk orientation, we fed the recorded joint angle trajectories into a realistic 3D biomechanical model of the hindlimb (Johnson et al., 2008) and we estimated through inverse kinematic the corresponding muscle stretch and stretch velocity profiles for three pairs of antagonistic muscles acting at each joint of the leg (ankle, knee and hip joints)
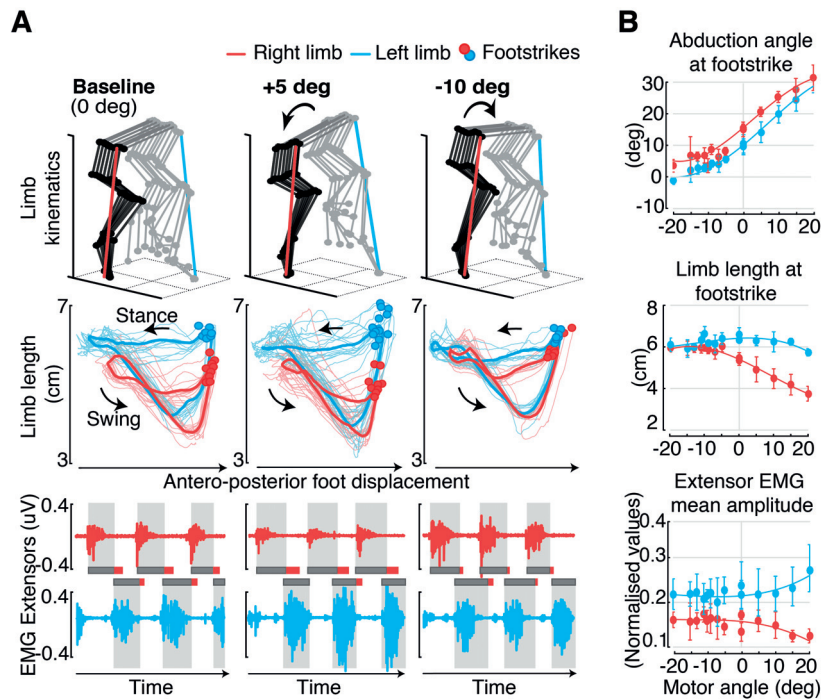
Figure 3.2 | Characterization of postural-effects on locomotor patterns. A, Representative stick diagram decomposition of hindlimb movements, bilateral limb length profiles and extensor EMG traces for one rat under different postural rotations. 'Baseline' corresponds to the posture manually defined by therapists during calibration prior to stepping. The animal exhibited weakness on his right limb and asymmetric stepping as a result of the contusion lesion. **B**, Comprehensive mapping of changes in locomotor features for trunk rotations ranging from -20 to 20 degrees for the same animal (n > 10 consecutive gait cycles for each condition). Data are means ± SD.

(**Figure 3.3**). We then used this information to derive the time profiles of group Ia and group II afferent firing rates during gait using a muscle spindle model (Prochazka & Gorassini, 1998b; Prochazka, 1999).

Computer simulations revealed that the trunk orientation profoundly altered the stretch profiles of all the simulated leg muscles, in particular those acting at proximal joints (**Figure 3.3B**). At the baseline trunk orientation, inter-limb asymmetries during stepping resulted in marked differences between the stretch profiles of the right and left leg muscles. For example, the profile of ankle flexor and knee extensor muscles diverged strongly at foot-strike and during early stance (i.e. for the weak leg, the Tibialis Anterior was under-stretched, while the Vastus Lateralis was over-stretched; the inverse occurred on the strong leg). These differences between left and right stretch profiles led to an excess of extensor-related muscle spindle feedback for the weak leg during stance, and an excess of flexor-related muscle spindle feedback for the strong leg (p < 0.05 between right and left, two-tail T-test, (**Figure 3.3C**) Graded adjustments in trunk orientation normalized the stretch profiles in all muscles, which reestablished the natural balance between flexor- vs. extensor-related muscle spindle feedback required to sustain appropriate stepping patterns (**Figure 3.3B,C**).

A **Simulation of posture-related afferent input**

B **Predicted muscle length**

— Right limb — Left limb
● Footstrikes -- Length at rest

C **Cumulative afferent input at footstrike**
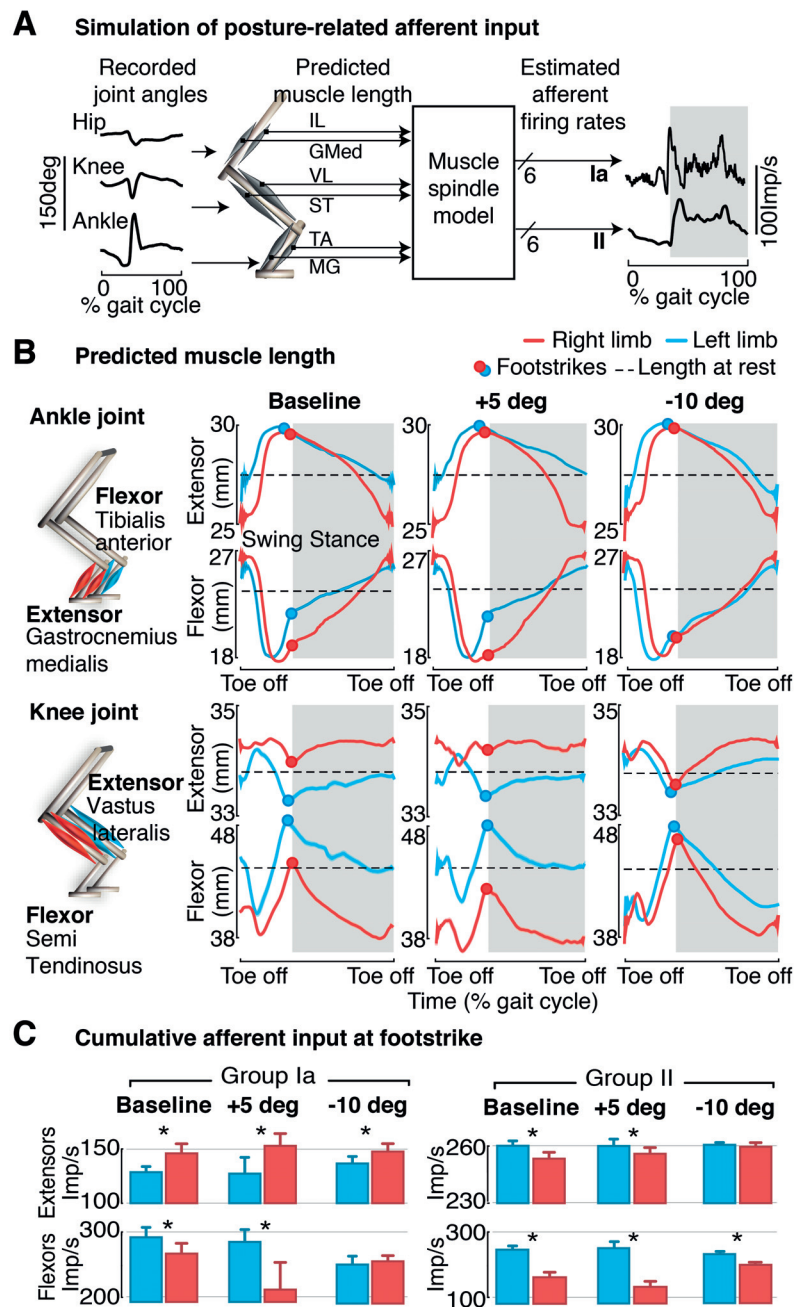
Figure 3.3 | Impact of trunk posture on afferent feedback ring rates. A, Computer simulations of muscle spindle feedback circuit dynamics. Joint angles recorded experimentally are fed into a musculoskeletal model of the rat hindlimb to predict the muscle stretch and stretch velocity profiles for 3 pairs of antagonist muscles (one per joint, for the hip, knee and ankle). Estimated firing rates for group Ia and group II afferent fibers are derived using a muscle spindle model. **B**, Comparison of estimated right and left stretch profiles throughout the gait-cycle for 3 postural rotations (same as shown in **Figure 3.2**). The red and cyan dots indicate the time of foot-strike events for each limb. **C**, Bar plots reporting the cumulative flexor- and extensor-related afferent firing rates at foot-strike for each trunk posture. Data are means ± SD. *$p < 0.05$ two-tailed T-test ($n = 11$ gait cycles).

3.3.4 Closed loop control of trunk posture

The impact of trunk orientation on muscle spindle feedback circuits stressed the importance to optimally define trunk orientation, accounting for deficits that arise throughout movement execution. Commonly, optimal trunk orientations are set empirically by therapists at the beginning of each session, and then remain constant throughout training. We sought to regulate trunk posture automatically based on continuous monitoring of locomotor performance.

We showed that trunk orientation monotonically modulates the abduction angles of the right and left legs, which in turn correlate with locomotor symmetry (**Supplementary Figure A.3** in the appendix). We thus employed the average of these angles as a biomarker to capture the impact of trunk posture on bilateral stepping performance. We then embedded a feedback control loop within the real-time monitoring platform. A proportional-integer (PI) controller extracted the mean abduction angles of the left and right legs at every gait cycle, and computed the appropriate adjustments in trunk orientation to track a desired reference abduction value (**Figure 3.4A**). To evaluate the performance of this control structure, we quantified its degree of controllability and stability (**Figure 3.4B**). We set the desired reference abduction value to 0 degrees (symmetry) and we evaluated the corrections provided as the controller converged towards the desired value. Regardless of rat-specific deficits or initial trunk orientations, the controller consistently minimized the amount of bilateral abduction and compensated for stepping asymmetries within a few gait cycles ($p < 0.05$ controlled vs. non controlled conditions for each rat, Ranksum test).

We then verified that the corrections of the controller converged towards optimal values for gait rehabilitation. We asked experienced trainers to fine-tune trunk posture for each rat during a training session in order to optimize locomotor performance, and compared the resulting trunk orientation with the rotation computed by the controller (**Figure 3.4C**). Despite its minimal structure, the closed-loop system provided adjustments that closely matched those of therapists, both in amplitude and speed to converge towards an optimal value ($p > 0.05$ controlled vs. manual for each rat, Ranksum test).

3.4 Materials and methods

For details regarding experimental procedures and the robotic interface used to control trunk posture see Moraud et al., 2018.

3.4.1 Neurobiomechanical computational model

Estimation of muscle stretch profiles during gait were derived from a realistic musculoskeletal model of the rat hindlimb implemented in OpenSim (Delp et al., 2007) and validated experimentally (Johnson et al., 2008, 2011). We fed the computer model with crest, hip, knee, ankle, and metatarsophalangeal joint angle traces recorded experimentally in rats under different postural conditions (n > 10 steps) and we calculated the corresponding muscle stretch and stretch velocity profiles through inverse kinematics for 3 pairs of antagonist muscles, i.e., Tibialis Anterior (TA) and Medial Gastrocnemius (GM) for the ankle joint, Vastus Lateralis (VL) and Semi Tendinosus (ST) for the knee joint, and Gluteus Medius (GMed) and Ilipsoas
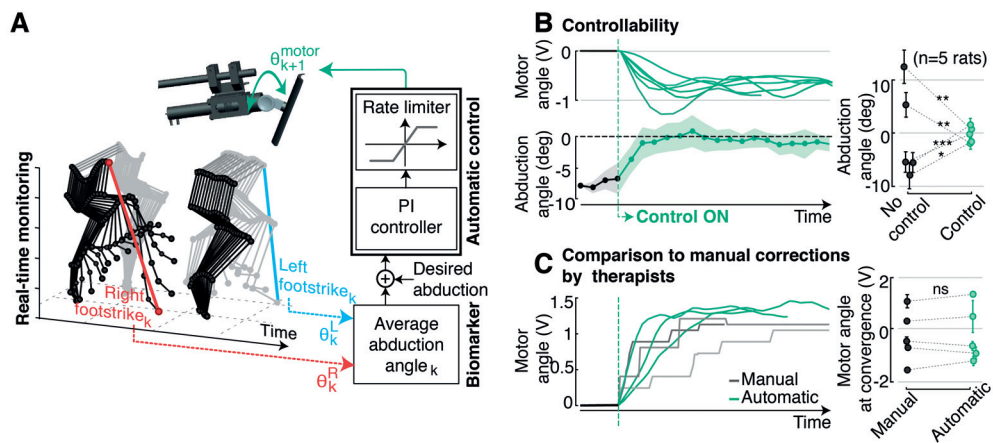
Figure 3.4 | Real-time control of trunk posture during locomotion. A, The closed-loop system continuously monitors bilateral limb kinematics and extracts, for each gait cycle k, the mean limb abduction angle at foot-strike (θ_k^R for the right limb, and θ_k^L for the left). This biomarker is fed into a PI controller that computes appropriate corrections in trunk rotation θ_{k+1}^{motor} to reduce the error with respect to a desired reference value. **B**, Performance of the control structure to correct animal-specific deficits. Representative traces of motor rotations and resulting corrections in mean limb abduction for one rat. The desired reference value is set to 0. Bar plots report the comparison of mean abduction angles with and without controlled postural adjustments for all animals (n = 5 rats). **C**, Example traces comparing automatic and manual trunk corrections provided by experienced therapists for one animal. No significant differences were observed for any rat. Data are means ± SD. *P < 0.05, **P < 0.01, ***P < 0.001, ns > 0.05 ranksum test (n > 10 gait cycles).

(IL) for the Hip joint (**Figure 3.3A**). Muscles lengths at rest were estimated by feeding the biomechanical model with experimental data from a calibration file in which animals were in the static, resting position prior to stepping.

The estimated firing rate profiles of group Ia and group II afferents fibers were computed using a spindle model (Prochazka & Gorassini, 1998b, 1998a; Prochazka, 1999). Although this model was originally established from cat electrophysiological recordings, dynamical relationships between muscle stretch and firing rate modulations are expected to be well preserved across mammals. Posture-related effects onto right and left dynamics are in all cases comparable to each other, and thus valid to conclude improvements in symmetry and balance. Firing rates of the different fibers were computed using **Equation 2.2** and **Equation 2.3**, reported in **Chapter 2**.

To derive the cumulative flexor- and extensor-related afferent input at foot-strike for each postural condition (**Figure 3.3C**), we defined a window (10 ms) around each foot-strike and calculated the mean firing rate (>10 gait cycles in each case) for each individual muscle. We then computed the Normal distribution corresponding to the sum for all three extensor muscles, and similarly for the three flexor muscles.

3.5 Discussion

Decades of research in gait rehabilitation have illustrated the importance of providing appropriate sensory afferent feedback in order to promote neuroplasticity leading to functional recovery after neurological disorders. Albeit known to play a pivotal role in modulating leg biomechanics, and consequently sensory afferent feedback, the regulation of trunk posture is

rarely optimized in training protocols. Here, we provide evidence that trunk posture induced robust, predictable effects on bilateral leg locomotor patterns, which directly impacted the dynamics of proprioceptive afferent feedback circuits. We exploited these results to design closed-loop control strategies that regulated the posture of the trunk in real-time based on simple biomarkers. These control policies substantially improved locomotor performance in rats with severe SCI. We discuss these findings with an emphasis on the implications for clinical translation aiming at integrating assistive trunk postural control within gait rehabilitation protocols for humans.

Locomotion involves the synergistic activation of multiple leg and trunk muscles to produce and sustain well-balanced motor patterns. While the legs produce the primary propulsive forces, the trunk actively assists in the coordination of inter-limb movements and the maintenance of equilibrium (Beloozerova et al., 2003). After spinal cord injury, the loss of trunk control adds up to impairments of leg motor control and strongly hinders the capacity to generate stable, coordinated gait patterns (Barbeau, 2003). Similarly, constraining pelvis movement in healthy individuals affects gait temporal patterns (Veneman et al., 2008). The interplay between trunk posture and leg biomechanics (Nott et al., 2010; Zajac et al., 2003) underscores the importance of assisting trunk posture during gait training. Our results reinforce this view with quantified outcomes in clinically relevant settings.

During gait rehabilitation, therapists are often forced to focus primarily on leg movements. They seek to correct asymmetries, reinforce weak muscles and prevent compensatory strategies (Harkema, Behrman, & Barbeau, 2011). When possible, they additionally provide manual corrections to pelvis movements, or deliver cues to the trunk in order to facilitate coordinated movements. However, bodyweight support systems and exoskeletons often restrict trunk posture, which strongly limits therapists' interventions. Our results showed that the regulation of trunk posture naturally addressed many gait deficits without direct assistance of leg movements. We found that gradual adjustments of trunk orientation mediated consistent and predictable modulations of key gait features related to both extension and flexion components, proportionally for each leg, which naturally restored stepping symmetry, reinforced loading and improved stepping quality. Computer simulations suggested that these postural adjustments were sufficient to reestablish the symmetry in muscle stretch profiles for multiple muscles spanning both legs, and thus to restore the appropriate balance between extensor- and flexor-related proprioceptive afferent feedback signals that modulate spinal circuits during stepping (Pearson, 2008; Yang & Gorassini, 2006). Considering the pivotal role of these pathways to steer recovery after injury and their remarkable conservation across mammals (Clarac et al., 2000), we conclude that real-time control of trunk movements to enable well-balanced modulation of proprioceptive feedback may play a critical role for gait rehabilitation in human patients with SCI.

Differences throughout training sessions and across animals also stressed the need to compute and adjust optimal trunk orientations for each subject during movement. Asymmetries and dynamic aspects of gait deficits only emerged during locomotion, and could hardly be predicted from the calibration phase prior to stepping. This implies that therapists ought

to manually re-adapt the positioning of the subject throughout the training session based on visual inspection, which is suboptimal to mediate maximal therapeutical effects. Here, we showed that real-time control policies are capable of providing continuous assistance of trunk movements automatically with the same level of accuracy as expert therapists.

Electrophysiological and experimental observations demonstrated that proprioceptive afferent feedback circuits, in particular from muscle spindles, play a major role in the generation of locomotor behavior (Akay et al., 2014), and in guiding functional recovery after injury (Takeoka et al., 2014). These circuits are known to be recruited by epidural electrical stimulation to facilitate motor control (Capogrosso et al., 2013; Moraud et al., 2016). Our computer model thus focused on the effects of trunk posture on these circuits. However, trunk postural adjustments undoubtedly modulate afferent pathways conveying gravity-related information to spinal circuits. Particularly critical in humans, inputs for cutaneous and Golgi tendon organ receptors continuously help stabilizing the dynamics governing bipedal gait (Prochazka et al., 1978; Harkema et al., 1997; Capaday, 2002). The inclusion of sensory feedback circuits related to Golgi tendon organs and skin mechanoreceptors in our computer simulations is thus a prerequisite to obtain complete neurobiomechanical insights into the effects of trunk posture on the sensory feedback circuits contributing to the production of gait.

Our results provide a conceptual and technical framework to design clinically-relevant assistive devices that tailor trunk posture in real-time in order to introduce precision medicine in gait rehabilitation after neurological disorders.

4 | Species-specific effects of epidural spinal cord stimulation

In the previous chapters we provided evidence that in rats epidural electrical stimulation (EES) facilitates locomotion by increasing the overall firing rate of the recruited proprioceptive afferents, without disrupting the ongoing sensory activity. We showed that this increase in afferent firing reinforces the excitation delivered to motoneurons and to reciprocal inhibitory networks controlling locomotion. In turn, the natural firing of the proprioceptive afferents modulates the activity of these networks, promoting the alternating recruitment of flexor and extensor muscles and thus the formation of locomotor patterns.

In this chapter we sought to assess whether these observation translate to humans. Specifically, we hypothesized that because of the difference in size between humans and rats, the activity induced by EES in the recruited afferents may interfere with the ongoing sensory activity through antidromic collisions — a phenomenon that we did not consider in our previous study. We assessed this possibility by performing computer simulations and a series of experiments in both humans and rats.

Related publication and personal contributions

The content of this chapter is adapted — with permission of the co-authors — form the following manuscript: **E. Formento**, K. Minassian, F. Wagner, JB. Mignardot, C.G. Le Goff, A. Rowald, J. Bloch, S. Micera⋆, M. Capogrosso⋆ and G. Courtine⋆, *"Electrical spinal cord stimulation must preserve proprioception to enable locomotion in humans with spinal cord injury"*, Nature Neuroscience (2018).

Personal contributions: conceived the study, designed and developed the computation model, performed computer simulations, designed and performed the experiments in rats and humans, data analysis, figures preparation, manuscript writing.

4.1   Abstract

Epidural electrical stimulation (EES) of the spinal cord restored locomotion in animal models of spinal cord injury (SCI) but has yet to reach similar efficacy in humans. Here, we hypothesized that this inter-species discrepancy is due to interferences between EES and proprioceptive information in humans. Computational simulations combined with preclinical and clinical experiments revealed that EES blocks a significant amount of proprioceptive information in humans, but not in rats. This transient deafferentation prevents the modulation of reciprocal inhibitory networks critically involved in locomotion and abolishes the conscious perception of leg position. Consequently, continuous EES can only facilitate locomotion within a narrow range of stimulation parameters and is therefore unable to provide meaningful locomotor improvements in humans without rehabilitation. Simulations showed that burst stimulation and spatiotemporal stimulation profiles mitigate the cancellation of proprioceptive information, enabling robust control over motoneuron activity. Our results demonstrate the importance of delivering stimulation protocols that preserve proprioceptive information to facilitate walking with EES.

4.2   Introduction

Spinal cord injury (SCI) has an immediate and devastating impact on the control of movement. These motor deficits result from the interruption of the communication between the brain and the spinal cord below the lesion, depriving the otherwise intact sensorimotor circuits from essential sources of modulation and excitation to produce movement (Kiehn, 2016). Due to the limited ability of the central nervous system for repair, the deficits are generally permanent. Currently, there is no medical treatment that significantly improves the recovery of motor control after SCI.

A variety of biological treatment paradigms aimed at inducing axonal regeneration, reducing inflammation and scar formation and reconstituting the cellular environment of the spinal cord have been tested with limited functional outcomes in animal models (O'Shea et al., 2017). Complementary strategies have capitalized on our understanding of motor physiology to improve functional recovery (Lovely et al., 1986; Barbeau & Rossignol, 1987; Wernig & Müller, 1992; Dimitrijevic et al., 1998; Herman et al., 2002; Mushahwar et al., 2007; Edgerton et al., 2008; Hofstoetter, Krenn, et al., 2015; Minassian et al., 2016). These engineering strategies tap into spared circuits and residual neural pathways to modulate and augment the ability of the central nervous system to produce movement.

Amongst all these biological and technological strategies, epidural electrical stimulation (EES) of the lumbar spinal cord showed the most striking preclinical outcomes. This treatment paradigm restored a broad range of adaptive motor behaviors in rodent, feline, and nonhuman primate models of leg paralysis (Van den Brand et al., 2012; Wenger et al., 2014; Musienko et al., 2012; Capogrosso et al., 2016).

EES has also been applied to the human spinal cord for several decades but has yet to promote the same degree of therapeutic efficacy as in animal models. EES induced rhythmic movements of the legs in people with complete paralysis (Dimitrijevic et al., 1998; Minassian et

al., 2004), and enables independent stepping when delivered over more than a year of intense rehabilitation (Herman et al., 2002; C. Angeli et al., 2018; Gill et al., 2018). Moreover, this stimulation enabled the volitional activation of paralyzed muscles to initiate isolated movements of the leg in five individuals with motor complete paralysis (Harkema, Gerasimenko, et al., 2011; C. A. Angeli et al., 2014; Grahn et al., 2017). These studies increased our understanding of spinal cord physiology, and drew attention to the potential of EES to improve motor control after SCI. However, in spite of the numerous successes reported in animal models, EES has failed to restore independent, weight-bearing locomotion in humans with severe SCI.

Currently, the mechanisms underlying species-specific responses to EES remain enigmatic. The identification of these mechanisms is not only essential for comparative spinal cord physiology, but also for guiding the development of evidence-based approaches that fulfill the potential of EES to improve recovery after SCI.

Computational models (Rattay et al., 2000; Ladenbauer et al., 2010; Capogrosso et al., 2013) and experimental studies (Gerasimenko et al., 2006; Minassian et al., 2007; Moraud et al., 2016; Hofstoetter et al., 2018) conducted in both animal models and humans have provided evidence suggesting that EES recruits afferent fibers conveying proprioceptive information. The recruitment of these afferent fibers leads to the activation of motoneurons through monosynaptic and polysynaptic proprioceptive circuits, and to an increase in the excitability of the lumbar spinal cord through the broad integration of these afferent inputs within the spinal motor system. This modulation enhances the responsiveness of spinal circuits to residual descending signals and sensory feedback. In turn, task-specific sensory information modulates the reciprocal inhibitory networks in the spinal cord that gate the excitatory drive produced by EES towards functionally relevant pathways. This mechanism enables the generation of well-organized and adaptive patterns of muscle activation in animal models of paralysis (Moraud et al., 2016).

This conceptual framework implies that task-specific sensory information plays a central role in the formation of motor patterns in response to EES after SCI. However, this viewpoint has not considered the possibility that the recruitment of proprioceptive fibers by EES may interfere with the natural flow of task-specific proprioceptive information traveling along the very same fibers.

Electrical stimulation triggers action potentials that travel in both directions along the recruited fiber. EES would thus elicit both orthodromic action potentials that are conveyed to the spinal cord, and antidromic action potentials that travel towards sensory organs (Su et al., 1992; Hunter & Ashby, 1994; Buonocore et al., 2008). Consequently, we hypothesized that antidromic action potentials may collide with action potentials conveying proprioceptive information, thus preventing the propagation of this information to the spinal cord, and even to the brain. The probability of these detrimental interactions is proportional to the stimulation frequency, the natural firing rate of sensory afferents, and the propagation time required by an action potential to travel along the entire length of the afferent fiber. These physiological parameters diverge dramatically between rats and humans. Indeed, the traveling time of action potentials along proprioceptive fibers is markedly longer in humans compared

to rats. Moreover, the firing rates of proprioceptive afferents is lower in humans (Prochazka, 1996). The resulting higher probability of collisions between natural and antidromic action potentials in humans may disrupt task-specific sensory information to unexpected levels. Here, we hypothesized that this phenomenon may explain the limited therapeutic efficacy of continuous EES in paraplegic individuals compared to rats.

Using computer simulations, electrophysiological evaluations, psychophysics tests and behavioral experiments, we show that antidromic collisions abolish the natural proprioceptive information in humans, but not in rats. These detrimental effects of EES restrict the range of stimulation frequencies and amplitudes that can facilitate locomotion in humans with SCI. Computer simulations identified strategies that mitigate this issue. For example, encoding the natural proprioceptive information in the spatiotemporal structure of EES stimulation protocols may maximize the range of useful EES parameters. These results demonstrate that EES must preserve proprioception to facilitate walking in humans with SCI.

4.3   Results

4.3.1   The probability of antidromic collisions during EES is higher in humans compared to rats

We first studied the occurrence probability of antidromic collisions along proprioceptive afferent fibers when delivering continuous EES to the lumbar spinal cord. For both rats and humans, we developed computational models of proprioceptive afferent fibers that take into account the length of axons innervating proximal and distal muscles, as well as the propagation times of action potentials along these axons. We modeled realistic interactions between the naturally occurring action potentials traveling along proprioceptive afferents and the action potentials elicited by EES (**Figure 4.1A**). We used these computational models to calculate the probability of antidromic collisions in muscle spindle afferents as a function of EES frequency and natural firing rate.

The model indicated that the occurrence probability of antidromic collisions was extremely low in rats, regardless of the tested EES frequencies and natural firing rates of muscle spindles (**Figure 4.1B**). While delivering EES at the frequency commonly used to enable locomotion in paralyzed rats (40 Hz Courtine et al., 2009; Van den Brand et al., 2012), this probability remained approximatively 20% across the entire range of physiological afferent firing rates.

The results of the simulations were dramatically different in humans. Due to the increase in action potential propagation times along human proprioceptive afferents, even relatively low frequencies of EES blocked most of the naturally occurring proprioceptive signals from reaching the spinal cord. For distal muscles, the occurrence probability of antidromic collisions reached nearly 100% for natural afferent firing rates of 30 impulses per second with an EES frequency of 30 Hz (**Figure 4.1C**). The disruption of natural proprioceptive information depends upon the distance of proprioceptive organs from the spinal cord. Accordingly, we found that the occurrence probability of antidromic collisions was markedly higher along afferents innervating proprioceptors located in distal muscles compared to proximal muscles

(**Figure 4.1C**).

These results suggest that continuous EES may disrupt the natural proprioceptive information in humans, but not in rats. To confirm this prediction, we conducted a series of electrophysiological and psychophysical experiments.
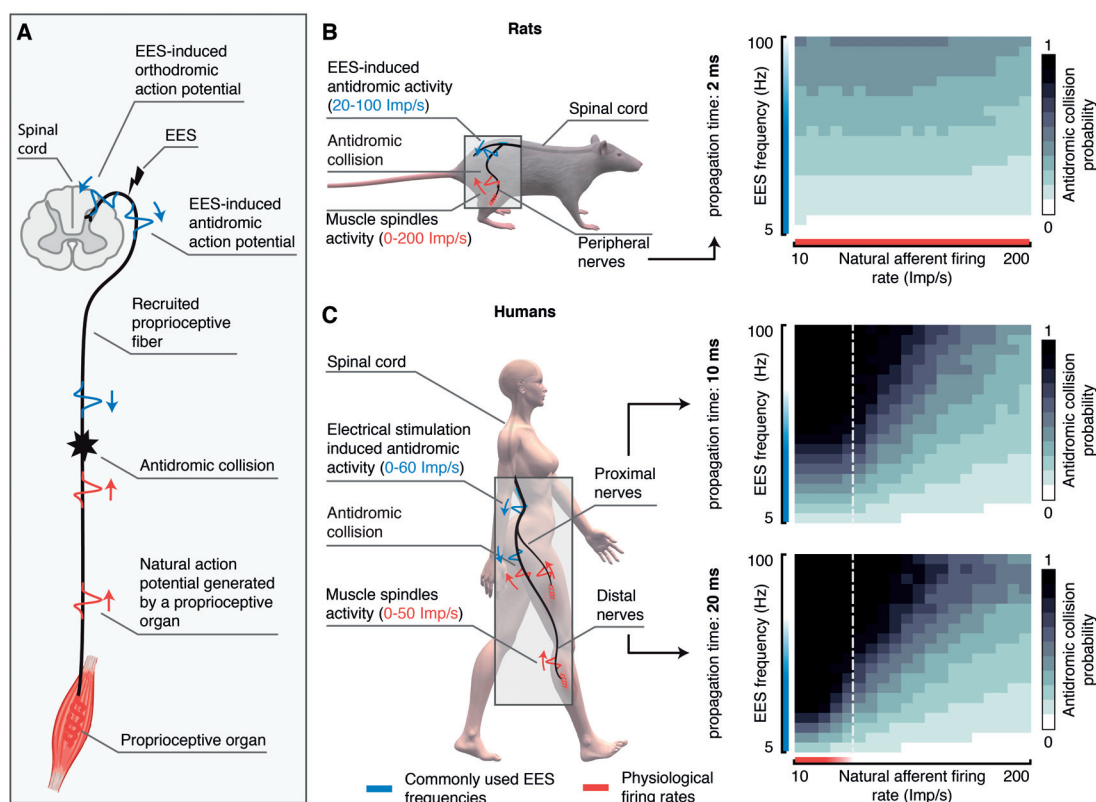
Figure 4.1 | Probability of antidromic collisions during EES in rats and humans. A, Schematic illustration of antidromic collisions between EES-induced antidromic action potentials and natural action potentials traveling along the recruited proprioceptive afferent fibers. **B**, **C**, Probability for a natural action potential to collide with EES-induced antidromic action potential in the proprioceptive afferent fibers of rats (**B**; action potential propagation time along the entire length of the fiber: 2 ms) and in the proximal and distal proprioceptive afferent fibers of humans (**C**; action potential propagation time along the entire length of the fiber: 10 and 20 ms, respectively). The probability is calculated as a function of EES frequency and natural firing rate along afferent fibers. EES frequencies that are commonly used to facilitate locomotion in rats (Van den Brand et al., 2012; Moraud et al., 2016; Courtine et al., 2009; Wenger et al., 2014) and humans (Minassian et al., 2004; Huang et al., 2006; Harkema, Gerasimenko, et al., 2011; C. A. Angeli et al., 2014) are highlighted in blue. Physiological proprioceptive firing rates reported in rats (Hník & Lessler, 1973; Prochazka, 1999) and humans (Prochazka, 1996; Albert et al., 2006) are highlighted in red. The vertical dashed white line highlights the estimated maximum firing rate of human proprioceptive afferents during gait. Imp, impulse.

4.3.2 Experimental evidence 1: EES induces antidromic activity along human afferents

We first verified whether EES produces antidromic activity along the recruited afferent fibers. We conducted concurrent recordings of the proximal and distal branches of the tibial nerve

(mixed nerve), the sural nerve (sensory nerve), and the soleus muscle during continuous EES of the lumbosacral spinal cord in two individuals with a chronic incomplete SCI (**Figure 4.2**; Subject #2 and #3 in **Table 4.1)**.

We selected a site of EES that elicited contractions of the soleus muscle and then reduced the stimulation amplitude in order to elicit a sensation of tingling in the corresponding dermatome without generating any visible muscle contractions. EES frequency was set at 20 Hz. In subject #2, each pulse of EES elicited a weak response in the soleus muscle with a latency of 25 ms. This response has been associated with the activation of group-Ia afferents and subsequent trans-synaptic recruitment of motoneurons (Capogrosso et al., 2013; Minassian et al., 2007; Hofstoetter et al., 2018). Concurrently, we detected two responses in the proximal branch of the tibial nerve, with latencies of 12.5 and 26.5 ms. Only one response (latency, 21 ms) was recorded in the distal branch of this nerve (**Figure 4.2**). The responses induced in the proximal (12.5 ms) and distal (21 ms) branches of the tibial nerve (**Figure 4.2**, blue windows) likely resulted from the same neural volley propagating from the site of stimulation to the periphery. Since the responses recorded in the distal branch occurred prior to any motor response, they cannot be attributed to orthodromic efferent activity. In this scenario, the response in the distal branch of the tibial nerve should have emerged after the motor response elicited in the more proximal soleus muscle. Therefore, we conclude that these responses likely corresponded to antidromic afferent volleys resulting from the recruitment of the dorsal roots. The response with a latency of 22 ms recorded in the exclusively sensory sural nerve is also compatible with this conclusion. Indeed, due to the lack of motor fibers, the antidromic recruitment of $A\beta$ afferents is the most probable explanation for this response. Finally, the second response recorded in the proximal branch of the tibial nerve (latency, 26.5 ms) is compatible with a far-field potential induced by the recruitment of the soleus muscle. More unequivocal results were obtained in subject #3. Each pulse of EES elicited a distinct response in both the proximal and distal branch of the tibial nerve (latencies, 12.5 and 22 ms respectively) and a response in the sural nerve (latency, 22.5ms). No motor responses were detected in the soleus muscle at this stimulation intensity.

These results support the hypothesis that EES elicits antidromic activity along both proprioceptive afferent fibers, opening the possibility that this stimulation interferes with the natural flow of sensory information in humans.

4.3.3   Experimental evidence 2: EES disrupts kinesthesia in humans

Cancellation of sensory information due to antidromic collision should result in a reduced or altered conscious perception of joint position and movement velocity. We thus predicted that continuous EES would affect the perception of passive leg movements. To test this hypothesis, we exposed three individuals with a chronic incomplete SCI **(Table 4.1)** to a threshold to detection of passive movement (TTDPM) test (Han et al., 2016). Due to impaired sensory functions, only subject #1 and subject #3 could complete the task without EES (**Figure 4.3A**).

Participants were sitting in a robotic system that imposed a passive isokinetic leg movement at the knee from a neutral resting position (**Figure 4.3B**). The participants were asked to
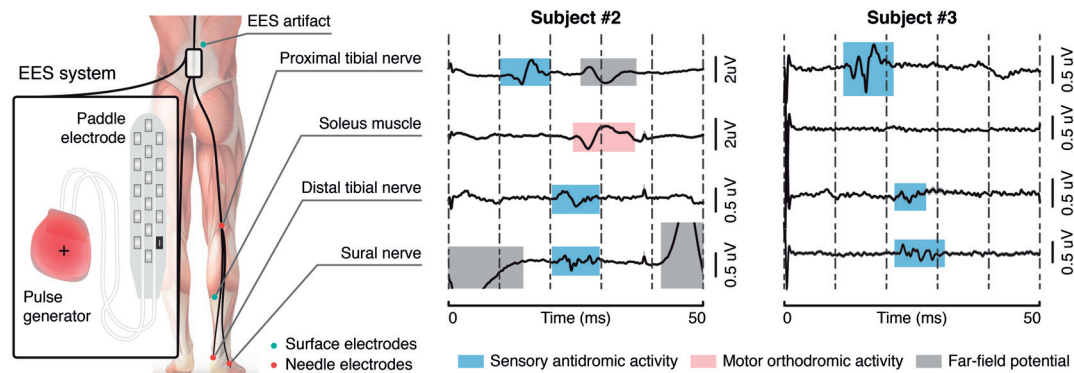
Figure 4.2 | EES induces antidromic activity along proprioceptive afferents. Recordings of antidromic activity from sensory nerves during EES. Needle electrodes were inserted subcutaneously close to peripheral nerves and surface electrodes over the soleus muscle, as depicted in the scheme. Continuous EES (20 Hz, monopolar stimulation, black cathode and red anode) was delivered for approximatively one minute. Averaged evoked potentials ($\pm$SEM, n $\geq$ 1200) are shown for subject #1 and subject #3. Evoked potentials highlighted in blue, red and grey were respectively classified as antidromic afferent volleys, efferent orthodromic activity, and far-field potentials (e.g. electromyographic activity of nearby muscles).

detect the direction of the movement as soon as they were able to perceive it, but before the knee joint angle had reached a predefined amplitude. Detection angle and trials error rate were used as measurements of performance.

Without EES, subject #1 was able to detect the extension and flexion of the knee with a 100% success rate (median detection angle: 7 deg, 95% CI: 3.9-11.9 deg). Subject #3 was able to detect the onset of knee movements but failed to detect their direction. Consequently, we increased the range and speed of the movement, and limited the movement to extension. Without stimulation, subject #3 successfully detected movement onset with a 100% success rate (median detection angle: 6.7 deg, 95% CI: 5.8-8.4 deg).

We then selected electrode configurations that targeted both extensor and flexor muscles of the knee, as verified from responses elicited in vastus lateralis and semitendinosus muscles. We first set the amplitude that elicited a tingling sensation in the knee without producing motor responses (x 0.8 muscle response threshold). At this intensity and over a broad range of frequencies, continuous EES did not alter the performance of subject #1, while it disrupted the ability of subject #3 to detect movement onset (error rate higher than 60%) (**Figure 4.3C**). At higher stimulation intensities (x 1.5 muscle response threshold), EES abolished the ability of both participants to detect the imposed passive movement (error rate higher than 80%). The participants reported a complete loss of awareness about the position and movement of their leg.

These psychophysical experiments corroborate our hypothesis that continuous EES disrupts and may even block the natural proprioceptive information in humans. This disruption occurred at amplitudes and frequencies that are commonly used in human studies (Minassian et al., 2004; Huang et al., 2006; Harkema, Gerasimenko, et al., 2011; C. A. Angeli et al., 2014).
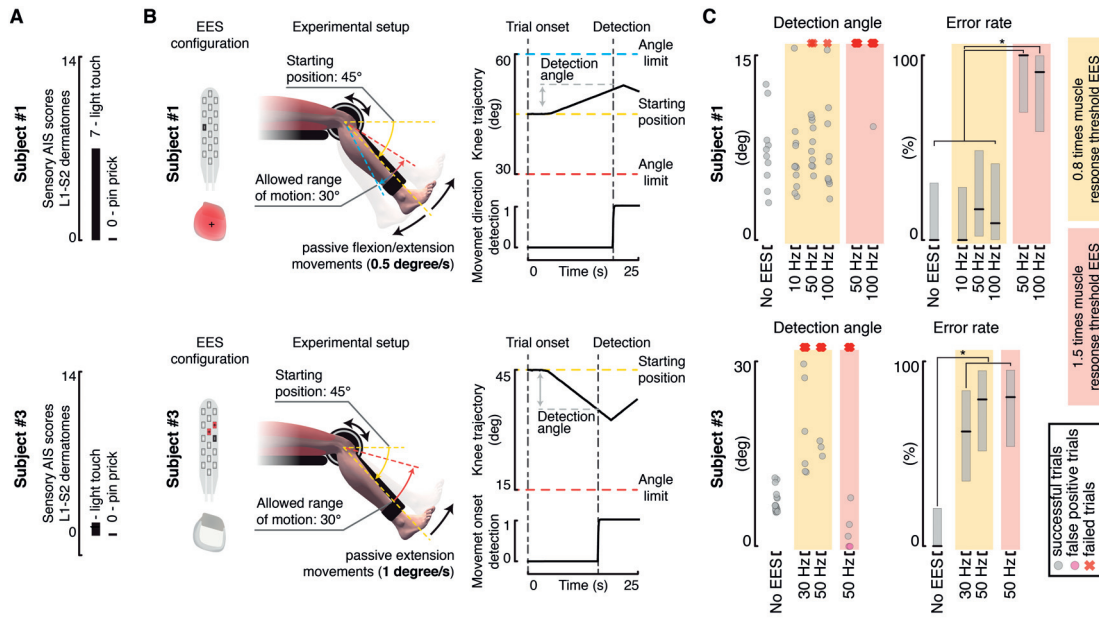
Figure 4.3 | Continuous EES disrupts proprioception in humans. A, Sensory subscores of the L1-S2 dermatomes for the two subjects that performed the threshold to detection of passive movement (TTDPM) test. **B**, Setup of the TTDPM test. Randomly selected flexion or extension movements were imposed to the knee joint of subject #1 (**top**). A movement speed of 0.5 degree per second and a maximum allowed range of motion of 15 degrees was used. Subject #3 (**bottom**) was not able to perceive movement direction. Hence, only the ability to detect extension movements was assessed. A movement speed of 1 degree per second and a maximum allowed range of motion of 30 degrees was used.EES configurations used to target knee flexor and extensor muscles were applied as indicated. **C**, Scatter plots reporting the detection angle and box plots reporting the error rate (percentage correct trials ± 95% CI) on the TTDPM test performance without EES and when delivering continuous EES at 0.8 and 1.5 times muscle response threshold amplitudes. Different EES frequencies were tested on subject #1 (10 Hz, 50 Hz, 100 Hz) and subject #3 (30 Hz, 50 Hz). At 1.5 motor response threshold amplitude, EES frequencies below 50 Hz induced spasms in the muscles and were thus not tested. Grey dots report the detection angle for successful trials, while pink dots and red crosses indicate false positive and failure to detect movement within the allowed range of motion, respectively. *, $P < 0.05$, Clopper-Pearson interval.

4.3.4 Experimental evidence 3: continuous EES alters afferent modulation of spinal circuits in humans but not in rats

Muscle spindles are the main sensory organs providing leg kinaesthesia (Proske & Gandevia, 2012). These primary afferents feed muscle spindle activity within spinal sensorimotor circuits (A. G. Brown & Fyffe, 1978), and neurons in the Clarke's column that relay this information centrally via the dorsal spinocerebellar tract (Proske & Gandevia, 2012). Since EES mainly recruits large primary afferents in the posterior roots, the observed disruption of leg kinaesthesia should be reflected in an altered modulation of propriospinal feedback circuits during EES. Indeed, sensory signals alter the excitability of sensorimotor circuits. For example, proprioceptive information during movement modulates the amplitude of reflex responses induced by peripheral nerve stimulation (Capaday & Stein, 1986; Courtine et al., 2007; Knikou et al., 2009; Dy et al., 2010). These observations imply that the cancellation of proprioceptive information would affect the modulation of reflex responses elicited by EES. Consequently, the cancellation of proprioceptive information during continuous EES in humans would reduce

the modulation of spinal reflex responses proportionally to the intensity and frequency of stimulation in humans, but not in rats.

To test this hypothesis, we studied the modulation of reflex responses elicited by various EES frequencies (5 to 60 Hz) during passive oscillations of the ankle or knee joint. The same participants with chronic SCI were seated in a robotic system that imposed passive rhythmic extension / flexion movements of the ankle or knee at a fixed angular velocity and amplitude (**Figure 4.4A**). Simultaneously, we delivered continuous EES with electrode configurations and stimulation intensities that induced consistent reflex responses in flexor and extensor muscles of the targeted joint (**Figure 4.4A**).

In all participants, the rhythmic flexion-extension movements of the joint induced a significant phase-dependent modulation of the reflex responses elicited by EES in the mobilized muscles (normalized modulation depth superior to 0.3; $p < 0.05$ for each frequency, bootstrap; (**Figure 4.4B-D**). However, the extent of this modulation depth strongly depended on the frequency of stimulation. Quantification of angle-dependent reflex responses revealed a pronounced monotonic decrease of the normalized modulation depth with EES frequency increments (**Figure 4.4D**).

We performed the same experiments in four lightly anesthetized rats with a chronic contusion SCI that were surgically implanted with a stimulating electrode over the lumbosacral spinal cord (**Figure 4.4E,G**). As observed in humans, robot-controlled oscillations of the ankle induced a robust modulation of reflex responses (normalized modulation depth superior to 0.18 ($p < 0.05$) for each frequency). However, we did not detect systematic relationships between EES frequencies and normalized modulation depth (**Figure 4.4G**). Modulation of motor responses was still present at frequencies as high as 100 Hz (**Figure 4.4F**). A linear fit of the median values yielded a slope close to 0 in all rats (median = 0.0003, 95% confidence interval = $[-0.0056, 0.0015]$, bootstrap), suggesting a lack of linear dependency between modulation depth and EES frequency.

Together, these experiments provide compelling evidence that continuous EES with stimulation features typically used for facilitating movement leads to a considerable cancellation of proprioceptive information in humans, but not in rats. Moreover, this disruption alters the ability of proprioceptive information to modulate the motor output elicited by EES. These mechanisms may explain the limited therapeutic efficacy of EES in people with SCI compared to rodent models.

4.3.5 Computational models of proprioceptive feedback circuits during locomotion

To address this question, we sought to assess the impact of continuous EES on the natural dynamics of proprioceptive feedback circuits during locomotion. Since these interactions cannot be studied in vivo, we synthesized EES properties, proprioceptive feedback circuits, and leg biomechanics into species-specific computational models (**Figure 4.5A**). Specifically, we adapted a previously validated dynamic computational model (Moraud et al., 2016) to the specific anatomical features of rats and humans. The model includes the minimal proprio-
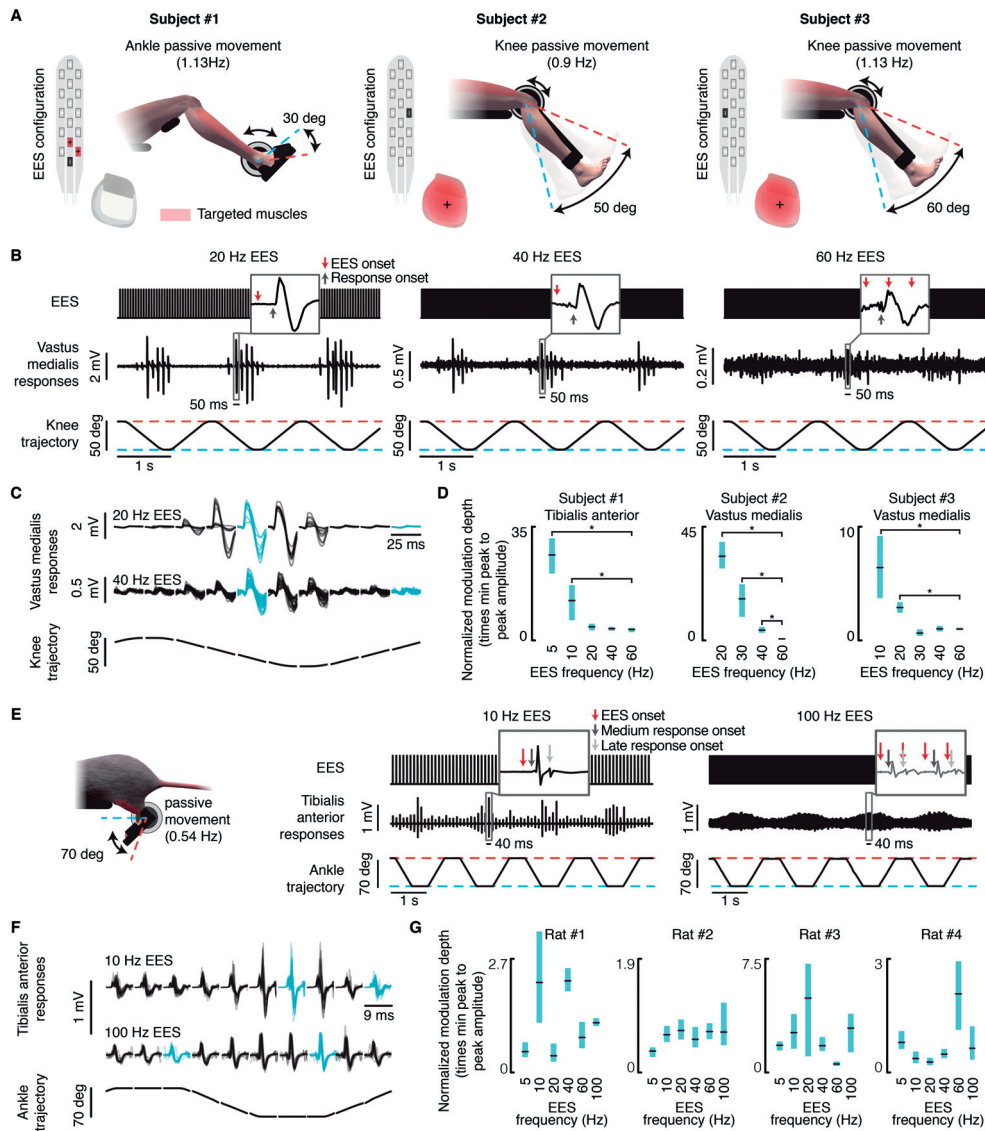
Figure 4.4 | Effect of EES on the natural modulation of proprioceptive circuits during passive movements. A, Configuration of the experimental setup for humans. The subjects were secured in a robotic system that moved the ankle or knee joint passively within the reported range of motion. EES electrodes were configured to target a muscle that underwent stretching cycles during the selected joint movement, as highlighted in red for each subject. **B**, Plots showing EES pulses, EMG activity of the vastus medialis, and changes in knee joint angle during passive oscillations of the knee for three different EES frequencies (20, 40 and 60 Hz) in subject #2.The rectangular windows highlight muscle responses induced by a single pulse of EES. Red and grey arrows depict the onset of the stimulation pulse and of the muscle response, respectively. **C**, The cycle of joint oscillation was divided into 10 bins of equal durations during which muscle responses were extracted and regrouped. Superimposed muscle responses are displayed for each bin for two EES frequencies (subject #2). Muscle responses used to compute the normalized modulation depth are depicted in light blue. **D**, Box plots reporting the median and 95% CI of the normalized modulation depth, for each EES condition tested and for the different subjects. Low frequencies of stimulation often induced spasms in the muscles. Consequently, subjects #2 and #3 could not be tested with EES frequencies below 20 and 10 Hz, respectively. *, $P < 0.05$, bootstrap. **E-G**, Configuration of the experimental setup for rats with severe contusion SCI (250 kdyn) and results following the same conventions as in (**B-D**) for human subjects.
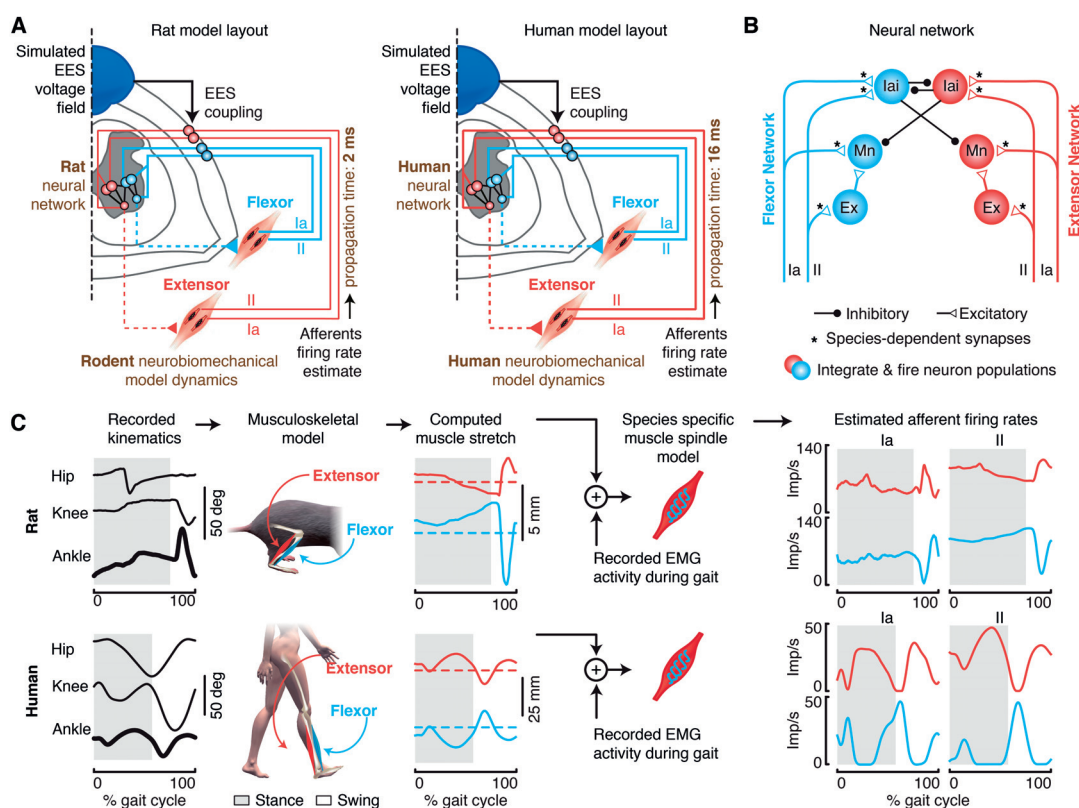
Figure 4.5 | Dynamic computational model of the rat and human muscle spindle circuitries during locomotion. A, Layout of the computational models built for rats and humans. The components highlighted in brown are tuned to match the anatomical and physiological features of rats versus humans. **B**, Spiking neural network model of muscle spindle feedback circuits for a pair of antagonist muscles. Mn, motoneuron. Ex, excitatory interneurons. Iai, Ia-inhibitory interneurons. The synapses highlighted with an asterisk (*) are tuned to match the known properties of humans and rats. **C**, Estimated stretch profiles and afferent firing rates of ankle flexor and extensor muscles over an entire gait cycle in rats (top) and humans (bottom).

ceptive neural network responsible for reciprocal activation of antagonist muscles (**Figure 4.5B**). We steered this network with proprioceptive afferent activity. For this, we used a validated biomechanical model of the rat and human lower limbs to estimate the stretch velocity profile of ankle antagonist muscles during locomotion. We exploited this information to estimate the firing rates of proprioceptive afferent fibers through species-specific muscle spindle models (**Figure 4.5C**). The model of proprioceptive afferent fibers also took into account the occurrence of orthodromic activity and antidromic collisions elicited by EES.

We first studied the impact of EES amplitude and frequency on the activity of proprioceptive afferent activity during locomotion. To model increments in EES amplitude and frequency, we scaled up the number of recruited afferent fibers and the rates of both orthodromic and antidromic induced activities, respectively. In rats, EES did not alter the modulation depth of proprioceptive information. The percentage of antidromic collisions remained low across a broad range of EES amplitudes and frequencies (**Figure 4.6**). In striking contrast, the same parameters of EES dramatically disrupted the modulation of proprioceptive information in humans. Increase in stimulation frequency augmented the firing rate of the recruited fibers. With

frequencies as low as 40 Hz, antidromic action potentials abolished the sensory information conveyed by each of the electrically stimulated fibers. The residual modulation of proprioceptive information solely resulted from the remaining incoming activity of non-recruited afferent fibers. Because increase in stimulation amplitude led to a higher number of recruited fibers, the percentage of erased proprioceptive information scaled up proportionally (**Figure 4.6**).
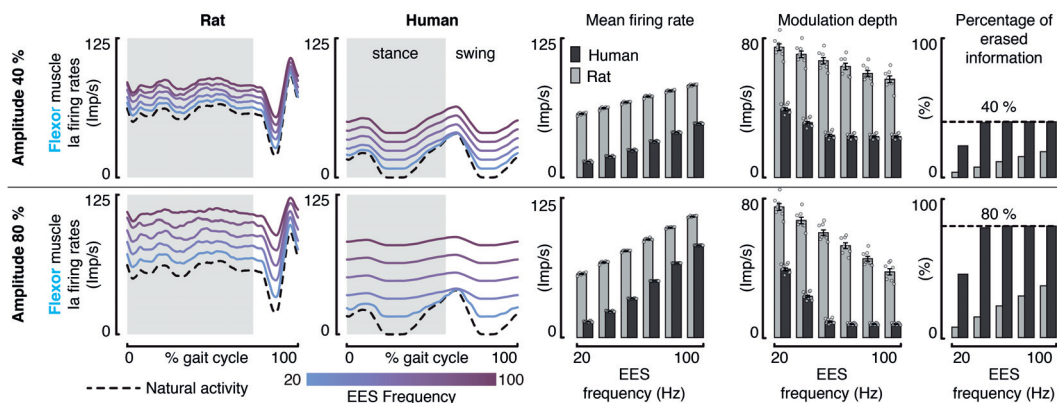
Figure 4.6 | Impact of continuous EES on proprioceptive afferent firings during locomotion in rats and humans. Impact of EES on the predicted natural firing rate profiles of group-Ia afferents innervating a flexor muscle of the ankle during locomotion in rats (left) and humans (right).From left to right: averaged firing rate profiles of the simulated population of afferent fibers over one gait cycle, mean afferent firing rate (± SEM, n = 8 gait cycles in rats, n = 11 gait cycles in humans), modulation depth of afferents firing rate profiles (mean ± SEM, n = 8 gait cycles in rats, n = 11 gait cycles in humans), and total amount of sensory information erased by EES. Results are reported over a range of EES frequencies. Top and bottom panels reports the results for EES amplitudes recruiting 40% (top) or 80% (bottom) of the entire population of modeled group-Ia afferents.

We then evaluated the impact of this cancellation on the ability of EES to steer reciprocal activation of motoneurons innervating antagonist muscles during locomotion. Continuous EES delivered excitation to Ia-inhibitory interneurons and motoneurons. In rats, the modulation of Ia-inhibitory interneurons driven by the natural proprioceptive information led to a reciprocal activation of antagonist motoneurons that was coherent with the stance and swing phases of gait (**Figure 4.7A**). As expected, increase in stimulation frequency or amplitude scaled up the firing rates of motoneurons. This increase was restricted to the phase of gait during which each pool of motoneurons was active.

The occurrence of antidromic collisions in the human model dramatically disrupted the dynamics of the neural network (**Figure 4.7B**). At low frequency and low amplitude, continuous EES steered the reciprocal activation of antagonist motoneurons, as observed in rats. With higher stimulation parameters, the cancellation of proprioceptive information prevented phase-dependent modulation of Ia-inhibitory interneurons. The resulting imbalance between antagonist pools of Ia-inhibitory interneurons led to a profound asymmetry in the excitatory drive delivered to motoneurons. Specifically, the extensor motoneuron pool became over-active while the flexor motoneuron pool received strong inhibition (**Figure 4.7B**).

These results suggest that only a narrow range of EES parameters could be exploited to

enhance the excitability of the human spinal cord after SCI without compromising the critical role of proprioceptive information in the production of locomotion. Therefore, while continuous EES might facilitate locomotion when optimally configured, the degree of controllability over human motoneurons is likely to be very limited compared to rats.
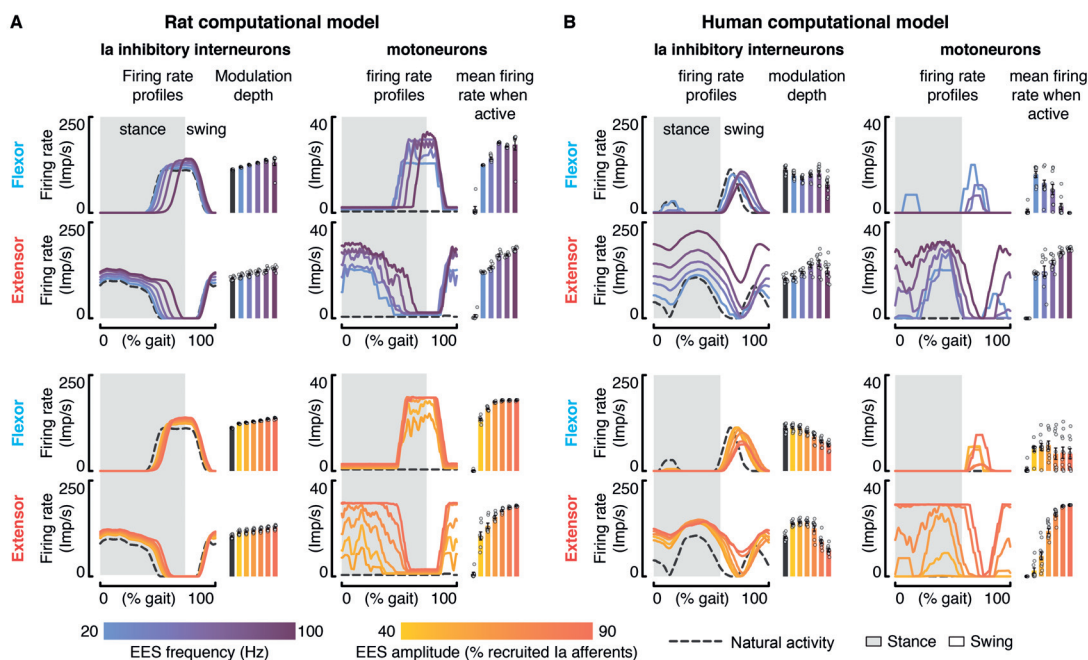
Figure 4.7 | Interactions between EES and muscle spindle feedback circuits during locomotion in rats and humans. A,B, Impact of EES on the modeled natural activity of Ia-inhibitory interneurons and on the activation of motoneurons during locomotion in rats and humans. Left, average firing rate profiles and modulation depth of the Ia-inhibitory interneuron populations embedded in the flexor or extensor part of the neural network (mean ± SEM., n = 8 gait cycles in rats, n = 11 gait cycles in humans). Right, average firing rate profiles and mean firing rate during the active phase for flexor and extensor motoneurons embedded in the flexor or the extensor neural network (mean ± SEM., n = 8 gait cycles in rats, n = 11 gait cycles in humans). The impact of EES frequencies and amplitudes are reported in the top and bottom panels, respectively. EES amplitude was set to a value recruiting 65% of the modeled Ia afferents when EES frequency was scaled up, while EES frequency was set to 60 Hz when the amplitude was increased.

4.3.6 The range of EES parameters facilitating locomotion is limited in humans compared to rats

We then evaluated the impact of tuning EES frequency and amplitude on the modulation of leg muscle activity during locomotion in rats and humans.

We tested rats with a clinically-relevant spinal cord contusion (Asboth et al., 2018) that were implanted with a pair of stimulating electrodes over L2 and L4 spinal segments (n = 4 rats). Rats were positioned bipedally in a robotic bodyweight support system over a treadmill (**Figure 4.8A**). Continuous EES (40 Hz) delivered through both electrodes induced robust locomotor movements of the otherwise paralyzed legs (**Figure 4.8B**). As previously reported (Wenger et al., 2014; Moraud et al., 2016; Wenger et al., 2016), increase in EES frequency (20-80 Hz) led to a linear modulation of leg muscle activity, which resulted in a graded tuning of

kinematic features such as the step height (**Figure 4.8B,C**).

The three participants with SCI were provided with a gravity-assist (Mignardot et al., 2017) that delivered personalized upward and forward forces to the trunk in order to facilitate walking over a treadmill (**Figure 4.8D**). Using the rails located on each side of the treadmill, subject #1 (60% body weight support) and subject #2 (70% body weight support) were able to take some steps on the moving treadmill belt and produce alternating activation of antagonist leg muscles without EES. However, this muscle activity did not translate into functional movements, as both feet essentially dragged along the treadmill belt at the end of the stance phases while the amplitude of leg movements remained limited. The delivery of continuous EES through manually-optimized electrode configurations and parameters (40 Hz, 3 to 9 mA) facilitated leg muscle activity and kinematic features (**Figure 4.8E,F** and **Figures 4.9** and **4.10**). Contrary to rats, however, the extent of this facilitation was insufficient to enable coordinated, weight-bearing locomotion. Subject #3 exhibited flaccid paralysis of all leg muscles in both legs. In this participant, continuous EES increased muscle activity, but failed to produce consistent modulation of this activity across the gait cycles (**Figure 4.11**). All participants reported a complete loss of limb position awareness during EES, which affected their ability to coordinate the timing of their locomotor movements.

Consequently, we explored the possibility to augment the motor output with modulation of EES frequency or amplitude. From optimal EES parameters, increase in frequency or in amplitude did not translate into improved facilitation of walking. Typically, the amplitude of EMG activity scaled up in flexor muscles, but this increase was associated with a concomitant decrease in extensor muscles, even leading to a complete suppression of extensor muscle activity in some instances (**Figure 4.8E,F** and **Figures 4.9** and **4.10**). Moreover, adjustments of EES parameters led to a co-activation of antagonist muscles, with the occurrence of abnormal bursting activity in flexor muscles during the stance phase of gait. Co-activation of muscles induced a sensation of stiff legs, reflected in the reduced range of motion of leg joints (**Figure 4.8E,F** and **Figures 4.9** and **4.10**). These experimental results are consistent with the predictions of our simulations, suggesting that only a narrow range of EES parameters can facilitate muscle activity without disrupting the natural modulation of reciprocal inhibitory networks due to the antidromic cancellation of proprioceptive feedback information.

These results confirm the predictions of the simulations, showing the limited efficacy of continuous EES for facilitating locomotion in humans with SCI compared to rats and thus providing a plausible explanation for this inter-species difference.

4.3.7 Spatiotemporal EES protocols may remedy the limitations of continuous EES

We next sought to exploit our computational model to identify stimulation strategies that may remedy the disruption of reciprocal inhibitory networks observed during continuous EES.

We reasoned that, to avoid this disruption, the temporal and spatial structure of the stimulation should encode the profile of proprioceptive feedback information. Specifically, we surmised that the amplitude / frequency of the stimulation targeting a specific muscle should
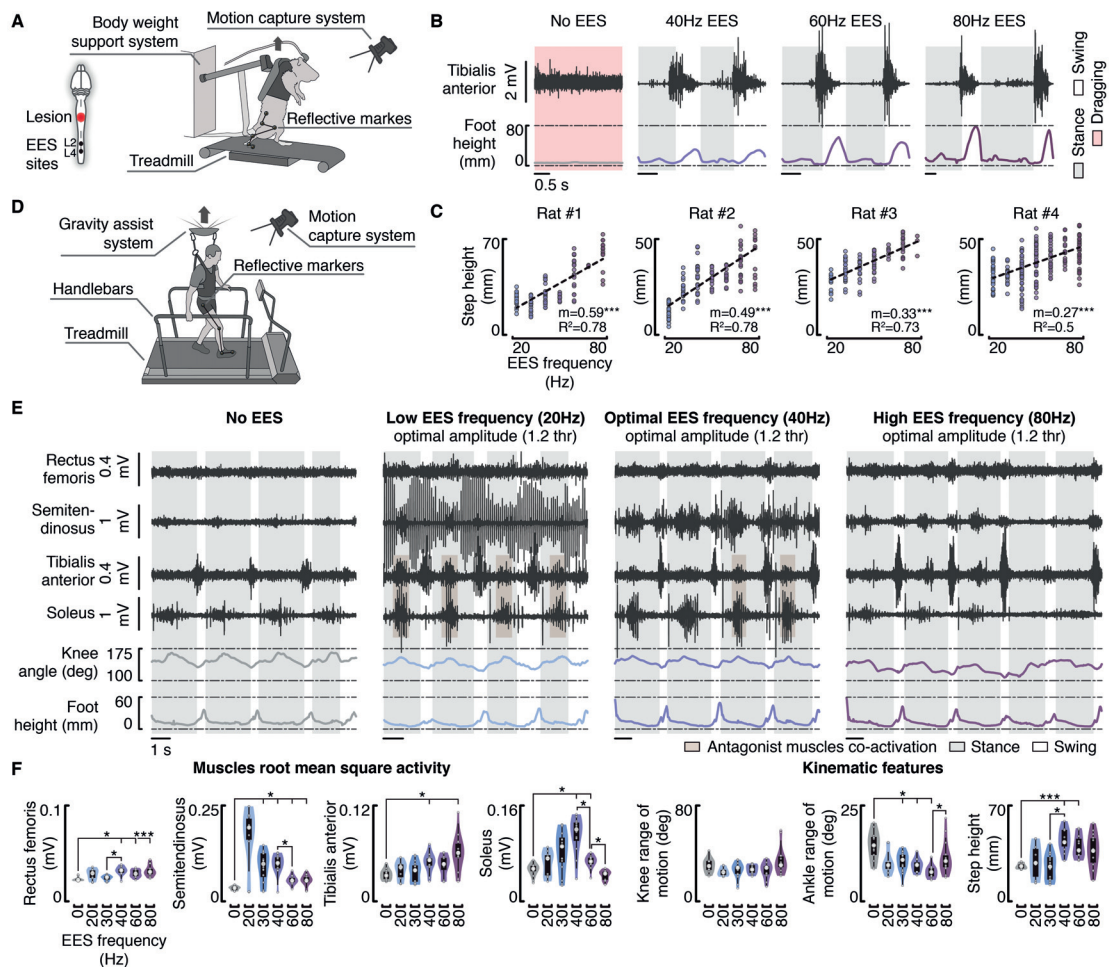
Figure 4.8 | Impact of EES frequencies on muscle activity and leg kinematics during locomotion in rats and humans. A, Experimental setup in rats. Rats with a severe contusion SCI were positioned in a robotic body weight support system located above a treadmill. Continuous EES was applied over L4 and L2 segments through chronically implanted electrodes secured over the midline of the dorsal spinal cord. **B**, EMG activity of the tibialis anterior muscle and foot height trajectory over two gait cycles without EES and with EES delivered at 40 Hz, 60 Hz and 80 Hz. **C**, Scatter plots reporting the step height at different gait cycles for the tested EES frequencies. Dashed lines report the linear regression between the EES frequency and the step height. Slope (m) and R^2 are reported. ***, $P < 0.001$ two-tailed Wald test slope $\neq 0$. **D**, Experimental setup in humans. Subjects were positioned in a gravity assist system that provided personalized forward and upward forces to the trunk. Subjects were asked to step on the treadmill while holding the handlebars, since they were not able to step independently with the hands free. **E**, EMG activity of flexor (semitendinosus/tibialis anterior) and extensor (rectus femoris/soleus) muscles spanning the right knee and ankle joints, together with the changes in the knee ankle angles and foot elevation over four gait cycles without EES and with EES delivered at 20 Hz, 40 Hz and 80 Hz in subject #1. EES amplitude was set to 1.2 times the muscle response threshold. Notice the opposite modulation of EMG activity in extensor and flexor muscles with increase in frequencies together with co-activation of flexor with extensor muscles. **F**, Violin plots reporting the root mean square activity of the recorded muscles, the range of motion of the knee and ankle angles, and the step height at different gait cycles for subject #1. Small grey dots represent the different data points, while the large white dots represent the median of the different distributions. Box and whiskers report the interquartile range and the adjacent values, respectively. *, $P < 0.05$, ***, $P < 0.001$, Wilcoxon rank-sum test with Bonferroni correction for multiple comparisons. The same results are reported for subjects #2 and #3 in **Figure 4.10** and **Figure 4.11**.

Figure 4.9 | Impact of EES amplitude on muscle activity and leg kinematics during locomotion on a treadmill — Subject #1. A, AIS leg motor score. **B**, Configuration of electrodes targeting the left and right posterior roots projecting to the L1 and L4 segments. Continuous EES was delivered through these electrodes to facilitate locomotion. **C**, EMG activity of flexor (semitendinosus/tibialis anterior) and extensor (rectus femoris/-soleus) muscles spanning the right knee and ankle joints, together with the changes in the knee ankle and foot height trajectories over four gait cycles without EES and with EES delivered at 0.9, 1.2 and 1.5 motor response threshold amplitude. EES frequency was set to 40Hz. **D**, Violin plots reporting the root mean square activity of the recorded muscles, the range of motion of the knee and ankle angles, and the step height for different gait cycles. Small grey dots represent the different data points, while the large white dots represent the median of the different distributions. Box and whiskers report the interquartile range and the adjacent values, respectively. *, $P < 0.05$, ***, $P < 0.001$, Wilcoxon rank-sum test with Bonferroni correction for multiple comparisons.
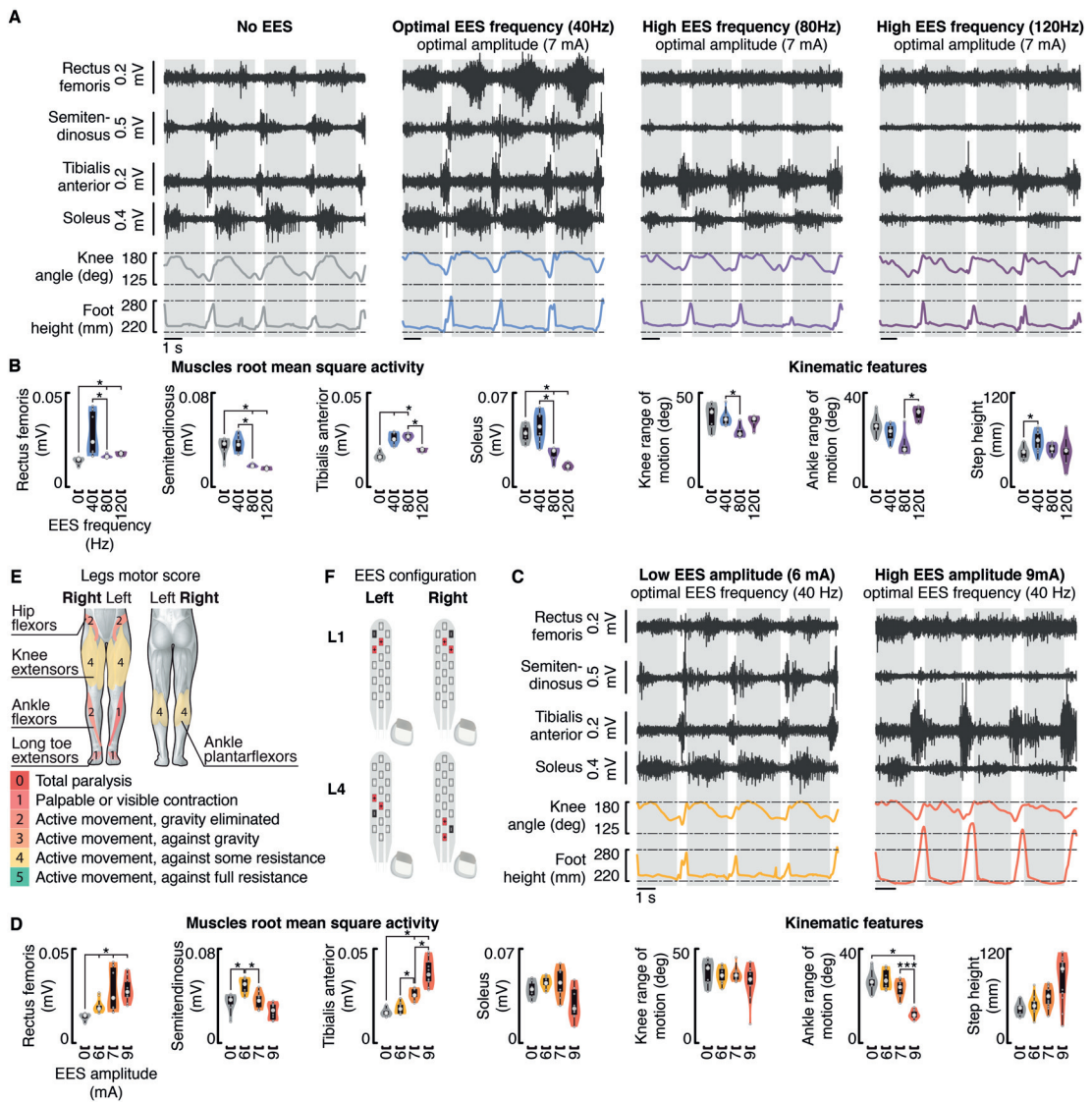
Figure 4.10 | Impact of EES frequency and amplitude on muscle activity and leg kinematics during locomotion on a treadmill — Subject #2. The results displayed in **Figure 4.8** and **Figure 4.9** for subject #1 are reported for subject #2 using the same conventions.
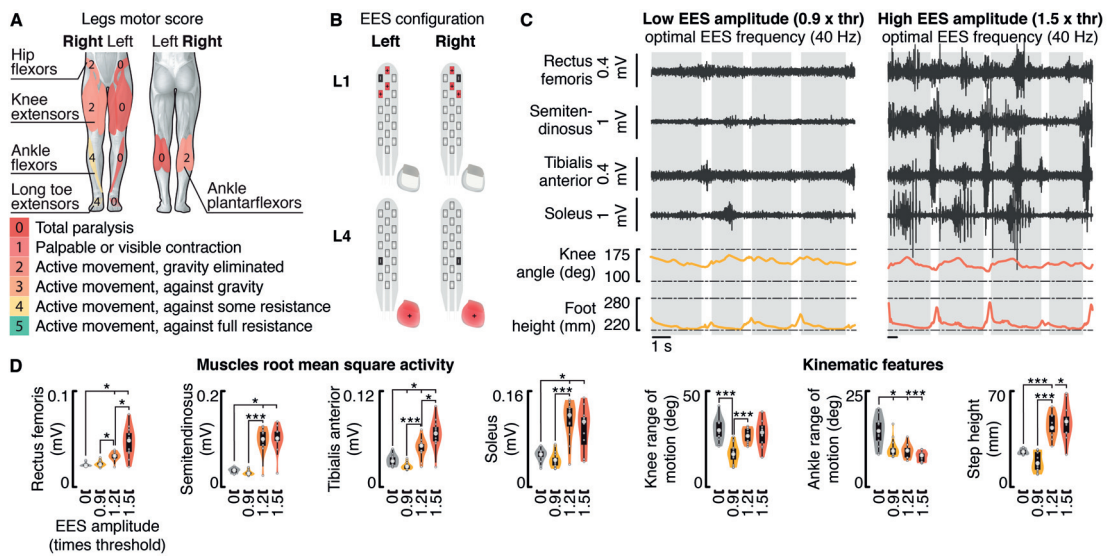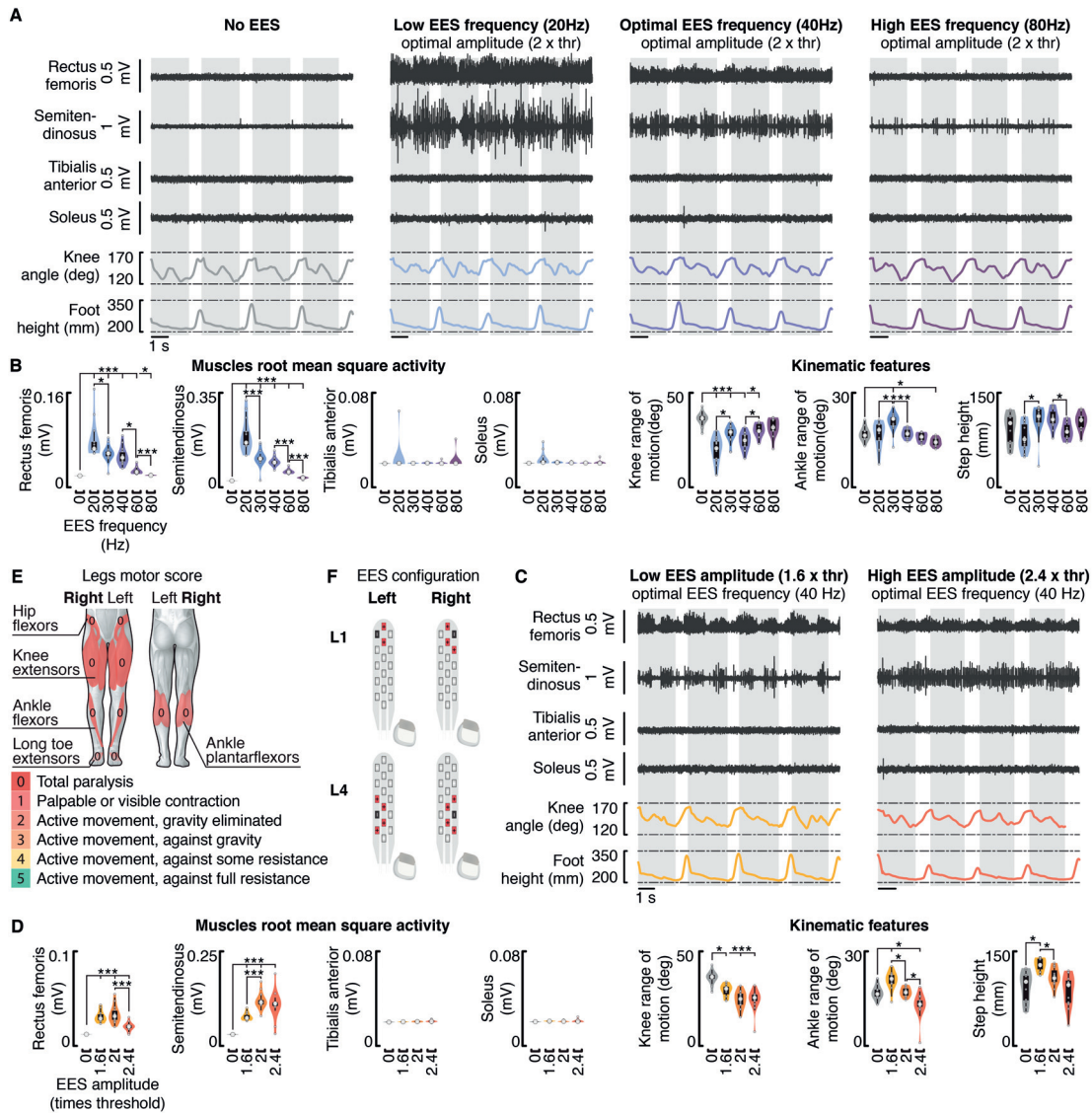
Figure 4.11 | Impact of EES frequency and amplitude on muscle activity and leg kinematics during locomotion on a treadmill — Subject #3. The results displayed in **Figure 4.8** and **Figure 4.9** for subject #1 are reported for subject #3 using the same conventions.

be proportional to the instantaneous firing rate of the proprioceptive afferents originating from the sensory organs located in this muscle. Due to the continuous match between the proprioceptive afferent activity and the stimulation profile, EES would augment the overall excitation delivered to the targeted motor pool without compromising the information conveyed by the proprioceptive afferents. Targeting antagonist motor pools with their specific stimulation profile would contribute to maintaining the modulation of reciprocal inhibitory networks that is necessary to facilitate walking with EES. In turn, we hypothesized that the degree of excitation delivered to motor pools could then be controlled by scaling the range of EES amplitudes and frequencies used to configure the stimulation profiles.

We implemented this stimulation strategy in the human dynamic computational model. We constructed stimulation profiles that combined the natural modulation of primary and secondary proprioceptive afferents (group-Ia, group-II, and Ib, **Figure 4.12A,B**) from the homonymous muscles; in our case a flexor and an extensor muscle of the ankle. We did not explicitly model Golgi tendon organs, although Ib-afferents are also recruited with EES and provide strong excitatory inputs during locomotion (Conway et al., 1987). Previous studies reported close correlations between the firing of Ib-afferents and the activity of the homonymous muscle (Prochazka, 1999). We thus used the EMG envelope as a surrogate for the firing profile of Ib-afferents.

Simulations revealed that this stimulation strategy erased the natural proprioceptive information to a similar extent as continuous stimulation (**Figure 4.12C**). Due to the continuous match between the natural proprioception and stimulation profile, however, the proprioceptive signals reaching the spinal cord contained the same amount of information, i.e., naturally generated action potentials annihilated by antidromic collision were replaced by EES-produced orthodromic action potentials. While the percentage of erased information steadily increased with the stimulation amplitude (**Figure 4.12C**), the depth of proprioceptive afferent modulation remained preserved, or even increased for higher stimulation amplitudes. Consequently, the stimulation artificially drove the reciprocal modulation of Ia-inhibitory interneurons, as would the natural proprioception during walking (**Figure 4.12C**). Scaling up the range of EES amplitudes with this stimulation strategy proportionally augmented the mean firing rates of proprioceptive afferents, which led to a linear increase in the excitation delivered to motoneurons. Since this excitation was restricted to the active phase of each motoneuron pool, increasing the amplitude or frequency of EES enabled a graded modulation of the firing rate of both extensor and flexor motoneurons (**Figure 4.12C**).

These results suggest that encoding the profile of proprioceptive afferent activity into the spatiotemporal structure of EES protocols may expand and refine the control over the amplitude of motoneuron activity while also reinforcing the modulation of reciprocal inhibitory networks, thereby enhancing the facilitation of walking compared to continuous EES.
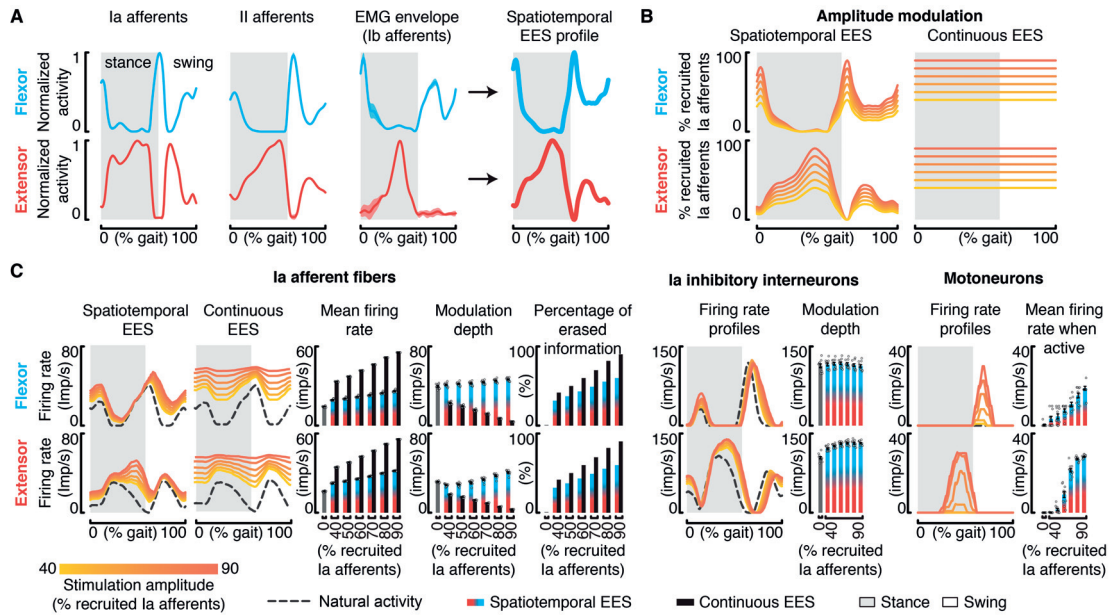
Figure 4.12 | Spatiotemporal EES protocols encoding proprioceptive sensory information. **A**,Estimation of spatiotemporal stimulation profiles that match the natural flow of proprioceptive information generated from flexor and extensor muscles of the ankle during gait. From left to right: estimated averaged firing rate profiles of group-Ia, group-II and group-Ib (equivalent to the muscle activity) afferents over a gait cycle, and the sum of these profiles that yielded the estimated stimulation profiles. **B**, Percentage of primary afferents that are recruited when applying the estimated spatiotemporal stimulation profile and during continuous stimulation. **C**, Impact of the estimated spatiotemporal stimulation profile on the modulation of muscle spindle feedback circuits from flexor and extensor muscles, including from left to right: group-Ia afferents firings, bar plots reporting the averaged mean firing rate and modulation depth of primary afferents (mean ± SEM., n = 11 gait cycles), overall percentage of sensory information erased by EES, modulation of Ia-inhibitory interneurons, and motoneuron activity. For comparison, the impact of continuous EES on the group-Ia afferent firings is also reported. Results of simulations are shown for a range of EES amplitudes. Conventions are the same as in **Figure 4.7**.

4.3.8 High-frequency low-amplitude EES alleviates the disruptive effects of continuous EES

We finally explored whether alternative strategies based on continuous EES could alleviate the cancellation of proprioception with EES.

We sought to design a stimulation strategy that minimizes the amount of erased proprioceptive information during continuous EES while providing high post-synaptic excitation to motoneurons. Each Ia-afferent synapses onto every single motoneuron that innervates the homonymous muscle (Mendell & Henneman, 1971; Segev et al., 1990). Moreover, electrophysiological studies showed that high-frequency stimulation of nerve afferents leads to a temporal summation of excitatory post-synaptic potentials (EPSP) delivered to the targeted cell (Collins et al., 1984; Koerber & Mendell, 1991; Bawa & Chalmers, 2008). Therefore, the recruitment of a limited number of Ia-afferents with a stimulation burst of low-amplitude but high-frequency could theoretically deliver the same excitation to motoneurons as the recruitment of a large number of Ia-afferents with single pulses of high amplitude. We thus hypothesized that each pulse of EES could be replaced by a high-frequency low-amplitude burst of EES that would provide the same overall excitation to motoneurons while reducing the overall amount of erased proprioceptive information. Indeed, while the proprioceptive information traveling along the recruited fibers would still be blocked by the stimulation, the reduced number of electrically recruited afferents would maintain a larger amount of fibers available to convey natural sensory signals to the spinal cord. Finally, the excitation delivered to motor pools could then be controlled by adjusting the inter-burst interval.

We tested the hypotheses underlying this stimulation strategy using computer simulations with multicompartmental motoneuron models and realistic distribution of Ia-afferent synaptic contacts (**Figure 4.13A**). As predicted, the temporal summation of EPSPs elicited by high-frequency low-amplitude bursts of stimulation enabled recruiting the same number of motoneurons as single pulses of high amplitude EES (**Figure 4.13B**).

To validate these results experimentally, we conducted electrophysiological experiments in five rats. **Figure 4.13C** shows representative motor responses recorded in the tibialis anterior when delivering single pulses of EES and single bursts of EES (25 ms duration with frequencies ranging from 100 to 1000 Hz) at increasing amplitudes. Compared to single pulses, high-frequency burst stimulation decreased the threshold to elicit a motor response by 39.8% (SEM: ± 4.4%). The largest reductions were obtained towards 500 Hz (SEM: ± 54.8 Hz). For a given frequency, a decrease in burst amplitude led to an increase in the latency of motor responses, suggesting that a higher number of pulses was necessary to recruit motoneurons through the temporal summation of EPSPs (**Figure 4.13D**).

The implantable pulse generator used to delivery EES in our participants could generate waveforms with a maximum frequency of 125 Hz. However, the simultaneous delivery of interleaved waveforms (2 ms hard-coded delay) enabled the configuration of single bursts composed of 4 pulses delivered at 500 Hz. While this feature was not sufficient to replicate the experiment conducted in rats, nor to test the efficacy of the proposed stimulation protocols to facilitate walking, it allowed us to evaluate the concept of high-frequency EES in humans.

As observed in rats, high-frequency bursts of EES required markedly reduced stimulation amplitudes to elicit a motor response compared to single pulses (**Figure 4.13E,F**).
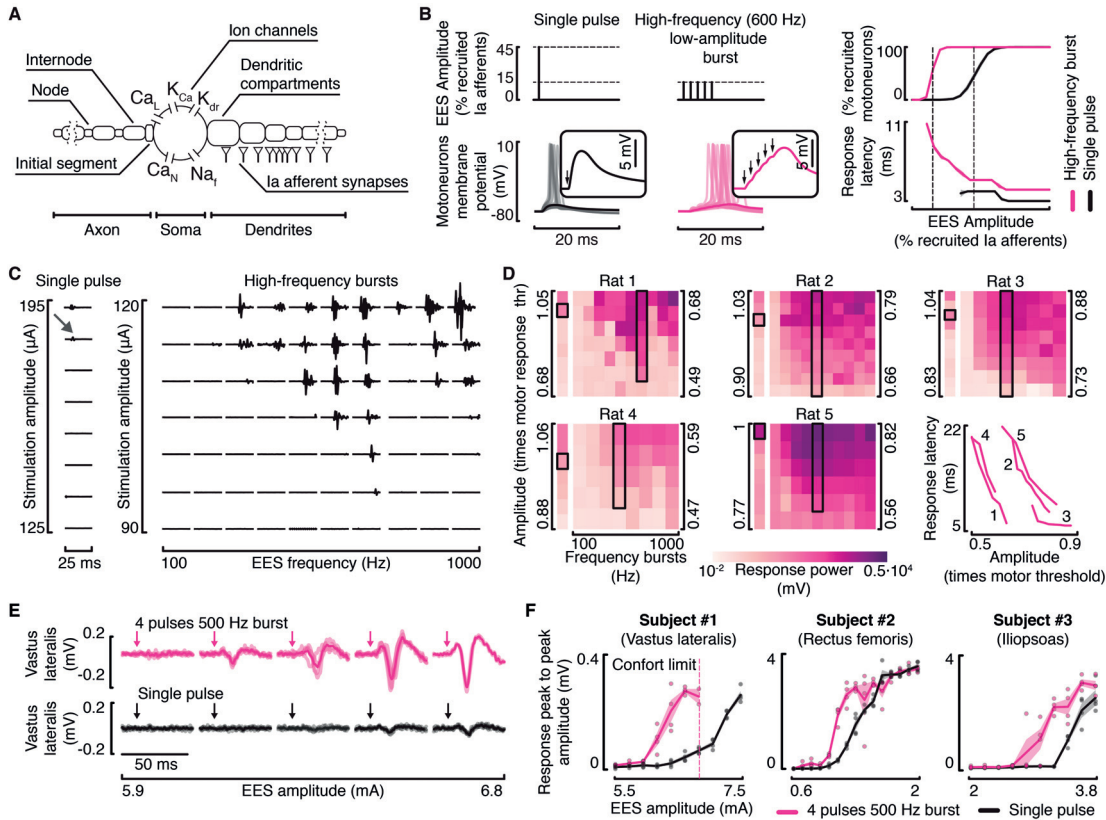
Figure 4.13 | High-frequency low-amplitude bursts of EES recruit motoneurons through temporal summation of EPSPs. A,Multicompartmental model of alpha motoneurons with realistic strength and distribution of group-Ia synaptic contacts. **B**, Simulations showing the response of motoneurons to a single pulse of EES at an amplitude recruiting 45% of the afferent population, and to a high-frequency bursts (5 pulses, 600 Hz) at an amplitude recruiting 15% of the afferent population. Windows show a zoomed view of the motoneuron membrane potential depolarizations in response to the pulses of EES (arrows). Right: plots showing the percentage of recruited motoneurons and the average (mean ± SEM) latency before the onset of an action potential. **C**, Responses recorded from the tibialis anterior muscle following a single pulse of EES (left) and high-frequency bursts of EES (right) applied to the lumbar (L2) spinal cord of rats with severe contusion SCI over a range of amplitudes and burst frequencies. The grey arrow indicates the responses induced by a single pulse of EES at the motor response threshold amplitude, emphasizing the need to deliver high amplitudes to elicit responses with single pulses compared to high-frequency bursts. **D**, Heatmaps representing the average power of motor responses (n=4) to single pulses (column on the left) and high-frequency bursts (matrix on the right) of EES over a range of EES amplitudes and bursts frequencies, for 5 rats. EES amplitude is reported as a multiple of motor response threshold, amplitude corresponding to the response highlighted by the black box. The highlighted column corresponds to the bursts with a frequency inducing the largest motor responses. Right, latencies of motor responses elicited by EES bursts with the frequency highlighted in the black boxes, at increasing amplitudes. **E**, Motor responses recorded from the vastus lateralis muscle induced by single pulses (bottom) and high-frequency bursts of EES for different stimulation amplitudes (subject #1). Shaded curves represent single trials, solid curves represent the average responses. Arrows indicate the onset of the stimulation. **F**, Plots representing the response peak to peak amplitudes (mean ± SEM) as a function of EES amplitude, for both single pulses (black) and high-frequency bursts (pink) and for the different subjects. In subject #1, EES amplitudes higher than 7 mA elicited uncomfortably powerful contractions and were thus not tested.

We finally implemented this stimulation strategy into our human computational model. In the simulation, we delivered EES bursts consisting of 5 pulses at 600 Hz with a stimulation amplitude recruiting 20% of all primary afferent fibers. Compared to continuous EES, this stimulation reduced the amount of erased proprioceptive information (**Figure 4.14**). Decreasing the duration between each EES burst led to a proportional increase in the excitability delivered to motoneurons.

These computational and experimental results suggest that high-frequency low-amplitude stimulation protocols may alleviate the detrimental impact of continuous EES on the modulation of proprioceptive feedback circuits in humans.
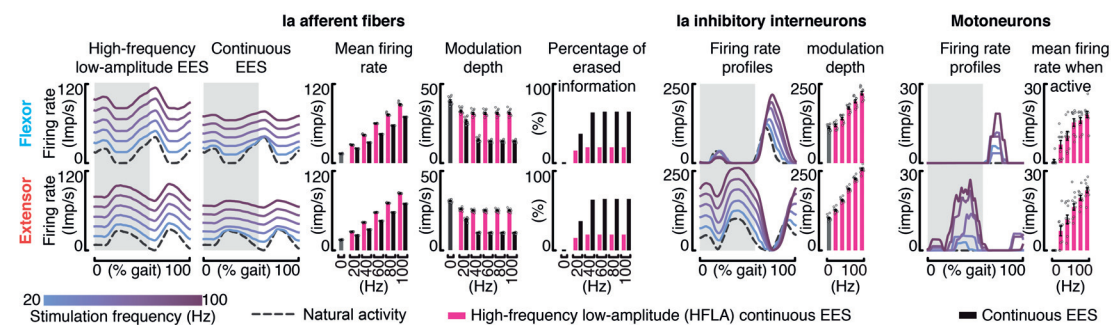
Figure 4.14 | High-frequency low-amplitude EES protocols preserve proprioceptive information and promote motor patterns formation. Impact of continuous high-frequency low-amplitude EES protocols (600 Hz, 20% recruited afferents) on the modulation of the muscle spindle feedback circuits, following the same conventions as in **Figure 4.7**. For comparison, the impact of continuous EES on the group-Ia afferent firings is also reported.

4.4 Materials and methods

4.4.1 Computer simulations

Computer simulations were performed in python 2.7 using the NEURON (Hines & Carnevale, 1997) simulation environment to run the spiking neural network models and OpenSim (Delp et al., 2007) for the biomechanical model of rats and humans. Both the NEURON simulation environment and OpenSim are open-source programs.

Model of a proprioceptive afferent fiber recruited by EES

The afferent fiber model was characterized by two parameters: (i) the propagation time required by an action potential (AP) to travel the whole length of the fiber, and (ii) the firing rate at which APs are generated by the sensory organ. These parameters were adjusted to meet the properties of all the modeled afferent fibers. For each AP, we simulated the propagation from the sensory organ of origin to the spinal cord and the refractory dynamics (mean refractory period ± standard deviation: 1.6 ± 0.16 ms) along the fiber. We modeled EES as a periodic event recruiting the most proximal portion of the fiber. The recruitment only occurred when the fiber was not under refractory period. When a fiber was electrically activated, an antidromic AP propagated towards the distal end of the fiber. The encounter of this antidromic AP with a sensory AP traveling towards the spinal cord led to an antidromic collision that cancelled both APs.

Estimation of antidromic collisions probability

The developed fiber model was used to assess the probability of antidromic collisions based on EES frequency, the firing rate of the sensory organs, and the propagation time required by an AP to travel along the whole length of the fiber. Propagation times were set to 2 ms in rat afferents. Due to the extended length of axons in humans, we modeled human afferents innervating proximal (10 ms) and distal (20 ms) muscles. Antidromic collision probability was defined as the probability of a natural sensory AP to collide with an EES-induced antidromic AP within a single fiber. For each tested model parameter and stimulation frequency, we integrated the dynamic of the fiber over 60 seconds and evaluated the number of antidromic collisions occurring within this time period. To estimate antidromic collisions probability, we averaged the results of 50 simulations initialized with different EES onset delays varying between 0 and 10 ms.

Rat model of proprioceptive feedback circuits

The rat model of proprioceptive feedback circuits was elaborated from a previously validated model (Moraud et al., 2016), which we modified to integrate a simpler and faster model of the motoneurons and the new model of proprioceptive afferents that considers the occurrence of antidromic collisions.

Briefly, this model is composed of four components: (i) a spiking neural network reproducing the proprioceptive feedback circuits associated with a pair of antagonist muscles, (ii)

a muscle spindle model, (iii) a musculoskeletal model of the rat hindlimb, and (iv) a finite element method model of EES of the rat lumbar spinal cord (**Figure 4.5A**).

The spiking neural network includes populations of group-Ia and group-II afferent fibers, Ia-inhibitory interneurons, group-II excitatory interneurons, and pools of alpha motoneurons. The number of cells, the number and the strength of the synapses contacting the different populations of neurons, and the characteristics of the cell models are described in our previous work (Moraud et al., 2016). To speed up the simulation time, we replaced our previous multicompartmental motoneuron model with an integrate and fire cell model designed to reproduce the realistic membrane response dynamics to excitatory and inhibitory stimuli (Burke, 1968; Munson et al., 1980; Harrison & Taylor, 1981; McIntyre & Grill, 2002). Specifically, we set the refractory period to 20 ± 1 ms and the membrane time constant τ_{membrane} to 6 ± 0.3 ms. Excitatory synapses were modeled as instantaneous changes in current exponentially decaying with time constant $\tau_{\text{excitatory}}$ 0.25 ms. Inhibitory synapses were modeled as alpha functions with a rise time constant $\tau_{\text{inhibitory\_1}}$ of 2 ms, and a decay time constant $\tau_{\text{inhibitory\_2}}$ of 4.5 ms (**Figure 4.15A**). We adjusted the motoneurons synaptic weights to match experimental excitatory and inhibitory post-synaptic potentials (EPSPs/IPSPs). For this, we normalized experimental EPSPs (Munson et al., 1980; Harrison & Taylor, 1981) and IPSPs (McIntyre & Grill, 2002) to the minimum depolarization necessary to induce an AP in our multicompartmental model (**Figure 4.15B,C**). Afferent fibers were modeled with an AP propagation time of 2 ms. This parameter was estimated to represent rat afferent fibers innervating the antagonist muscles of the ankle.

The musculoskeletal (Johnson et al., 2008, 2011) and muscle spindle (Prochazka, 1999) models were used to calculate the firing rate profiles of group-Ia and group-II afferent fibers innervating the flexor (tibialis anterior) and extensor (gastrocnemius medialis) muscles of the ankle during locomotion. For this purpose, we steered the musculoskeletal model with previously obtained recordings of the rat hindlimb kinematics during locomotion to estimate the ankle muscles stretch profiles through inverse kinematics. We then used the muscle spindle model to compute the firing rate profiles. To mimic the alpha-gamma linkage, muscles stretch and stretch velocity were linked to the envelope of EMG activity from the homonymous muscle (**Equation 4.1** and **Equation 4.2**, Prochazka, 1999). The estimated afferent firing rate profiles drove the activity of the modeled proprioceptive afferents.

A validated finite element method model of EES of the lumbar spinal cord (Capogrosso et al., 2013) was finally used to estimate the proportion of afferent and efferent fibers recruited at a given stimulation amplitude. Realistic interactions between EES and the natural sensory activity along the modeled afferent fibers were integrated using the developed proprioceptive afferent model.

$$
\begin{aligned}
IaFiringRate = {} & 50 + 2 \times stretch \\
& + 4.3 \times sign(stretchVelocity) \times |stretchVelocity|^{0.6} \quad \textbf{(Equation 4.1)} \\
& + 50 \times EMG_{env}
\end{aligned}
$$

$$IIFiringRate = 80 + 13.5 \times stretch + 20 \times EMG_{env} \qquad \textbf{(Equation 4.2)}$$

Human model of proprioceptive feedback circuits

The layout of the rat model served as a basis to build the human model of proprioceptive feedback circuits. To take into account the specific anatomical and physiological features of humans, we adapted the musculoskeletal model, the muscle spindle model, the weights of the synapses in the network, the length of the modeled afferent fibers, and the output of the finite element method model of EES (**Figure 4.5A**).

To estimate the stretch of flexor (tibialis anterior) and extensor (soleus) muscles spanning the ankle joints, we used the 3DGaitModel2392 OpenSim lower limb model (Delp et al., 1990) and kinematic data of healthy subjects during locomotion on a treadmill (Wojtusch & von Stryk, n.d.; Mignardot et al., 2017). We tuned the muscle spindle model to account for the lower firing rates of human proprioceptive afferents compared to those of rodents (Prochazka, 1996; Hník & Lessler, 1973). Specifically, we scaled **Equation 4.1** and **Equation 4.2** down by 0.2 and 0.25, respectively, to produce firing rates that remained within the range of values generally observed in humans (rarely exceeding 30 Impulse/second, Prochazka, 1996, 1999;

D		s_1	s_2	s_3
Number of synapses		60	116	232
Experimental IPSP/EPSP		52 / 212 μV	~ 0.33·s_1 EPSP	~ -0.13 μV
Integrate and fire IPSP/EPSP		1.4% excitation threshold	0.7% excitation threshold	-0.2% excitation threshold
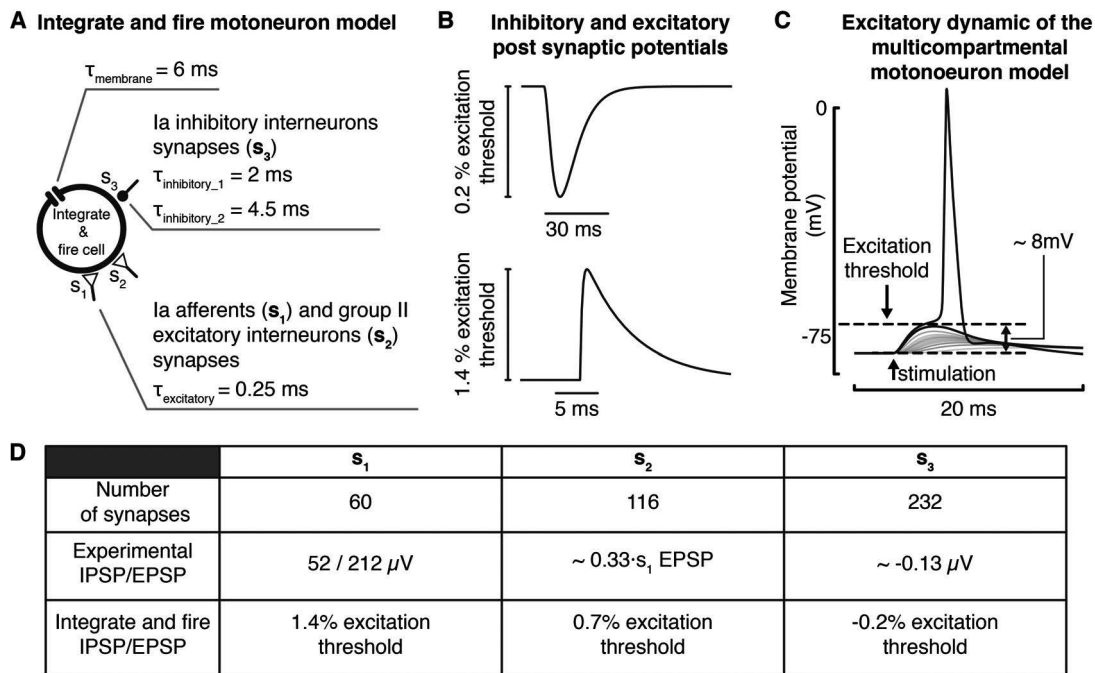
Figure 4.15 | Integrate and fire motoneuron model. **A**, Schematic of the integrate and fire model and of the different synapses contacting this cell. **B**, Simulated inhibitory and excitatory post synaptic potentials (IPSPs/EPSPs) induced by the activation of a single Ia-inhibitory interneuron or a single group-Ia afferent fiber, respectively. **C**, Excitation threshold of our multicompartmental alpha motoneuron model (Moraud et al., 2016). **D**, Number and amplitude of experimental (Munson et al., 1980; Harrison & Taylor, 1981; McIntyre & Grill, 2002) and modeled EPSP/IPSPs induced from the synaptic contacts originating from group-Ia afferents (s1), group-II excitatory interneurons (s2), and Ia-inhibitory interneurons (s3).

Albert et al., 2006). The envelopes of EMG activity were extracted from the same subjects from whom we also extracted the kinematic data (Wojtusch & von Stryk, n.d.; Mignardot et al., 2017).

We assumed that if the occurrence probability of antidromic collisions would be the same in humans and rodents, the human model should reproduce results that are qualitatively similar to the simulations obtained in rats. Hence, we optimized the weight of the synaptic connections between the afferent fibers and their target spinal neurons by driving the network with the estimated human afferent firings but without modifying the propagation time required by sensory APs to reach the spinal cord — a parameter proportional to the occurrence probability of antidromic collisions (**Figure 4.16A**). To this purpose we performed a systematic search by progressively increasing the synaptic weights of connections from afferent fibers. EES frequency and percentage of Ia-afferents recruited by EES were set to 60 Hz and to 60%, respectively. We defined a set of fitness functions and relative minimum scores to define the range of synaptic weights that produce the desired behavior of the network (**Equation 4.3**) and selected one set of weights for further simulations (**Figure 4.16B,C**).

$$\begin{cases} \text{percentile\_90}(\boldsymbol{MotoneuronsFR_{ext}}) > 5 \; Imp/s \\ \text{percentile\_90}(\boldsymbol{MotoneuronsFR_{flex}}) > 5 \; Imp/s \\ 1 - mean(\boldsymbol{MotoneuronsFR_{ext}} \odot \boldsymbol{MotoneuronsFR_{flex}}) > 0.9 \end{cases} \qquad (\textbf{Equation 4.3})$$

We then modified the AP propagation time parameter of the afferent fiber models to 16 ms, which is a representative value for the proprioceptive afferents of the ankle muscles in humans (Hofstoetter et al., 2018; Restuccia, 2000).

We assumed that the ratio between the amount of primary and secondary afferent fibers recruited by EES while increasing the stimulation amplitude is similar in rats and humans. We thus used the finite element method model of the rat spinal cord to estimate the percentage of primary and secondary afferents recruited by the stimulation. However, to take into account the considerably larger distance of the ventral roots from the epidural electrodes, we did not simulate the direct recruitment of motor axons. This phenomenon commonly occurs in rats but is limited in humans (Rattay et al., 2000; Capogrosso et al., 2013). While this decision was taken in order to build a more realistic model, simulating the direct recruitment of motor axons as in the rat model would have not influenced the significance of the presented results. Indeed, given the relatively low amplitudes tested in this work, only 7% of the simulated rat motoneuron axons were recruited directly by EES at the highest stimulation amplitude tested (**Figure 4.7A**).

Spatiotemporal stimulation profiles

Spatiotemporal EES profiles encoding the natural proprioceptive information originating from a pair of antagonist muscles spanning the ankle joint were estimated in two steps. First, we computed the normalized average firing rate profiles of group-Ia, group-II and group-Ib
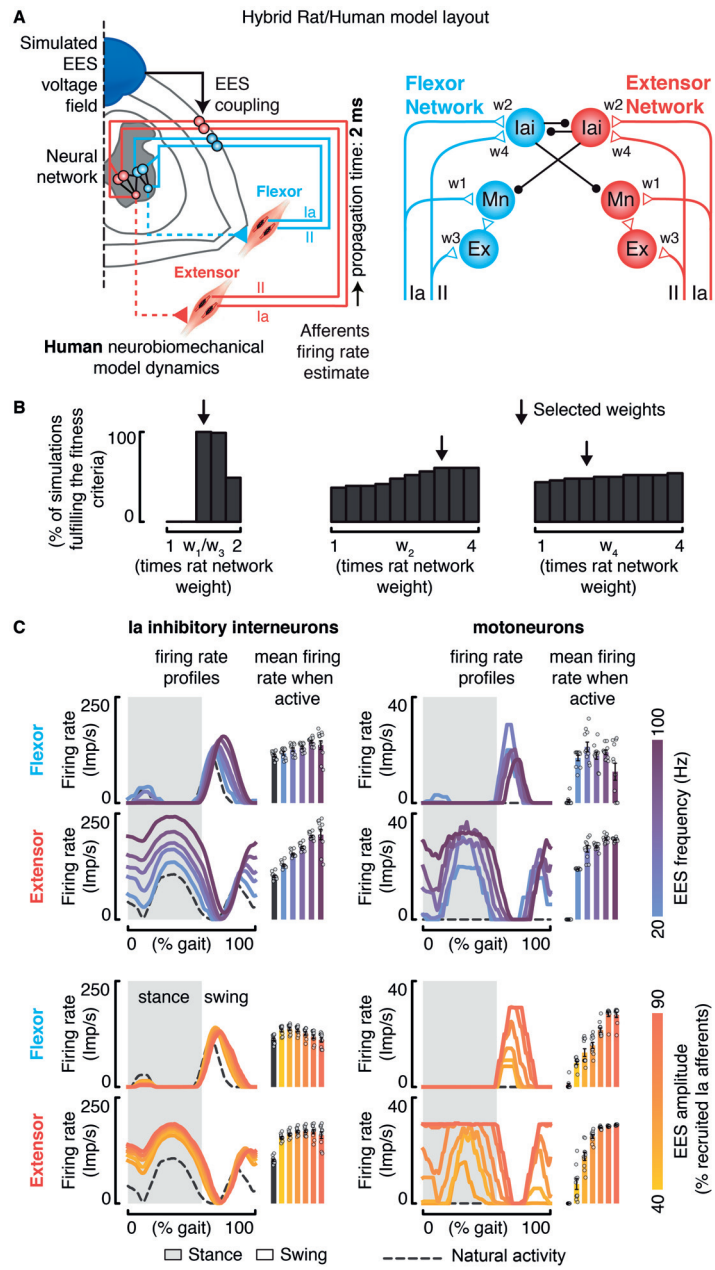
Figure 4.16 | Adaptation of the rat neural network to humans. A, Model layout of the hybrid rat-human computational model used to tune the human neural network weights. W_1, w_2, w_3 and w_4 represent the weights of the neural network connections that have been modified to adapt the rat neural network to the human one. **B**, Systematic search results. W_1 and w_3 were ranged together between 1 and 2 times the weight used in the rat network, while w_2 and w_4 were ranged between 1 and 4 times. Bar plots report the percentage of simulations that fulfilled the defined fitness criteria. Selected weights that have been used for further simulations are highlighted with an arrow. **C**, Effect of EES on the natural activity of Ia-inhibitory interneurons and on the production of motor patterns during locomotion, in the hybrid rat-human model for the selected set of synaptic weights. Panels on the left report the average firing rate profiles of the Ia-inhibitory interneuron populations associated to either the flexor or the extensor network, as well as their modulation depth (mean ± SEM, n = 11 gait cycles). Similarly, right-most panels represent the average firing rate profiles of motoneurons and their mean firing rate activity during the phase in which they are active (mean ± SEM, n = 11 gait cycles). Effects of different EES frequencies and amplitudes are reported on the top and bottom panels, respectively.

afferents over a gait cycle. Second, these three profiles were averaged to produce a stimulation profile that encodes the global proprioceptive information (**Figure 4.12A**). Since group-Ib afferent firing is closely correlated to the activity of the muscle along which the associated Golgi tendon organ is connected (Prochazka, 1999), we approximated the firing rates of group-Ib afferents with the envelope of the EMG activity from the homonymous muscle during gait. Simulations were conducted using the estimated stimulation profile for each muscle. EES amplitude was adjusted proportionally to the changes in the estimated stimulation profile while the length of the stimulation profile was adjusted based on the duration of each gait cycle.

High-frequency low-amplitude EES model

To assess the effect of high-frequency low-amplitude EES on the membrane potentials of motoneurons, we used our previously validated multicompartmental motoneuron model that integrates realistic synaptic boutons from group-Ia afferents (**Figure 4.13A,B**, Moraud et al., 2016). However, simulations on the effect of high-frequency low-amplitude EES on the muscle spindle feedback circuits were still performed using the simplified integrate and fire motoneuron model (**Figure 4.13E**). The more realistic multicompartmental model was used in order to obtain a more accurate estimate of motoneurons' soma responses to high-frequency bursts of EES.

Limitations of the human computational model

Microneurographic recordings of group-Ia and group-II afferents during slow movements reported that firing rates rarely exceed 30 Imp/s in humans (Prochazka, 1996; Vallbo & al Falahe, 1990; Roll et al., 2004). In the human computational model, we thus limited muscle spindle firing to 50 Imp/s during gait, which is markedly lower than peak firings of up to 200 Imp/s reported during locomotion in quadrupedal mammals. Nevertheless, we cannot exclude the possibility that human muscle spindle afferents fire at higher rates during specific phases of the gait. Indeed, normal locomotion involves higher joint angle velocities than those commonly tested during microneurographic recordings in humans. Consequently, the actual range of firing rates underlying the activity of group-Ia fibers during human gait remains unknown. It should be considered however, that the gait cycle frequencies occurring in individuals with SCI, even with EES, are considerably lower than those during normal walking. Furthermore, the firing rates of group-II afferents are not proportional to movement velocity. While higher firing rates might affect the results of our model to some degree, the overall predictions would remain unchanged, since EES would still block a significant amount of proprioceptive information. Therefore, the degree of disruption may scale with the actual range of afferent firings, but the conclusion derived from this model would still hold.

4.4.2 Experimental procedures in humans

Spinal cord stimulation system implanted in human subjects with SCI

Experiments conducted in human subjects with SCI were carried out within the framework of an ongoing clinical study that has been approved by Swiss authorities (Swissethics protocol number 04/2014 ProjectID: PB_2016-00886, Swissmedic protocol 2016-MD-0002). The study is conducted at the Lausanne University Hospital (CHUV). All subjects signed written inform consent prior to their participation. The subjects were surgically implanted with a spinal cord stimulation system comprising an implantable pulse generator (Activa™RC, Medtronic plc, Fridley, Minnesota, SA) connected to a 16-electrode paddle array (Medtronic Specify™5-6-5 surgical lead) that was placed over the lumbosacral segments of the spinal cord. Subject related data and details on their neurological status at their entry into the clinical study, evaluated according to the International Standards for Neurological Classification of Spinal Cord Injury, are provided in **Table 4.1**.

Recording of EES-induced antidromic activity along human afferents

Recordings of the neural activity induced by EES were performed with the NIM Eclipse system (Medtronic plc, Fridley, Minnesota, USA). The activity of the soleus muscle was recorded with surface EMG electrodes (Ambu Neuroline 715, Ambu Sarl, Bordeaux, France), while the activity of the sural and of the proximal and distal branches of the tibial nerve were recorded using percutaneous disposable needle electrodes (Ambu Neuroline Twisted Pair Subdermal 12×0.4 mm, Ambu Sarl, Bordeaux, France). The proximal branch of the tibial nerve was recorded at the level of the popliteal fossa (**Figure 4.2**). The recording needle electrode insertion point was at the site that elicited an H-reflex at the lowest stimulation amplitude, identified by using a stimulation probe. The distal branch of the tibial nerve was recorded at the level of the medial malleolus (**Figure 4.2**). The recording electrode position was determined by applying electrical stimulation to this site and by verifying the evoked potentials at the level of the proximal branch of the tibial nerve. The sural nerve was recorded at the level of the lateral malleolus. The specific location of the electrode was defined following the same procedure as for the distal branch of the tibial nerve. Neural and EMG signals were sampled at 10000 Hz, amplified, and band-pass filtered (30-1000 Hz) online. For the entire duration of the experiment, participants remained relaxed in a supine position. EES was delivered at 20 Hz for 60 seconds in order to collect a total of approximately 1200 pulses. We selected EES sites that mainly recruited the posterior root innervating the S1 spinal segment, as verified in the presence of reflex responses in the soleus muscle following each pulse of EES. For the experiment, the stimulation amplitude was reduced until no muscle contraction was noticeable to avoid contaminating neural recordings with electromyographic activity or movement artifacts. To verify that the stimulation amplitude was sufficient to recruit afferent fibers in the recorded nerves, we controlled that the stimulation elicited a sensation of tingling in the corresponding dermatome. We recorded EES artifacts with surface electrodes positioned over the vertebral levels of the implanted paddle array. The artifacts were used as triggers to extract and average the evoked potentials.

Subject	#1	#2	#3
Gender	m	m	m
Age (y)	28	35	47
Years after SCI	6	6	4
WISCI II score	13	6	0
AIS	C	D	C*
Neurological level of injury	C7	C4	C7
UEMS total (max 50)	46	31	45
LER motor subscore (max 25)	14	13	0
LEL motor subscore (max 25)	0	12	0
LE motor score L2 (R/L)	2/0	2/2	0/0
LE motor score L3 (R/L)	2/0	4/4	0/0
LE motor score L4 (R/L)	4/0	2/1	0/0
LE motor score L5 (R/L)	4/0	1/1	0/0
LE motor score S1 (R/L)	2/0	4/4	0/0
LTR sensory subscore	38	29	26
LTL sensory subscore	37	36	29
LE sensory score L1 (R/L)	1/1	1/1	0/0
LE sensory score L2 (R/L)	1/1	1/1	0/0
LE sensory score L3 (R/L)	1/1	1/1	0/1
LE sensory score L4 (R/L)	1/1	1/2	0/0
LE sensory score L5 (R/L)	1/1	1/1	0/1
LE sensory score S1 (R/L)	1/1	0/1	1/1
LE sensory score S2 (R/L)	1/1	0/1	0/1
PPR sensory subscore	17	29	13
PPL sensory subscore	16	36	15
PPR, dermatome L1-S2	0	4	0
PPL, dermatome L1-S2	0	8	0

AIS, American Spinal Injury Association Impairment Scale; LEMS, Lower extremity motor score; SCI, spinal cord injury; LEL, Lower extremity left; LER, lower extremity right; LTL, Light touch left; LTR, Light touch right; PPL, Pin prick left; PPR, Pin prick right; R/L, right/left; UEMS, Upper extremity motor score; WISCI, Walking index for spinal cord injury.

*Reason of AIS C classification in spite of motor scores of 0 throughout all lower extremity key muscles is the presence of voluntary anal contraction.

Table 4.1 | Subjects' data and neurological status according to the International Standards for Neurological Classification of Spinal Cord Injury. All the values were collected before the surgical implantation.

Assessment of proprioceptive function during EES

The threshold to detection of passive movement test (Han et al., 2016) was performed with the Humac Norm Cybex system (Computer Sports Medicine Inc., Stoughton, US). Subjects were first tested without EES and then during continuous EES. Throughout the experiment, participants' tactile, visual, and aural information were occluded by using foam cushions, blindfolds, and headphones with pink noise. The experimental protocol was tailored for each participant, since each of them presented distinct levels of residual proprioceptive functions. At the beginning of each trial, the participant's knee joint was moved to an initial position of 45 degrees of extension. The participant was informed with a tap on the shoulder that a new trial was about to start. The trial was then started after a randomised time delay to assess false positive detections. In subject #1, we imposed movements of knee extension or knee flexion from the initial position at a constant angular velocity of 0.5 degrees per second. Flexion and extension were delivered randomly. The participant was instructed to report the movement direction, as soon as he became aware of it, by pushing a button. A maximum displacement of 15 degrees was allowed (**Figure 4.3B**). Button-triggered digital signal and joint kinematics were recorded at a sampling frequency of 5000 Hz. The trial was considered successful if the direction of the movement was correctly identified. A trial was considered unsuccessful when the movement was either misclassified or not perceived at all within the limited range of movement. Subject #3 was not able to detect the direction of the imposed movement, even in the absence of continuous EES. To simplify the task, we limited the movement to knee extension only, increased the movement speed to 1 degree per second, and allowed a maximum displacement of 30 degrees (**Figure 4.3B**). A trial was considered successful if the movement was detected within the allowed range of movement. Subject #2 was not able to perceive the imposed movements and was thus excluded from this experiment.

A total number of 15 repetitions or 10 successful repetitions were performed to complete an assessment for a given EES condition. The proportion between successful and unsuccessful trials was used to compute participants' error rate and 95% confidence interval by using the Clopper-Pearson interval method based on Beta distribution.

We adjusted the configuration of EES electrodes to target both flexor and extensor muscles of the knee. Recordings of the EMG activity from the vastus lateralis and semitendinosus muscles allowed the identification of the minimum stimulation amplitude necessary to recruit these muscles. We then assessed the proprioceptive functions of the subjects during continuous EES that was delivered with amplitudes below (0.8 times) and above (1.5 times) the muscle response threshold. For both amplitudes, we tested a range of frequencies: 10, 30, 50 and 100 Hz. At 1.5 the muscle response threshold amplitude, frequencies below 50 Hz induced spastic contractions, and were thus not tested.

Assessment of EES-induced responses modulated during passive joint movements

The Humac Norm Cybex was used to impose passive joint movements with a sinusoidal profile of fixed amplitude and frequency, while continuous EES was delivered to produce motor responses in the muscles spanning this joint. The subjects were asked to relax, neither to

resist, follow, nor facilitate the movements. Muscle responses and EES artifacts were recorded with wireless surface EMG electrodes (Myon 320, Myon AG, Schwarzenberg, Switzerland) at a sampling frequency of 5000 Hz. Joint kinematics was recorded with the Cybex system at 5000 Hz. EES parameters, as well as the targeted joint, the angular velocity and the amplitude of the movement were set depending on subject-specific constraints (**Figure 4.4A**). In subject #1, the Cybex system was used to produce flexion and extension movements of the ankle joint at a frequency of 1.13 Hz and a range of motion of 30 degrees. These parameters were chosen to be as large as possible in order to maximize the amount of proprioceptive signals generated from the targeted muscles while minimizing discomfort. EES electrodes were configured in order to recruit the targeted muscles. EES was delivered with frequencies ranging from 5 to 60 Hz. The stimulation amplitude was set to induce consistent muscle responses across the range of tested frequencies, corresponded to 1.25 times the muscle response threshold. For each condition tested, a minimum of 1 minute of recording was performed. Recording duration was extended to 2 minutes when EES was delivered at 5 Hz. In subject #2 and #3, we could not find electrode configurations that recruited the targeted muscles without causing discomfort at the required EES amplitudes and frequencies. Therefore, we adapted the experiment and targeted the knee joint instead of the ankle joint. Moreover, we limited the range of tested frequencies. Specifically, for subject #3 we kept an oscillation frequency of 1.13 Hz, set a movement range of 60 degrees, and limited the range of EES frequencies from 10 to 60 Hz. These settings also led to spastic contractions in subject #2. Consequently, we reduced the movement range and frequency to 50 degrees and 0.9 Hz, respectively, and limited the range of EES frequencies between 20 and 60 Hz.

To quantify the modulation of muscle responses during the passive movements, we extracted the timing of each EES pulse with the recorded stimulation artifacts. We then extracted the muscles responses and grouped them according to the phase of the cyclic movement (n = 10 bins) (**Figure 4.4B**). When more than one EES pulse occurred within a given bin, only the response with highest amplitude was selected. We bootstrapped the normalized modulation depth median and 95% confidence interval (**Equation 4.4**) by computing the median peak to peak amplitudes (mP2Ps) of the responses occurred in the different bins. Normalization was performed in order to account for frequency-dependent depression of EES-induced muscle responses (Ishikawa et al., 1966; Calancie et al., 1993; Schindler-Ivens & Shields, 2000).

$$Normalized Modulation Depth = \frac{|max(mP2Ps) - min(mP2Ps)|}{min(mP2Ps)} \quad \textbf{(Equation 4.4)}$$

Continuous EES during locomotion on a treadmill

The FLOAT robotic suspension system (Lutz Medical Engineering AG, Rudlingen, Switzerland) was used to provide the participants with personalized upward and forward forces to the trunk during locomotion on a treadmill (Vallery et al., 2013; Mignardot et al., 2017). EES was delivered through four independent configurations of electrodes. Each configuration involved

one or multiple anodes and cathodes. We configured these electrode combinations to target the left and right posterior roots projecting to the L1 and L4 segments. For this purpose, we searched the electrode configurations that activated preferentially the iliopsoas and the tibialis anterior. These motor pools spanned the L1/L2 segments and L4/L5 segments, respectively. The amplitude and frequency of these four electrode configurations were optimized by visual inspection of the induced EMG activity and facilitation of kinematics when subjects were asked to step on the treadmill. EMG recordings were performed with wireless surface electrodes (Myon 320, Myon AG, Schwarzenberg, Switzerland) and recorded at 1000 Hz. Leg kinematics was recorded using the Vicon motion capture system (Vicon Motion Systems, Oxford, UK) at 100 Hz. Subjects were allowed to use the handrails of the treadmill to facilitate their leg movements. Analysis of EMG activity and kinematics was conducted using methods reported in details previously (Mignardot et al., 2017).

Electrophysiological recordings of high-frequency low-amplitude EES

EES was delivered through electrode configurations that were used to facilitate locomotion. Motor responses to both single pulses and bursts of 4 pulses at 500 Hz were recorded from different lower limb muscles with wireless surface electrodes at a sampling rate of 5000 Hz (Myon 320, Myon AG, Schwarzenberg, Switzerland). The responses of the muscle that was recruited the most were used for the analyses. During the experiment, the participants were in the supine position.

4.4.3   Experimental procedures in rats

Animal husbandry

All procedures and surgeries were approved by the Veterinary Office of the canton of Geneva in Switzerland. The experiments were conducted in 9 adult female Lewis rats (220 g body weight) and 4 Long-Evans rats (240 g body weight). Rats were housed separately with a light/dark cycle of 12 hours.

Surgical procedures

Surgical procedures have been described in detail previously (Courtine et al., 2009; Van den Brand et al., 2012). All the interventions were performed in aseptic conditions and under general anesthesia. Briefly, rats received a severe thoracic (T8) contusion SCI (250 kdyn) by using a force-controlled spinal cord impactor (IH-0400 Impactor, Precision Systems and Instrumentation LLC, USA). During the same surgery, EES electrodes were sutured to the dura overlying the midline of S1 and L2 spinal segments in Lewis rats, and of L4 and L2 spinal segments in Long-Evans rats. Electrodes were created by removing a small part of insulation (400 μm) from Teflon-coated stainless-steel wires (AS632, Cooner Wire, USA). A common ground wire electrode (1 cm of active site) was placed subcutaneously over the right shoulder. Finally, bipolar electrodes (same type as used for EES) were implanted bilaterally in the left and right tibialis anterior muscles to record the EMG activity.

Assessment of EES induced responses modulated during passive joint movements

Lewis rats (n=4) were lightly anesthetized (Ketamine: 75 mg/kg and Xylazine 5 mg/kg, ip) and positioned in a prone position within a support system that let the hindlimbs hanging freely. The right paw was secured within a 3D printed pedal connected to a stepper motor (QSH4218-51-10-049, Trinamic Motion Control GmbH, Waterloohain, Germany). We used this robotic platform to impose cyclic movements of the ankle with a fixed amplitude (70 degrees) and frequency (0.54 Hz), while continuous EES was delivered to evoke responses in the tibialis anterior muscle (**Figure 4.4E**). EES was delivered using an IZ2H Stimulator controlled by a RZ2 BioAmp Processor (Tucker-Davis Technologies, Alachua, US). EES amplitude was set to approximately 1.2 times the muscle response threshold. We tested EES frequencies ranging from 5 to 100 Hz. EMG activity of the tibialis anterior was amplified with a PZ3 Low Impedance Amplifier (Tucker-Davis Technologies, Alachua, US) and recorded with the RZ2 BioAmp Processor at a sampling frequency of 24414 Hz. Ankle kinematics was record with the Vicon motion capture system at sampling frequency of 200 Hz. For each tested EES condition a minimum of 1 minute of recording was performed. To analyze the modulation of the muscle responses, we used the same procedures that we adopted in the equivalent experiment carried out in human subjects.

Electrophysiological recordings of high-frequency low-amplitude EES

We tested the impact of high-frequency low-amplitude EES in 5 Lewis rats. EES and EMG recordings were performed with the setup used for assessing the modulation of muscle responses during passive movements. The muscle response threshold was measured using single pulses of EES that were delivered at amplitudes close to this threshold, thus allowing to obtain a precise value. High-frequency bursts were then delivered at amplitudes below the identified motor response threshold. The aim was to evaluate whether high-frequency stimulation was able to recruit trans-synaptically motoneurons at lower amplitudes than single pulses. For each amplitude, we tested burst frequencies ranging from 100 to 1000 Hz. The duration of each burst was kept constant at 25 ms. During the experiments, the rats were held in a resting position with the hindlimbs hanging freely.

Continuous EES during locomotion on a treadmill

Behavioural experiments during locomotion were performed in 4 Long-Evans rats. Following one to two weeks of rehabilitation using previously described procedures (Courtine et al., 2009; Van den Brand et al., 2012), we evaluated the impact of different EES frequencies on the modulation of muscle activity and hindlimb kinematics during bipedal locomotion on a treadmill. Locomotion was recorded without EES and with EES at frequencies ranging from 20 to 80 Hz. EES amplitude was kept fixed at the optimal value found during training. For each experimental condition, a minimum of 10 steps or 20 seconds of minimal leg movements were recorded.

Hindlimb kinematics was recorded with the Vicon motion capture system (Vicon Motion Systems, Oxford, UK) at a sampling frequency of 200 Hz. EMG signals were amplified and

filtered online (10–10000 Hz band-pass) by a Differential AC Amplifier (A-M System, Sequim, US) and recorded at 2000 kHz with the Vicon system.

4.4.4 Statistics

Data are reported as mean ± standard error of the mean (SEM.) or median values ± 95% confidence interval (CI.). Confidence intervals and significance were analyzed using the non-parametric Wilcoxon rank-sum test with Bonferroni correction for multiple comparisons, student's t-test, the Clopper-Pearson interval based on Beta distribution method, or a bootstrapping approach based on the Monte Carlo algorithm resampling scheme (n=10'000 iterations).

4.5 Discussion

We have accumulated evidence that the antidromic recruitment of proprioceptive afferent axons during continuous EES blocks the propagation of naturally-generated proprioceptive signals to the brain and spinal cord. Computer simulations suggest that this cancellation of proprioceptive information disrupts the natural activity of reciprocal inhibitory networks that are essential to produce alternating recruitment of antagonist motor pools during locomotion. Consequently, only a narrow range of EES parameters can facilitate walking in people with SCI, which is insufficient to mediate clinically meaningful improvements of locomotion without extensive rehabilitation (C. Angeli et al., 2018; Gill et al., 2018). Computer simulations guided the design of EES protocols that not only preserve proprioceptive information but also enable a robust control over motoneuron activity. Here, we discuss the significance of these results, stress the dramatic consequences of the transient proprioceptive deafferentation during EES, and envision the avenues for translating these new stimulation protocols into clinical settings.

4.5.1 EES erases proprioceptive information in humans, but not in rats

Mounting evidence indicates that EES primarily recruits large-diameter afferent fibers within the posterior roots (Rattay et al., 2000; Ladenbauer et al., 2010; Capogrosso et al., 2013; Gerasimenko et al., 2006; Hofstoetter et al., 2018; Hofstoetter, Danner, et al., 2015). These afferent fibers mainly originate from proprioceptive organs, which sense changes in muscle length and tension, and to a lesser extent, mechanoreceptors within the skin. EES elicits orthodromic action potentials along the recruited afferent fibers that mediate the therapeutic effects of the stimulation (Moraud et al., 2016). However, we show that EES also induces antidromic action potentials that travel in the opposite direction. Indeed, recordings of peripheral nerve activity identified antidromic volleys propagating toward sensory organs in response to EES in humans. Previous studies documented the presence of antidromic action potentials traveling along the sensory fibers of the sciatic, peroneal and sural nerves in rats, dogs, nonhuman primates and humans in response to EES applied to thoracic segments (Su et al., 1992; Hunter & Ashby, 1994; Buonocore et al., 2008). Here, we establish the high occurrence of antidromic action potentials when EES targets the posterior roots of lumbar spinal cord segments.

We reasoned that EES-induced antidromic action potentials may collide with the action potentials conveying the natural proprioceptive information. The annihilation of action potentials following these collisions is due to the refractory period of Ranvier's nodes. Computer simulations predicted a high occurrence probability of these collisions along the recruited afferent fibers when EES is delivered at frequencies commonly used in human studies to facilitate movements after SCI. Due to the longer length and therefore larger propagation time of action potentials along human proprioceptive afferent axons, the incidence of these collisions is considerably higher than in rats. These results suggested that EES may partially cancel the natural proprioceptive information in humans.

To assess this possibility, we conducted experiments that highlighted the dramatic consequences of these collisions on the integration of proprioceptive information in the brain

and spinal cord of humans with SCI. First, we found that the delivery of continuous EES abolishes the conscious perception of leg position and displacement. Second, we showed that proprioceptive information drives the modulation of spinal circuits during movement, and consequently, that the cancellation of proprioceptive information during continuous EES disrupts this modulation.

During the past two decades, EES was applied to thousands of people for alleviating pain, and for improving motor functions after SCI (Herman et al., 2002; Carhart et al., 2004; Huang et al., 2006; Harkema, Gerasimenko, et al., 2011; C. A. Angeli et al., 2014; Grahn et al., 2017). For pain treatments, the stimulation is applied at the thoracic level at relatively low intensities. Consequently, the loss of sensation in the legs was not obvious. For SCI, the involved participants generally exhibited no or limited sensations in the legs, which may explain why this unexpected cancellation of proprioception information remained unnoticed. However, this phenomenon has far-reaching implications for the development of a therapy to restore locomotion with EES. Indeed, this transient proprioceptive deafferentation not only alters the conscious control of movement and the modulation of spinal circuits with EES, but may also compromise the reorganization of residual descending pathways during rehabilitation enabled by EES, as we discuss below.

4.5.2 Proprioceptive information must be preserved to enable locomotion with EES

Bipedal locomotion requires the integration of information from a multiplicity of sensory modalities. Proprioception may be the most important of these modalities. Proprioceptive information gives rise to a conscious perception of limb positions that play a critical role during walking (Dietz, 2002; Proske & Gandevia, 2012; Tuthill & Azim, 2018). For example, the sudden loss of proprioception induces severe gait deficits (Sanes et al., 1985; Cole, 1995). Individuals with a chronic loss of proprioception can learn to compensate for this loss with other sensory modalities, especially vision (Cole, 1995). While this adaptation enables them to walk again, the cognitive load associated with this execution obliged them to rely on a wheelchair in their daily life. All the human subjects involved in our study reported a loss of limb position awareness during EES. Consequently, this disruption of proprioception strongly limits the clinical relevance of continuous EES to support locomotor functions during daily living activities in people with SCI.

In addition to its integration in the brain, the information derived from proprioceptive organs is distributed throughout the spinal cord via a dense network of afferent feedback circuits that directly activate motoneurons and shape motor pattern formation during locomotion. Signals from muscle spindles and Golgi tendon organs determine the timing of phase transitions, contribute substantially to the recruitment of leg motoneuron pools, and coordinate the adaptions of leg movements to unpredictable perturbations and task-specific requirements (Dietz & Duysens, 2000; Rossignol et al., 2006; Hultborn & Nielsen, 2007). Our results suggest that these key mechanisms of motor control are obstructed during continuous EES. Moreover, the interruption of descending pathways reinforces the critical role of these

proprioceptive feedback circuits, which then become the primary source of control for motor pattern formation (Edgerton et al., 2004). For example, the integration of proprioceptive information enables the spinal cord to coordinate locomotion across a broad range of speeds, loads and directions in animal models of complete SCI (Courtine et al., 2009). The disruption of proprioceptive information during EES would severely deteriorate this ability of the spinal cord to coordinate motor pattern formation after SCI.

We previously documented some of the mechanisms through which EES facilitates locomotion in rats. In particular, we showed that the modulation of reciprocal inhibitory circuits via proprioceptive feedback during each phase of gait directs the excitatory drive elicited by EES towards the motoneuron pools that are functionally relevant at this specific time (Moraud et al., 2016). This mechanism transforms the unspecific excitatory drive into a spatially and temporally specific pattern of excitation delivered in an alternating manner to the motoneuron pools whose activation is required in the flexion and extension phases of the locomotor step cycle. The spinal cord thus acts as an elegant filter that endows EES with the necessary specificity for therapeutic applications. Due to the cancellation of proprioceptive information in humans, only narrow ranges of EES frequencies and amplitudes are able to take advantage of this mechanism. As soon as the stimulation elicits responses in muscles, computer simulations indicate that EES disrupts movement-related modulation of reciprocal inhibitory circuits. The resulting destabilization of the network leads to an imbalance in the excitation delivered to antagonist motor pools, favoring one motor pool over the other. Consequently, the modulation of EES parameters failed to enable the graded control over motoneuron activity that was observed in the rodent computational model. Experimental recordings confirmed these results, both in rodents and humans with SCI. We previously showed that this controllability enables targeting lesion-specific gait deficits and mediating task-specific adjustments of leg movements through closed-loop controllers and brain-spine interfaces in rats and nonhuman primates (Wenger et al., 2014; Capogrosso et al., 2016; Moraud et al., 2016). These features may be essential to facilitate the complex postural and propulsive requirements underlying the bipedal gait of humans.

Finally, input from proprioceptive organs plays a determinant role in steering the reorganization of residual descending pathways that help restore locomotion after SCI. Genetically modified mice lacking functional proprioceptive circuits display defective rearrangements of descending projections after SCI, which abolish the extensive recovery occurring spontaneously in wild-type mice after the same injury (Takeoka et al., 2014). Similarly, clinical studies reported that the preservation of proprioceptive information is a key predictor of recovery after neurotrauma (Park et al., 2008), suggesting that this specific sensory channel may also contribute to steering the reorganization of residual neuronal pathways in humans. Therefore, the disruption of natural proprioception may reduce the ability of EES to augment neuroplasticity and recovery when delivered during rehabilitation.

The multifaceted roles of proprioceptive information for coordinating locomotor functions and steering functional recovery after SCI emphasize the critical importance of identifying EES protocols that preserve proprioceptive information in order to fulfill the therapeutic

potential of this treatment paradigm for clinical applications.

4.5.3 EES strategies that replace or preserve proprioceptive information

We exploited this new understanding to design sensory-compliant EES protocols that circumvent the cancellation of natural proprioception during EES and may therefore augment the therapeutic efficacy of EES in humans. We identified two protocols, which we discuss below.

We first conceptualized a strategy that aims to replace the cancelled proprioceptive information with a spatiotemporal stimulation profile that encodes the natural firing rates of proprioceptive afferents from each muscle during locomotion. Computer simulations confirmed that this EES protocol not only preserves proprioceptive information but also augments the degree of control over motoneuron activity while preserving the alternation between antagonist muscles. Realistically, the afferents originating from a single muscle cannot be targeted specifically with current stimulation technologies. However, these stimulation protocols could be approximated with EES bursts delivered over spatially–selective spinal cord regions using a temporal sequence that coincides with the firing profile of the proprioceptive afferents innervating these specific spinal cord regions. This approach shares similarities with EES protocols that encode the spatiotemporal sequence of motoneuron activation during locomotion (Wenger et al., 2016). Compared to continuous EES, this targeted stimulation strategy enables a markedly higher degree of control over motoneuron activity in rodent and nonhuman primate models of SCI (Capogrosso et al., 2016; Wenger et al., 2016). Incidentally, the alternation of spatially-selective bursts also preserves the natural proprioceptive information flowing in the dorsal/posterior roots that are not engaged by the stimulation. Our simulations suggest that the delivery of EES bursts should coincide with the profile of proprioceptive afferent firing, which can be partially out of phase with motoneuron activity. However, we believe that this protocol would enhance the control over motoneuron activity, while additionally maximising the amount of preserved proprioceptive information. Such a stimulation strategy shares striking similarities with biomimetic approaches developed for the delivery of realistic tactile sensations in human amputees (Saal & Bensmaia, 2015). These similarities highlight the importance of developing biomimetic stimulation protocols to improve or restore nervous system functions in humans with disabilities.

We found that the delivery of EES bursts with a low amplitude, but high frequency may be an alternative or even a complementary stimulation strategy to minimize the cancellation of proprioceptive information. Due to the low amplitude, the stimulation recruits a limited number of afferents. Each proprioceptive afferent establishes synapses onto all the homonymous motoneurons (Mendell & Henneman, 1971; Segev et al., 1990). Consequently, the repeated recruitment of these afferents with EES bursts at high-frequency leads to a summation of excitatory post-synaptic potentials in motoneurons, which receive an overall amount of excitation that is equivalent to that induced by continuous EES at high amplitude and low frequency. However, all the non-recruited afferents continue providing essential information about the change in length and tension in the muscles. These results have general implications for EES protocols. First, the modulation of EES bursts allows them to augment the amount of

excitation delivered to motoneurons without the need to increase the stimulation amplitude. Second, the lower amplitude requirements would improve the spatial selectivity of the stimulation, since the volume of the electrical field is proportional to the current amplitude.

These novel stimulation protocols require dedicated implantable pulse generators that allow the delivery of EES bursts with high-frequency resolution through independent current sources that are controllable independently in real-time. Various companies are developing next-generation implantable pulse generators that partially meet these requirements. In parallel, we are conducting a clinical study using a commercially available stimulator that we upgraded to enable real-time control of spatially selective EES trains. We found that within 1 week, spatiotemporal stimulation enables independent weight-bearing locomotion in the three participants of the present study (Wagner et al., 2018). These combined findings stress the necessity of developing new neurotechnologies that support the implementation of strategies that preserve proprioception to facilitate motor control and steer plasticity with EES in humans.

5 Conclusions and perspectives

This thesis aimed at studying the mechanisms through which epidural electrical stimulation (EES) of the spinal cord facilitates movements in animal models and people with paralysis, and at exploiting the acquired knowledge to design hypothesis-driven strategies augmenting the efficacy of this therapy.

The prevailing view is that EES excites the whole spinal locomotor network by recruiting large-diameter proprioceptive afferents (Minassian et al., 2007; Capogrosso et al., 2013), and thus increases the responsiveness of spinal circuits to peripheral sensory signals and residual descending commands (C. A. Angeli et al., 2014; Danner et al., 2015). However, the mechanisms through which the recruitment of proprioceptive afferents leads to motor pattern formation remains mostly unclear. Consequently, the development of EES strategies has been mainly supported by inductive, empirical observations, which restricted the delivery of EES to continuous, non-modulated stimulation patterns. While these EES strategies were shown to enable locomotion in rodent models of SCI (Courtine et al., 2009), they failed to provide similar results in people with paralysis (Carhart et al., 2004; C. A. Angeli et al., 2014). In order to optimize the therapeutic efficacy of EES in humans, here we explored how EES interacts with the recruited sensorimotor circuits, and investigated the possible mechanisms underlying these species-specific responses to EES. For this, we used a deductive approach based on computer simulation and hypothesis-driven behavioral, electrophysiological and psychophysical experiments.

In this chapter, first I briefly summarize the main findings of this thesis, then I discuss the proposed strategies to augment the efficacy of EES therapies. I also discuss current and future works in perspective of these results, and I finally highlight the most important outcomes of this work.

5.1 Summary of the main findings

In **Chapter 2**, we studied the mechanisms through which continuous EES promotes locomotion in rat models of SCI. For this, we developed a dynamic model of rat muscle spindle feedback circuits during locomotion, and modeled the interaction between these circuits and EES. Using this model, we showed that EES increases the mean firing rate of the recruited

proprioceptive afferents, without interfering with the ongoing natural activity during locomotion. This increased afferent activity — integrated into muscle spindle feedback circuits — was then sufficient to elicit alternating flexor and extensor motoneuron bursts, which resembled those recorded during EES-induced locomotion. Notably, the modulation of EES parameters allowed for fine control over the amplitude of motoneuron bursts, as observed in behavioral experiments. We proposed that two synergistic mechanisms enable EES to promote this locomotor-like activity. First, EES supports the emergence of motor activity by increasing the excitatory drive reaching motoneurons. Second, EES promotes the phasic recruitment of flexor an extensor muscles by strengthening the activity of reciprocal inhibitory networks. In turn, the natural activity of proprioceptive afferents generated during movement controls the alternation of these reciprocal inhibitory networks, and thus allows the generation of functional motor patterns. As such, proprioceptive signals act as a source of control that gates the unspecific excitation provided by EES towards functionally relevant pathways. This mechanistic understanding allowed us to develop an EES strategy that improved the general locomotor performance by exploiting the natural dynamics of the engaged sensorimotor circuits. Given the broad conservation of the recruited circuits across mammals, similar strategies may have the potential to promote locomotion also in humans. These results reveal the critical role of proprioceptive signals and muscle spindle feedback circuits in mediating the therapeutic effect of continuous EES.

In **Chapter 3**, we explored whether acting on proprioceptive signals by adjusting trunk posture allow refining stepping performance during EES-enabled treadmill locomotion in rat models of SCI. By combining computer simulations and behavioral experiments, we showed that adjustments in the mediolateral trunk orientation significantly affect bilateral leg proprioceptive signals and muscle activities. We found that because of lesion-specific inter limb asymmetries during stepping, a vertical trunk orientation commonly caused profound differences between the stretch profiles of bilateral flexor and extensor muscles. We showed that controlling trunk posture is possible to restore balanced proprioceptive feedback signals, and thus to promote the production of stable bilateral motor patterns. We leveraged this understanding to design a trunk-posture control paradigm that automatically restored proprioceptive feedback signals balance during gait, and thus improved the locomotor performance. Similar trunk posture control paradigms might promote the efficacy of EES during gait rehabilitation in humans. These results highlight the remarkable influence both of trunk posture on proprioceptive feedback circuits during locomotion and of proprioceptive signals on the effect of EES.

In **Chapter 4**, we investigated species-specific effects of EES. Hypothesis-driven simulations revealed that in humans, as opposed to rats, the antidromic recruitment of proprioceptive afferents by continuous EES prevents a significant proportion of proprioceptive signals from reaching the spinal cord. We explained that this phenomenon arises from the difference in size between humans and rats, and from the lower firing rate of proprioceptive afferents in humans. We validated this prediction with a series of experiments in rats and people with SCI. We showed that continuous EES — delivered at amplitudes and frequencies commonly used to facilitate locomotion — abolishes the conscious ability to perceive leg

movements, and disrupts the afferent modulation of spinal sensorimotor circuits in humans, but not in rats. Due to this phenomenon, simulations suggested that in humans only a limited range of stimulation parameters can be used to excite spinal sensorimotor circuits without compromising the natural modulation of reciprocal inhibitory networks. Thus, only a limited facilitation of locomotion can be achieved compared to rats. We corroborated these predictions by performing behavioral experiments in rats and people with severe SCI. While continuous EES enabled robust control over locomotion in rats, the limited range of functional EES parameters prevented a similar facilitation of gait in the study participants. Lastly, we proposed two novel stimulation strategies that might augment the therapeutic efficacy of EES by limiting the amount of sensory information disrupted. These sensory-compliant strategies involve the use of spatiotemporal stimulation profiles encoding the natural proprioceptive signals generated during locomotion (sensory-encoding spatiotemporal EES), and the continuous delivery of high-frequency low-amplitude bursts of EES. These results reveal a critical limitation of continuous EES therapies, and hold crucial implications for the design of novel EES therapies that aims at promoting the recovery of locomotion after SCI.

5.2 Proposed strategies to increase the efficacy of EES therapies

In this thesis, we proposed multiple, complementary strategies to increase the efficacy of EES-based therapies in humans; namely, to increase the amount of motor facilitation that can be provided by EES, and to augment the level of controllability over the motor patterns produced during gait. Here, I discuss these strategies in light of the limitations of continuous EES found in Chapter 4, and how they can be combined together to maximize the ability of EES to address patient-specific locomotor deficits.

In Chapter 2, we argued that addressing lesion-specific gait deficits is fundamental to optimize the outcome of rehabilitation strategies. Therefore, we proposed a stimulation protocol that allowed correcting bilateral gait deficits in rats with SCI, by modulating the stimulation frequency during different phases of gait. This stimulation protocol was based on the observation that adjusting the frequency of continuous EES protocols allows one to finely control muscle activities produced during gait. Since EES recruits similar neural circuits across species, we argued that adopting the same strategy in humans might provide similar effects. However, in Chapter 4, we found that only a limited range of EES parameters can be used to facilitate locomotion in humans. This phenomenon — that we suggest is due to the interference of continuous EES with proprioceptive signals — critically limits the amount of facilitation that can be provided during walking, and the level of control over motor patterns. Therefore, modulating the stimulation frequency during different phases of gait would only result in minor benefits. As such, the protocol proposed in Chapter 2 is not fully translatable to humans.

To overcome the limitations of continuous EES, we proposed two sensory-compliant EES protocols, i.e., continuous High-Frequency Low-Amplitude (HFLA) EES and Sensory-Encoding Spatiotemporal (SES) EES. Simulations showed that both protocols provide a larger facilitation of movements and an increased level of controllability over motoneuronal firing

during gait. In particular, simulations showed that using HFLA bursts of EES, motoneurons firings can be precisely controlled by modulating the inter-burst interval. Therefore, HFLA EES protocols would enable one to address gait deficits as proposed in Chapter 2. On the other hand, simulations showed that SES EES protocols can modulate motoneurons firings by scaling up the temporal profiles used to control the stimulation parameters. Since this strategy intrinsically relies on the selective recruitment of different muscle groups, patient-specific deficits can be addressed by independently modulating the amplitude of the waveforms used to stimulate the different spinal segments. Finally, in Chapter 3, we showed that lesion-specific gait deficits can also be addressed by adjusting trunk posture during stepping. This assistive strategy directly acts on the proprioceptive signals reaching the spinal cord, and thus is complementary to the proposed stimulation strategies. Therefore, we propose that the combination of this assistive strategy with sensory-compliant EES protocols modulated during gait will allow for the highest level of controllability over the effects of EES.

While the proposed stimulation strategies need to be validated, these paradigms provide a new range of opportunities to facilitate locomotion and to address patient-specific gait deficits in people with SCI using EES.

5.3 Perspectives

The work presented in this thesis represents a significant step towards the development of successful EES rehabilitation paradigms that might promote a full recovery of locomotion in people with SCI. However, there are still several challenges that need to be faced before reaching this milestone. Here, I discuss three lines of research that we are currently addressing to translate EES into a viable clinical application.

5.3.1 Towards sensory-compliant EES protocols that enable locomotion in people with SCI

In Chapter 4, we proposed two sensory-compliant stimulation strategies that might overcome the highlighted limitations of continuous EES; namely, SES EES, and continuous HFLA EES. Testing the therapeutic efficacy of both these strategies in clinical settings is one of our strongest priorities. To date, however, neurostimulation technologies fail to provide the required features to deliver continuous HFLA EES, and limit the implementation of SES EES protocols.

Despite these limitations, our research group recently validated the relevance of sensory-compliant EES protocols in a pilot clinical study on people with severe SCI (Wagner et al., 2018). In this study, we used commercially available electrode arrays and implantable pulse generators (IPGs) with an upgraded firmware allowing for near real-time triggering capabilities. These technologies prevented the direct implementation of the proposed SES EES. Yet, they allowed developing a comparable spatiotemporal EES strategy that we used to facilitate gravity-assisted walking. Specifically, we defined electrode configurations that selectively recruited group of muscles acting at distinct lower limb joints. We then built trains of stimulation pulses that targeted these distinct muscle groups at different phases of the gait cycle. The timing

and duration of these stimulation bursts were optimized in order to produce the strongest facilitation of locomotion, and were largely in accordance with the sensory profiles emerging from the targeted muscles. By controlling the described stimulation strategy via a closed loop controller monitoring body kinematics, participants immediately regained voluntary control over previously paralyzed muscles during walking — to a degree that exceeded what has been achieved with continuous EES (Chapter 4). The application of this EES strategy during gait rehabilitation was shown to promote the recovery of voluntary control over previously paralyzed muscles, even in the absence of stimulation. At the end of the rehabilitation program, all participants had marked improvements in locomotor functions, with two subjects (over three) regaining the ability to transit from sitting to standing and walking with crutches.

These results demonstrate the critical relevance of spatiotemporal EES protocols and stress the importance of developing sensory-compliant stimulation strategies to further promote the recovery of locomotion after SCI. It is therefore essential to push forward the development of neurostimulation technologies that fulfill the requirements of the proposed strategies, as described in the next section.

5.3.2 Next generation technologies for EES-based rehabilitation strategies

The results presented in this thesis have highlighted the need for developing new neurostimulation and assistive technologies to augment the efficacy of current EES-based rehabilitation strategies.

Regarding neurostimulation technologies, the implementation of the proposed sensory-compliant stimulation strategies (SES EES and continuous HFLA EES) would need a redesign of both current electrode arrays and IPGs. First, both strategies would benefit from high-density electrode arrays. In particular, SES EES would take advantage of high-density electrode arrays to achieve the required stimulation selectivity. Conversely, continuous HFLA EES would benefit from this technology to ensure an unspecific recruitment of multiple dorsal roots — despite the low amplitude involving this strategy. Second, current IPGs fail to provide the required level of control over the stimulation waveforms. Specifically, SES EES requires IPGs able to generate multiple waveforms that can be independently controlled in real-time, with a high frequency and amplitude resolution. Alternatively, HFLA EES requires IPGs that can deliver high-frequency bursts (up to approximately 700 Hz), of length and frequency that can be precisely controlled, through multiple independent current sources.

Regarding assistive technologies, we showed that by adjusting trunk posture it is possible to ameliorate the motor patterns generated by EES, and restore stepping symmetry in rat models of SCI. However, current bodyweight support systems or exoskeletons used in gait rehabilitation often restrict trunk movements. Therefore, to further promote the efficacy of EES-based therapies and gait rehabilitation, future assistive technologies will need to allow for a greater control over trunk posture.

Currently, several companies are focusing on the development of new technologies fulfilling most of these requirements, promising a forthcoming clinical fruition of the rehabilitation strategies here proposed.

5.3.3 Towards the design of targeted drugs to augment the efficacy of EES

A complementary approach to overcome the highlighted limitations of continuous EES in humans might be to modulate pharmacologically the sensorimotor circuits engaged by EES. Specifically, increasing the excitability of proprioceptive feedback circuits would provide two benefits. First, it might reduce the amount of excitation that needs to be provided by EES to allow the formation of motor patterns. Consequently, it would allow using lower EES amplitudes and frequencies, and thus reduce the amount of proprioceptive information blocked by EES. Second, it might reduce the amount of proprioceptive signals required to steer the excitation delivered by EES. Therefore, a larger amount of sensory signals could be blocked without disrupting the natural modulation of proprioceptive sensorimotor circuits. As such, a larger range of stimulation parameters would be available to facilitate locomotion. This would translate in a larger control over motoneurons firings, thus enhancing the ability of EES to facilitate locomotion.

Several studies in rodents demonstrated that different pharmacological agents can enhance the efficacy of EES (Courtine et al., 2009; Musienko et al., 2011). Among these, serotonin receptor agonists (5-HT and 8-OHDPAT) were shown to be the most effective (Courtine et al., 2009). As described in Chapter 2, the use of 5-HT agonists increases the overall excitability of the spinal locomotor network, thus further facilitating the production of locomotion during EES. In particular, we showed that these drugs significantly reduce the amount of excitation that needs to be delivered by EES to produce desired levels of motoneuronal activity. For example, delivering 40 Hz EES together with serotonin agonists elicited motoneuronal activity profiles similar to those induce by EES delivered at 80 Hz in the absence of serotonin (**Figure 2.11**). Applying these drugs in humans might provide similar facilitatory effects. However, due to the broad distribution of serotonin receptors across the whole peripheral and central nervous systems, this strategy remains inadequate for clinical applications. Compared to serotonin agonists, several studies suggest that α_2 adrenergic receptors might allow for a more targeted modulation of spinal sensorimotor circuits engaged by EES (Chau et al., 1998; Musienko et al., 2011). However, the functional organization and anatomical distribution of these receptors are still unclear. In addition, the ability of pharmacological agents acting on these receptors to facilitate locomotion in combination with EES is controversial (Chau et al., 1998; Musienko et al., 2011).

To address these questions, we are currently investigating the organization of noradrenergic circuits in the rodent spinal cord and their interaction with EES. For this, we first studied the spatial and functional distribution of the α_2 receptor subtypes (α_{2a} and α_{2c}) in the lumbar mammal spinal cord (Bartholdi et al., 2016). We found that α_{2a} receptors modulate proprioceptive feedback circuits, whereas α_{2c} receptors regulate the activity of cutaneous sensorimotor pathways. Although EES mainly recruits large proprioceptive afferents (group-Ia and Ib), Aβ afferents innervating low-threshold mechanoreceptors have also been suggested to be recruited by EES (Capogrosso et al., 2013). These results suggest that both α_2 receptor subtypes could potentially disrupt or enhance the effect of EES. To evaluate these possibilities, we are expanding the neuromusculoskeletal computational model developed within this the-

sis to include the cutaneous sensorimotor pathways targeted by the α_{2c} receptor subtype. Our goal is to take advantage of this model to engineer a pharmaceutical neuromodulation strategy that augments the efficacy of EES by specifically modulating the recruited sensorimotor circuits.

5.3.4 Towards a closed loop neuromusculoskeletal model of locomotion

In this thesis, we developed a neuromusculoskeletal model of the spinal sensorimotor circuits that controls a couple of antagonist muscles. While this model improved our understanding of how EES interacts with the recruited proprioceptive afferents to facilitate locomotion, two main limitations need to be addressed to allow future investigations. First, the model is feedforward, i.e., the coupling between the musculoskeletal and the neural components is unidirectional. Specifically, here the musculoskeletal model was used to estimate the afferent firings from experimental data. In turn, the estimated firings were used to drive the neural network activity, together with EES. Finally, motoneuronal activity was computed by integrating the neural network over time, and used as a proxy to evaluate the effect of EES on the motor output. However, there was no link between the neural network and the musculoskeletal model. Therefore, the effectiveness of this model in investigating the mechanisms of motor pattern formation is restricted. Secondly, the developed model only considered muscle spindle feedback circuits. However, several other spinal circuits are engaged during locomotion.

We are currently addressing these limitations in collaboration with the Human Brain Project. In particular, we are developing a closed loop neuromusculoskeletal model of rodent and human treadmill locomotion. To this end, we created a simulation platform that allows running closed loop neuromusculoskeletal simulations, in which the motor output generated by the modeled neural networks is used to drive the musculoskeletal model with muscle activations, while the musculoskeletal model is used to drive the neural network with sensory activity. We are now extending the modeled network to include the sensorimotor circuits integrating load information generated by Golgi tendon organs and cutaneous mechanoreceptors. These sensory signals are fundamental to shape locomotor patterns (Pearson, 1993; Rossignol et al., 2006; Lacquaniti et al., 2012). In parallel, we are expanding the network to control all main muscles of the lower limbs, and integrating populations of commissural interneurons to control left-right limb coordination (Shevtsova et al., 2015).

The benefits of such a closed loop model are multiple. First, it will allow predicting with a higher precision the motor output produced by a given EES paradigm, and thus to further optimize current simulation protocols. Second, it will provide a mechanistic tool to assess how different neuronal networks in the spinal cord can control movement by integrating the natural flow of sensory information. Finally, it will allow probing how supraspinal centers interact with the spinal circuits to control locomotion.

The ultimate objective is to create an accurate neuromusculoskeletal model of locomotion that will allow using optimization algorithms to develop new strategies to enable locomotion after SCI.

5.4   General conclusion

In this thesis, we uncovered key mechanisms through which EES facilitates locomotion, and we highlighted critical limitations of continuous EES therapies when applied to humans. We provided compelling evidence suggesting that proprioceptive signals are essential for guiding the therapeutic effect of EES, and that acting on these signals through assistive technologies can augment the efficacy of this therapy. In addition, we demonstrated that in rodents EES works in synergy with these signals to promote locomotion. Conversely, we showed that in humans continuous EES blocks the sensory information traveling along the recruited afferent fibers. We argued that this difference explains, at least partially, why current stimulation strategies failed to translate into viable clinical applications, despite the promising results achieved in preclinical experiments. Finally, we proposed novel stimulation paradigms that might limit the interference of EES with proprioceptive signals, and thus augment the therapeutic efficacy of EES in humans. While partially validated, new neurostimulation technologies will be essential to thoroughly test the potential of these strategies to restore locomotion in people with SCI.

6 Bibliography

References

Abraira, V. E., & Ginty, D. D. (2013, August). The sensory neurons of touch. *Neuron*, *79*(4), 618–639.

Akay, T., Tourtellotte, W. G., Arber, S., & Jessell, T. M. (2014, November). Degradation of mouse locomotor pattern in the absence of proprioceptive sensory feedback. *Proceedings of the National Academy of Sciences of the United States of America*, *111*(47), 16877–16882.

Albert, F., Bergenheim, M., Ribot-Ciscar, E., & Roll, J.-P. (2006, June). The Ia afferent feedback of a given movement evokes the illusion of the same movement when returned to the subject via muscle tendon vibration. *Experimental brain research*, *172*(2), 163–174.

Amos, A., Armstrong, D. M., & Marple-Horvat, D. E. (1990, February). Changes in the discharge patterns of motor cortical neurones associated with volitional changes in stepping in the cat. *Neuroscience letters*, *109*(1-2), 107–112.

Anderson, K. D. (2004, October). Targeting recovery: priorities of the spinal cord-injured population. *Journal of neurotrauma*, *21*(10), 1371–1383.

Angeli, C., Boakye, M., Morton, R. A., Vogt, J., Benton, K., Chen, Y., ... Harkema, S. J. (2018, September). Recovery of over-ground walking after chronic motor complete spinal cord Injury . *New England Journal of Medicine*.

Angeli, C. A., Edgerton, V. R., Gerasimenko, Y. P., & Harkema, S. J. (2014, May). Altering spinal cord excitability enables voluntary movements after chronic complete paralysis in humans. *Brain : a journal of neurology*, *137*(Pt 5), 1394–1409.

Arber, S. (2012, June). Motor circuits in action: specification, connectivity, and function. *Neuron*, *74*(6), 975–989.

Armour, B. S., Courtney-Long, E. A., Fox, M. H., Fredine, H., & Cahill, A. (2016, October). Prevalence and Causes of Paralysis-United States, 2013. *American journal of public health*, *106*(10), 1855–1857.

Asboth, L., Friedli, L., Beauparlant, J., Martinez-Gonzalez, C., Anil, S., Rey, E., ... Courtine, G. (2018, April). Cortico-reticulo-spinal circuit reorganization enables functional recovery after severe spinal cord contusion. *Nature Neuroscience*, *21*(4), 576–588.

Barbeau, H. (2003, March). Locomotor training in neurorehabilitation: emerging rehabilitation

concepts. *Neurorehabilitation and neural repair*, *17*(1), 3–11.

Barbeau, H., McCrea, D. A., O'Donovan, M. J., Rossignol, S., Grill, W. M., & Lemay, M. A. (1999, July). Tapping into spinal circuits to restore motor function. *Brain research. Brain research reviews*, *30*(1), 27–51.

Barbeau, H., & Rossignol, S. (1987, May). Recovery of locomotion after chronic spinalization in the adult cat. *Brain research*, *412*(1), 84–95.

Barbeau, H., & Rossignol, S. (1990, April). The effects of serotonergic drugs on the locomotor pattern and on cutaneous reflexes of the adult chronic spinal cat. *Brain research*, *514*(1), 55–67.

Barrière, G., Mellen, N., & Cazalets, J. R. (2004, March). Neuromodulation of the locomotor network by dopamine in the isolated spinal cord of newborn rat. *The European journal of neuroscience*, *19*(5), 1325–1335.

Bartels, A. L., & Leenders, K. L. (2008). Brain imaging in patients with freezing of gait. *Movement Disorders*, *23*(S2), S461–S467.

Bartholdi, K., Barraud, Q., Formento, E., Rowald, A., Musienko, P., Capogrosso, M., & Courtine, G. (2016). Noradrenergic pathways and epidural electrical stimulation synergistically modulate proprioceptive feedback circuits in order to restore locomotion after spinal cord injury . *Program No. 158.21 SS6. Neuroscience Meeting Planner. San Diego, CA Society for Neuroscience, 2016 . Online.*.

Basbaum, A. I., & Fields, H. L. (1984). Endogenous pain control systems: brainstem spinal pathways and endorphin circuitry. *Annual review of neuroscience*, *7*(1), 309–338.

Bawa, P., & Chalmers, G. (2008, December). Responses of human motoneurons to high-frequency stimulation of Ia afferents. *Muscle & nerve*, *38*(6), 1604–1615.

Belanger, M., Drew, T., Provencher, J., & Rossignol, S. (1996, July). A comparison of treadmill locomotion in adult cats before and after spinal transection. *Journal of Neurophysiology*, *76*(1), 471–491.

Beloozerova, I. N., & Sirota, M. G. (1993, February). The role of the motor cortex in the control of accuracy of locomotor movements in the cat. *The Journal of physiology*, *461*(1), 1–25.

Beloozerova, I. N., Zelenin, P. V., Popova, L. B., Orlovsky, G. N., Grillner, S., & Deliagina, T. G. (2003, December). Postural control in the rabbit maintaining balance on the tilting platform. *Journal of Neurophysiology*, *90*(6), 3783–3793.

Berniker, M., Jarc, A., Bizzi, E., & Tresch, M. C. (2009, May). Simplified and effective motor control based on muscle synergies to exploit musculoskeletal dynamics. *Proceedings of the National Academy of Sciences of the United States of America*, *106*(18), 7601–7606.

Booth, V., Rinzel, J., & Kiehn, O. (1997). Compartmental model of vertebrate motoneurons for Ca2+-dependent spiking and plateau potentials under pharmacological treatment. *Journal of Neurophysiology*.

Borton, D., Bonizzato, M., Beauparlant, J., DiGiovanna, J., Moraud, E. M., Wenger, N., . . . Courtine, G. (2014, January). Corticospinal neuroprostheses to restore locomotion after spinal cord injury. *Neuroscience Research*, *78*, 21–29.

Borton, D., Micera, S., Millán, J. d. R., & Courtine, G. (2013, November). Personalized neuro-prosthetics. *Science Translational Medicine*, *5*(210), 210rv2–210rv2.

Bouyer, L. J. G., & Rossignol, S. (2003a, December). Contribution of cutaneous inputs from the hindpaw to the control of locomotion. I. Intact cats. *Journal of Neurophysiology*, *90*(6), 3625–3639.

Bouyer, L. J. G., & Rossignol, S. (2003b, December). Contribution of cutaneous inputs from the hindpaw to the control of locomotion. II. Spinal cats. *Journal of Neurophysiology*, *90*(6), 3640–3653.

Brown, A. G., & Fyffe, R. E. (1978, January). The morphology of group Ia afferent fibre collaterals in the spinal cord of the cat. *The Journal of physiology*, *274*(1), 111–127.

Brown, T. G. (1911, December). The Intrinsic Factors in the Act of Progression in the Mammal. *Proceedings of the Royal Society B: Biological Sciences*, *84*(572), 308–319.

Brown, T. G. (1912, July). The Factors in Rhythmic Activity of the Nervous System. *Proceedings of the Royal Society B: Biological Sciences*, *85*(579), 278–289.

Brown, T. G. (1914, March). On the nature of the fundamental activity of the nervous centres; together with an analysis of the conditioning of rhythmic activity in progression, and a theory of the evolution of function in the nervous system. *The Journal of physiology*, *48*(1), 18–46.

Buchanan, T. S., Lloyd, D. G., Manal, K., & Besier, T. F. (2004, November). Neuromusculoskeletal Modeling: Estimation of Muscle Forces and Joint Moments and Movements from Measurements of Neural Command. *Journal of Applied Biomechanics*, *20*(4), 367–395.

Buonocore, M., Bonezzi, C., & Barolat, G. (2008, February). Neurophysiological evidence of antidromic activation of large myelinated fibres in lower limbs during spinal cord stimulation. *Spine*, *33*(4), E90–3.

Burke, R. E. (1968, June). Group Ia synaptic input to fast and slow twitch motor units of cat triceps surae. *The Journal of physiology*, *196*(3), 605–630.

Burkitt, A. N. (2006, July). A review of the integrate-and-fire neuron model: I. Homogeneous synaptic input. *Biological cybernetics*, *95*(1), 1–19.

Butt, S. J. B., & Kiehn, O. (2003). Functional Identification of Interneurons Responsible for Left-Right Coordination of Hindlimbs in Mammals. *Neuron*, *38*(6), 953–963.

Calancie, B., Broton, J. G., John Klose, K., Traad, M., Difini, J., & Ram Ayyar, D. (1993, June). Evidence that alterations in presynaptic inhibition contribute to segmental hypo- and hyperexcitability after spinal cord injury in man. *Electroencephalography and Clinical Neurophysiology/Evoked Potentials Section*, *89*(3), 177–186.

Capaday, C. (2002). The special nature of human walking and its neural control. *Trends in Neurosciences*, *25*(7), 370–376.

Capaday, C., & Stein, R. B. (1986, May). Amplitude modulation of the soleus H-reflex in the human during walking and standing. *Journal of Neuroscience*, *6*(5), 1308–1313.

Capogrosso, M., Milekovic, T., Borton, D., Wagner, F., Moraud, E. M., Mignardot, J.-B., … Courtine, G. (2016, November). A brain–spine interface alleviating gait deficits after spinal cord injury in primates. *Nature Publishing Group*, *539*(7628), 284–288.

Capogrosso, M., Wenger, N., Raspopovic, S., Musienko, P., Beauparlant, J., Bassi Luciani, L., … Micera, S. (2013, December). A computational model for epidural electrical stimulation of spinal sensorimotor circuits. *The Journal of neuroscience : the official journal of the*

Society for Neuroscience, *33*(49), 19326–19340.

Carhart, M. R., He, J., Herman, R., D'Luzansky, S., & Willis, W. T. (2004, March). Epidural spinal-cord stimulation facilitates recovery of functional walking following incomplete spinal-cord injury. *IEEE transactions on neural systems and rehabilitation engineering : a publication of the IEEE Engineering in Medicine and Biology Society*, *12*(1), 32–42.

Carrier, L., Brustein, E., & Rossignol, S. (1997, April). Locomotion of the hindlimbs after neurectomy of ankle flexors in intact and spinal cats: model for the study of locomotor plasticity. *Journal of Neurophysiology*, *77*(4), 1979–1993.

Cavagna, G. A., Willems, P. A., & Heglund, N. C. (2000). The role of gravity in human walking: pendular energy exchange, external work and optimal speed. *The Journal of physiology*, *528*(3), 657–668.

Chandler, S. H., Baker, L. L., & Goldberg, L. J. (1984). Characterization of synaptic potentials in hindlimb extensor motoneurons duringl-DOPA-induced fictive locomotion in acure and chronic spinal cats. *Brain research*, *303*(1), 91–100.

Chau, C., Barbeau, H., & Rossignol, S. (1998, January). Early locomotor training with clonidine in spinal cats. *Journal of Neurophysiology*, *79*(1), 392–409.

Christie, K. J., & Whelan, P. J. (2005, August). Monoaminergic establishment of rostrocaudal gradients of rhythmicity in the neonatal mouse spinal cord. *Journal of Neurophysiology*, *94*(2), 1554–1564.

Clarac, F., Cattaert, D., & Le Ray, D. (2000, May). Central control components of a 'simple' stretch reflex. *Trends in Neurosciences*, *23*(5), 199–208.

Cole, J. (1995). *Pride and a Daily Marathon*. MIT Press.

Collins, W. F., Honig, M. G., & Mendell, L. M. (1984, November). Heterogeneity of group Ia synapses on homonymous alpha-motoneurons as revealed by high-frequency stimulation of Ia afferent fibers. *Journal of Neurophysiology*, *52*(5), 980–993.

Conway, B. A., Hultborn, H., & Kiehn, O. (1987, November). Proprioceptive input resets central locomotor rhythm in the spinal cat. *Experimental brain research*, *68*(3).

Courtine, G., & Bloch, J. (2015, April). Defining ecological strategies in neuroprosthetics. *Neuron*, *86*(1), 29–33.

Courtine, G., Gerasimenko, Y. P., Van den Brand, R., Yew, A., Musienko, P., Zhong, H., … Edgerton, V. R. (2009, September). Transformation of nonfunctional spinal circuits into functional states after the loss of brain input. *Nature Neuroscience*, *12*(10), 1333–1342.

Courtine, G., Harkema, S. J., Dy, C. J., Gerasimenko, Y. P., & Dyhre-Poulsen, P. (2007, August). Modulation of multisegmental monosynaptic responses in a variety of leg muscles during walking and running in humans. *The Journal of physiology*, *582*(Pt 3), 1125–1139.

Danner, S. M., Hofstoetter, U. S., Freundl, B., Binder, H., Mayr, W., Rattay, F., & Minassian, K. (2015, January). Human spinal locomotor control is based on flexibly organized burst generators. *Brain : a journal of neurology*.

de Leon, R. D., Tamaki, H., Hodgson, J. A., Roy, R. R., & Edgerton, V. R. (1999, July). Hindlimb locomotor and postural training modulates glycinergic inhibition in the spinal cord of the adult spinal cat. *Journal of Neurophysiology*, *82*(1), 359–369.

Deliagina, T. G., Zelenin, P. V., & Orlovsky, G. N. (2012, August). Physiological and circuit

mechanisms of postural control. *Current opinion in neurobiology, 22*(4), 646–652.

Delp, S. L., Anderson, F. C., Arnold, A. S., Loan, P., Habib, A., John, C. T., . . . Thelen, D. G. (2007, November). OpenSim: open-source software to create and analyze dynamic simulations of movement. *Biomedical Engineering, IEEE Transactions on, 54*(11), 1940–1950.

Delp, S. L., Loan, J. P., Hoy, M. G., Zajac, F. E., Topp, E. L., & Rosen, J. M. (1990, August). An interactive graphics-based model of the lower extremity to study orthopaedic surgical procedures. *Biomedical Engineering, IEEE Transactions on, 37*(8), 757–767.

Dietz, V. (2002, October). Proprioception and locomotor disorders. *Nature Reviews Neuroscience, 3*(10), 781–790.

Dietz, V. (2003, August). Spinal cord pattern generators for locomotion. *Clinical Neurophysiology, 114*(8), 1379–1389.

Dietz, V., Colombo, G., Jensen, L., & Baumgartner, L. (1995, May). Locomotor capacity of spinal cord in paraplegic patients. *Annals of neurology, 37*(5), 574–582.

Dietz, V., & Duysens, J. (2000, April). Significance of load receptor input during locomotion: a review. *Gait & Posture, 11*(2), 102–110.

Dietz, V., Wirz, M., Curt, A., & Colombo, G. (1998, May). Locomotor pattern in paraplegic patients: training effects and recovery of spinal cord function. *Spinal Cord, 36*(6), 380–390.

Dimitrijevic, M. R., Gerasimenko, Y. P., & Pinter, M. M. (1998, November). Evidence for a spinal central pattern generator in humans. *Annals of the New York Academy of Sciences, 860*, 360–376.

Dominici, N., Ivanenko, Y. P., Cappellini, G., d'Avella, A., Mondì, V., Cicchese, M., . . . Lacquaniti, F. (2011, November). Locomotor primitives in newborn babies and their development. *Science, 334*(6058), 997–999.

Donelan, J. M., & Pearson, K. G. (2004, October). Contribution of Force Feedback to Ankle Extensor Activity in Decerebrate Walking Cats. *Journal of Neurophysiology, 92*(4), 2093–2104.

Drew, T., Jiang, W., Kably, B., & Lavoie, S. (1996, April). Role of the motor cortex in the control of visually triggered gait modifications. *Canadian Journal of Physiology and Pharmacology, 74*(4), 426–442.

Drew, T., Jiang, W., & Widajewicz, W. (2002). Contributions of the motor cortex to the control of the hindlimbs during locomotion in the cat. *Brain Research Reviews, 40*(1-3), 178–191.

Drew, T., & Marigold, D. S. (2015, August). Taking the next step: cortical contributions to the control of locomotion. *Current opinion in neurobiology, 33*, 25–33.

Duysens, J., & Van de Crommert, H. W. A. A. (1998, March). Neural control of locomotion; Part 1: The central pattern generator from cats to humans. *Gait & Posture, 7*(2), 131–141.

Dy, C. J., Gerasimenko, Y. P., Edgerton, V. R., Dyhre-Poulsen, P., Courtine, G., & Harkema, S. J. (2010, May). Phase-dependent modulation of percutaneously elicited multisegmental muscle responses after spinal cord injury. *J Neurophysiol, 103*(5), 2808–2820.

Edgerton, V. R., Courtine, G., Gerasimenko, Y. P., Lavrov, I. A., Ichiyama, R. M., Fong, A. J., . . . Roy, R. R. (2008, January). Training locomotor networks. *Brain Research Reviews, 57*(1), 241–254.

Edgerton, V. R., Tillakaratne, N. J. K., Bigbee, A. J., de Leon, R. D., & Roy, R. R. (2004). Plasticity of the spinal neural circuitry after injury. *Annual review of neuroscience*, *27*, 145–167.

Ekeberg, Ö., & Pearson, K. (2005). Computer Simulation of Stepping in the Hind Legs of the Cat: An Examination of Mechanisms Regulating the Stance-to-Swing Transition. *Journal of Neurophysiology*, *94*(6), 4256–4268.

Endo, T., & Kiehn, O. (2008, December). Asymmetric operation of the locomotor central pattern generator in the neonatal mouse spinal cord. *Journal of Neurophysiology*, *100*(6), 3043–3054.

Fawcett, J. W., Curt, A., Steeves, J. D., Coleman, W. P., Tuszynski, M. H., Lammertse, D., . . . Short, D. (2007, March). Guidelines for the conduct of clinical trials for spinal cord injury as developed by the ICCP panel: spontaneous recovery after spinal cord injury and statistical power needed for therapeutic clinical trials. *Spinal Cord*, *45*(3), 190–205.

Fleshman, J. W., Lev-Tov, A., & Burke, R. E. (1984, February). Peripheral and central control of flexor digitorum longus and flexor hallucis longus motoneurons: The synaptic basis of functional diversity. *Experimental brain research*, *54*(1).

Fleshman, J. W., Rudomin, P., & Burke, R. E. (1988, February). Supraspinal control of a short-latency cutaneous pathway to hindlimb motoneurons. *Experimental brain research*, *69*(3), 449–459.

Forssberg, H., & Grillner, S. (1973). The locomotion of the acute spinal cat injected with clonidine i.v. *Brain research*, *50*(1), 184–186.

Forssberg, H., Grillner, S., HALBERTSMA, J., & Rossignol, S. (1980, March). The locomotion of the low spinal cat. II. Interlimb coordination. *Acta physiologica Scandinavica*, *108*(3), 283–295.

Frankemolle, A. M. M., Wu, J., Noecker, A. M., Voelcker-Rehage, C., Ho, J. C., Vitek, J. L., . . . Alberts, J. L. (2010, March). Reversing cognitive-motor impairments in Parkinson's disease patients using a computational modelling approach to deep brain stimulation programming. *Brain : a journal of neurology*, *133*(Pt 3), 746–761.

Friedli, L., Rosenzweig, E. S., Barraud, Q., Schubert, M., Dominici, N., Awai, L., . . . Courtine, G. (2015, August). Pronounced species divergence in corticospinal tract reorganization and functional recovery after lateralized spinal cord injury favors primates. *Science Translational Medicine*, *7*(302), 302ra134.

Friel, K. M., Drew, T., & Martin, J. H. (2007, May). Differential activity-dependent development of corticospinal control of movement and final limb position during visually guided locomotion. *Journal of Neurophysiology*, *97*(5), 3396–3406.

Geertsen, S. S., Stecina, K., Meehan, C. F., Nielsen, J. B., & Hultborn, H. (2011, January). Reciprocal Ia inhibition contributes to motoneuronal hyperpolarisation during the inactive phase of locomotion and scratching in the cat. *The Journal of physiology*, *589*(Pt 1), 119–134.

Gerasimenko, Y. P., Lavrov, I. A., Courtine, G., Ichiyama, R. M., Dy, C. J., Zhong, H., . . . Edgerton, V. R. (2006, October). Spinal cord reflexes induced by epidural spinal cord stimulation in normal awake rats. *Journal of Neuroscience Methods*, *157*(2), 253–263.

Gerasimenko, Y. P., Sayenko, D., Gad, P., Liu, C.-T., Tillakaratne, N. J. K., Roy, R. R., . . . Edgerton,

V. R. (2016, December). Feed-Forwardness of Spinal Networks in Posture and Locomotion. *The Neuroscientist : a review journal bringing neurobiology, neurology and psychiatry*, 1073858416683681.

Geyer, H., & Herr, H. (2010, June). A muscle-reflex model that encodes principles of legged mechanics produces human walking dynamics and muscle activities. *IEEE Transactions on Neural Systems and Rehabilitation Engineering*, *18*(3), 263–273.

Gill, M. L., Grahn, P. J., Calvert, J. S., Linde, M. B., Lavrov, I. A., Strommen, J. A., . . . Zhao, K. D. (2018, September). Neuromodulation of lumbosacral spinal networks enables independent stepping after complete paraplegia. *Nature Medicine*, *377*, 1938.

Goldberger, M. E. (1977). Locomotor recovery after unilateral hindlimb deafferentation in cats. *Brain research*, *123*(1), 59–74.

Goulding, M. (2009, July). Circuits controlling vertebrate locomotion: moving in a new direction. *Nature Reviews Neuroscience*, *10*(7), 507–518.

Grahn, P. J., Lavrov, I. A., Sayenko, D. G., Van Straaten, M. G., Gill, M. L., Strommen, J. A., . . . Lee, K. H. (2017, April). Enabling Task-Specific Volitional Motor Functions via Spinal Cord Neuromodulation in a Human With Paraplegia. *Mayo Clinic Proceedings*, *92*(4), 544–554.

Grillner, S. (2011, November). Human Locomotor Circuits Conform. *Science*, *334*(6058), 912–913.

Grillner, S., & Rossignol, S. (1978). On the initiation of the swing phase of locomotion in chronic spinal cats. *Brain research*, *146*(2), 269–277.

Grillner, S., & Zangger, P. (1979, January). On the central generation of locomotion in the low spinal cat. *Experimental brain research*, *34*(2).

Grillner, S., & Zangger, P. (1984, March). The effect of dorsal root transection on the efferent motor pattern in the cat's hindlimb during locomotion. *Acta physiologica Scandinavica*, *120*(3), 393–405.

Guest, R. S., Klose, K. J., Needham-Shropshire, B. M., & Jacobs, P. L. (1997). Evaluation of a training program for persons with SCI paraplegia using the Parastep®1 ambulation system: Part 4. Effect on physical self-concept and depression. *Archives of Physical Medicine and Rehabilitation*, *78*(8), 804–807.

Hägglund, M., Borgius, L., Dougherty, K. J., & Kiehn, O. (2010, February). Activation of groups of excitatory neurons in the mammalian spinal cord or hindbrain evokes locomotion. *Nature Neuroscience*, *13*(2), 246–252.

Hägglund, M., Dougherty, K. J., Borgius, L., Itohara, S., Iwasato, T., & Kiehn, O. (2013, July). Optogenetic dissection reveals multiple rhythmogenic modules underlying locomotion. *Proceedings of the National Academy of Sciences of the United States of America*, *110*(28), 11589–11594.

Han, J., Waddington, G., Adams, R., Anson, J., & Liu, Y. (2016, March). Assessing proprioception: A critical review of methods. *Journal of Sport and Health Science*, *5*(1), 80–90.

Harkema, S. J., Behrman, A. L., & Barbeau, H. (2011). *Locomotor Training*. Oxford University Press, USA.

Harkema, S. J., Gerasimenko, Y. P., Hodes, J., Burdick, J., Angeli, C., Chen, Y., . . . Edgerton, V. R.

(2011, June). Effect of epidural stimulation of the lumbosacral spinal cord on voluntary movement, standing, and assisted stepping after motor complete paraplegia: a case study. *The Lancet*, *377*(9781), 1938–1947.

Harkema, S. J., Hurley, S. L., Patel, U. K., Requejo, P. S., Dobkin, B. H., & Edgerton, V. R. (1997, February). Human lumbosacral spinal cord interprets loading during stepping. *Journal of Neurophysiology*, *77*(2), 797–811.

Harrison, P. J., & Taylor, A. (1981, March). Individual excitatory post-synaptic potentials due to muscle spindle Ia afferents in cat triceps surae motoneurones. *The Journal of physiology*, *312*, 455–470.

Harvey, C. D., Coen, P., & Tank, D. W. (2012, April). Choice-specific sequences in parietal cortex during a virtual-navigation decision task. *Nature Publishing Group*, *484*(7392), 62–68.

Herman, R., He, J., D'Luzansky, S., Willis, W., & Dilli, S. (2002, February). Spinal cord stimulation facilitates functional walking in a chronic, incomplete spinal cord injured. *Spinal Cord*, *40*(2), 65–68.

Hines, M. L., & Carnevale, N. T. (1997, August). The NEURON simulation environment. *Neural computation*, *9*(6), 1179–1209.

Hník, P., & Lessler, M. J. (1973, June). Changes in muscle spindle activity of the chronically de-efferented gastrocnemius of the rat. *Pflugers Archiv : European journal of physiology*, *341*(2), 155–170.

Hochman, S., & Schmidt, B. J. (1998, February). Whole cell recordings of lumbar motoneurons during locomotor-like activity in the in vitro neonatal rat spinal cord. *Journal of Neurophysiology*, *79*(2), 743–752.

Hodgkin, A. L., & Huxley, A. F. (1952, August). A quantitative description of membrane current and its application to conduction and excitation in nerve. *The Journal of physiology*, *117*(4), 500–544.

Hofstoetter, U. S., Danner, S. M., Freundl, B., Binder, H., Mayr, W., Rattay, F., & Minassian, K. (2015, July). Periodic modulation of repetitively elicited monosynaptic reflexes of the human lumbosacral spinal cord. *J Neurophysiol*, *114*(1), 400–410.

Hofstoetter, U. S., Freundl, B., Binder, H., & Minassian, K. (2018). Common neural structures activated by epidural and transcutaneous lumbar spinal cord stimulation: Elicitation of posterior root-muscle reflexes. *PLOS ONE*, *13*(1), e0192013.

Hofstoetter, U. S., Krenn, M., Danner, S. M., Hofer, C., Kern, H., McKay, W. B., … Minassian, K. (2015, October). Augmentation of Voluntary Locomotor Activity by Transcutaneous Spinal Cord Stimulation in Motor-Incomplete Spinal Cord-Injured Individuals. *Artificial Organs*, n/a–n/a.

Huang, H., He, J., Herman, R., & Carhart, M. R. (2006, March). Modulation effects of epidural spinal cord stimulation on muscle activities during walking. *IEEE transactions on neural systems and rehabilitation engineering : a publication of the IEEE Engineering in Medicine and Biology Society*, *14*(1), 14–23.

Hultborn, H. (1976). Transmission in the pathway of reciprocal Ia inhibition to motoneurones and its control during the tonic stretch reflex. *Progress in brain research*, *44*, 235–255.

Hultborn, H. (2003, May). Changes in neuronal properties and spinal reflexes during develop-

ment of spasticity following spinal cord lesions and stroke: studies in animal models and patients. *Journal of rehabilitation medicine*(41 Suppl), 46–55.

Hultborn, H., Jankowska, E., & Lindström, S. (1971, July). Recurrent inhibition of interneurones monosynaptically activated from group Ia afferents. *The Journal of physiology, 215*(3), 613–636.

Hultborn, H., & Nielsen, J. B. (2007, February). Spinal control of locomotion–from cat to man. *Acta physiologica (Oxford, England), 189*(2), 111–121.

Hunter, J. P., & Ashby, P. (1994, February). Segmental effects of epidural spinal cord stimulation in humans. *The Journal of physiology, 474*(3), 407–419.

Ijspeert, A. J., Crespi, A., Ryczko, D., & Cabelguen, J.-M. (2007, March). From swimming to walking with a salamander robot driven by a spinal cord model. *Science, 315*(5817), 1416–1420.

Ishikawa, K., Ott, K., Porter, R. W., & Stuart, D. (1966, May). Low frequency depression of the H wave in normal and spinal man. *Experimental neurology, 15*(1), 140–156.

Jahn, K., Deutschländer, A., Stephan, T., Kalla, R., Hüfner, K., Wagner, J., . . . Brandt, T. (2008). Supraspinal locomotor control in quadrupeds and humans. *Progress in brain research, 171*, 353–362.

Jankowska, E. (1992). Interneuronal relay in spinal pathways from proprioceptors. *Progress in neurobiology, 38*(4), 335–378.

Jankowska, E. (2008, January). Spinal interneuronal networks in the cat: elementary components. *Brain Research Reviews, 57*(1), 46–55.

Jankowska, E., Krutki, P., & Matsuyama, K. (2005, October). Relative contribution of Ia inhibitory interneurones to inhibition of feline contralateral motoneurones evoked via commissural interneurones. *The Journal of physiology, 568*(Pt 2), 617–628.

Johnson, W. L., Jindrich, D. L., Roy, R. R., & Edgerton, V. R. (2008). A three-dimensional model of the rat hindlimb: musculoskeletal geometry and muscle moment arms. *Journal of biomechanics, 41*(3), 610–619.

Johnson, W. L., Jindrich, D. L., Zhong, H., Roy, R. R., & Edgerton, V. R. (2011, December). Application of a rat hindlimb model: a prediction of force spaces reachable through stimulation of nerve fascicles. *IEEE Transactions on Biomedical Engineering, 58*(12), 3328–3338.

Jones, K. E., & Bawa, P. (1997). Computer simulation of the responses of human motoneurons to composite 1A EPSPS: effects of background firing rate. *Journal of Neurophysiology*.

Jordan, L. M., Liu, J., Hedlund, P. B., Akay, T., & Pearson, K. G. (2008, January). Descending command systems for the initiation of locomotion in mammals. *Brain Research Reviews, 57*(1), 183–191.

Keizer, K., & Kuypers, H. G. J. M. (1989). Distribution of corticospinal neurons with collaterals to the lower brain stem reticular formation in monkey (Macaca fascicularis). *Experimental brain research, 74*(2).

Kiehn, O. (2006). Locomotor circuits in the mammalian spinal cord. *Annual review of neuroscience, 29*(1), 279–306.

Kiehn, O. (2016, March). Decoding the organization of spinal circuits that control locomotion.

Nature Publishing Group, 1–15.

Knikou, M., Angeli, C. A., Ferreira, C. K., & Harkema, S. J. (2009, March). Soleus H-reflex modulation during body weight support treadmill walking in spinal cord intact and injured subjects. *Experimental brain research*, *193*(3), 397–407.

Koerber, H. R., & Mendell, L. M. (1991, March). Modulation of synaptic transmission at Ia-afferent fiber connections on motoneurons during high-frequency stimulation: role of postsynaptic target. *Journal of Neurophysiology*, *65*(3), 590–597.

Lacquaniti, F., Ivanenko, Y. P., & Zago, M. (2012, October). Development of human locomotion. *Current opinion in neurobiology*, *22*(5), 822–828.

Ladenbauer, J., Minassian, K., Hofstoetter, U. S., Dimitrijevic, M. R., & Rattay, F. (2010, December). Stimulation of the human lumbar spinal cord with implanted and surface electrodes: a computer simulation study. *IEEE transactions on neural systems and rehabilitation engineering : a publication of the IEEE Engineering in Medicine and Biology Society*, *18*(6), 637–645.

Le Ray, D., Juvin, L., Ryczko, D., & Dubuc, R. (2011). *Chapter 4 - Supraspinal control of locomotion: The mesencephalic locomotor region* (1st ed., Vol. 188). Elsevier BV.

Levine, A. J., Hinckley, C. A., Hilde, K. L., Driscoll, S. P., Poon, T. H., Montgomery, J. M., & Pfaff, S. L. (2014, March). Identification of a cellular node for motor control pathways. *Nature Neuroscience*, *17*(4), 586–593.

Lovely, R. G., Gregor, R. J., Roy, R. R., & Edgerton, V. R. (1986, May). Effects of training on the recovery of full-weight-bearing stepping in the adult spinal cat. *Experimental neurology*, *92*(2), 421–435.

Marigold, D. S., & Drew, T. (2011, May). Contribution of cells in the posterior parietal cortex to the planning of visually guided locomotion in the cat: effects of temporary visual interruption. *J Neurophysiol*, *105*(5), 2457–2470.

Masdeu, J. C., Alampur, U., Cavaliere, R., & Tavoulareas, G. (1994, May). Astasia and gait failure with damage of the pontomesencephalic locomotor region. *Annals of neurology*, *35*(5), 619–621.

Matsuyama, K., & Drew, T. (1997, December). Organization of the projections from the pericruciate cortex to the pontomedullary brainstem of the cat: A study using the anterograde tracer Phaseolus vulgaris-leucoagglutinin. *Journal of Comparative Neurology*, *389*(4), 617–641.

McIntyre, C. C., & Foutz, T. J. (2013). Computational modeling of deep brain stimulation. *Handbook of clinical neurology*, *116*, 55–61.

McIntyre, C. C., & Grill, W. M. (2002, October). Extracellular stimulation of central neurons: influence of stimulus waveform and frequency on neuronal output. *Journal of Neurophysiology*, *88*(4), 1592–1604.

McIntyre, C. C., & Richardson, A. G. (2002). Modeling the excitability of mammalian nerve fibers: influence of afterpotentials on the recovery cycle. *Journal of . . . .*

McNeal, D. R. (1976). Analysis of a Model for Excitation of Myelinated Nerve. *IEEE Transactions on Biomedical Engineering*, *BME-23*(4), 329–337.

McVea, D. A., Donelan, J. M., Tachibana, A., & Pearson, K. G. (2005). A Role for Hip Position in

Initiating the Swing-to-Stance Transition in Walking Cats. *Journal of Neurophysiology*, *94*(5), 3497–3508.

McVea, D. A., Taylor, A. J., & Pearson, K. G. (2009, July). Long-lasting working memories of obstacles established by foreleg stepping in walking cats require area 5 of the posterior parietal cortex. *The Journal of neuroscience : the official journal of the Society for Neuroscience*, *29*(29), 9396–9404.

Mendell, L. M., & Henneman, E. (1971, January). Terminals of single Ia fibers: location, density, and distribution within a pool of 300 homonymous motoneurons. *Journal of Neurophysiology*, *34*(1), 171–187.

Middleton, F. A., & Strick, P. L. (2000, March). Basal ganglia and cerebellar loops: motor and cognitive circuits. *Brain research. Brain research reviews*, *31*(2-3), 236–250.

Mignardot, J.-B., Le Goff, C. G., Van den Brand, R., Capogrosso, M., Fumeaux, N., Vallery, H., . . . Courtine, G. (2017). A multidirectional gravity-assist algorithm that enhances locomotor control in patients with stroke or spinal cord injury. *Science Translational Medicine*, *9*(399).

Minassian, K., Hofstoetter, U. S., Danner, S. M., Mayr, W., Bruce, J. A., McKay, W. B., & Tansey, K. E. (2016, March). Spinal Rhythm Generation by Step-Induced Feedback and Transcutaneous Posterior Root Stimulation in Complete Spinal Cord-Injured Individuals. *Neurorehabilitation and neural repair*, *30*(3), 233–243.

Minassian, K., Jilge, B., Rattay, F., Pinter, M. M., Binder, H., Gerstenbrand, F., & Dimitrijevic, M. R. (2004, July). Stepping-like movements in humans with complete spinal cord injury induced by epidural stimulation of the lumbar cord: electromyographic study of compound muscle action potentials. *Spinal Cord*, *42*(7), 401–416.

Minassian, K., Persy, I., Rattay, F., Pinter, M. M., Kern, H., & Dimitrijevic, M. R. (2007, April). Human lumbar cord circuitries can be activated by extrinsic tonic input to generate locomotor-like activity. *Human movement science*, *26*(2), 275–295.

Minev, I. R., Musienko, P., Hirsch, A., Barraud, Q., Wenger, N., Moraud, E. M., . . . Lacour, S. P. (2015, January). Biomaterials. Electronic dura mater for long-term multimodal neural interfaces. *Science*, *347*(6218), 159–163.

Moraud, E. M., Capogrosso, M., Formento, E., Wenger, N., DiGiovanna, J., Courtine, G., & Micera, S. (2016, February). Mechanisms Underlying the Neuromodulation of Spinal Circuits for Correcting Gait and Balance Deficits after Spinal Cord Injury. *Neuron*, *89*(4), 814–828.

Moraud, E. M., von Zitzewitz, J., Miehlbradt, J., Wurth, S., Formento, E., DiGiovanna, J., . . . Micera, S. (2018, January). Closed-loop control of trunk posture improves locomotion through the regulation of leg proprioceptive feedback after spinal cord injury. *Scientific reports*, *8*(1), 76.

Mori, S., Matsui, T., Kuze, B., Asanome, M., Nakajima, K., & Matsuyama, K. (1999, July). Stimulation of a restricted region in the midline cerebellar white matter evokes coordinated quadrupedal locomotion in the decerebrate cat. *Journal of Neurophysiology*, *82*(1), 290–300.

Munson, J. B., Fleshman, J. W., & Sypert, G. W. (1980, October). Properties of single-fiber

spindle group II EPSPs in triceps surae motoneurons. *Journal of Neurophysiology, 44*(4), 713–725.

Mushahwar, V. K., Jacobs, P. L., Normann, R. A., Triolo, R. J., & Kleitman, N. (2007, September). New functional electrical stimulation approaches to standing and walking. *Journal of Neural Engineering, 4*(3), S181.

Musienko, P., Courtine, G., Tibbs, J. E., Kilimnik, V., Savochin, A., Garfinkel, A., ... Gerasimenko, Y. P. (2012, April). Somatosensory control of balance during locomotion in decerebrated cat. *J Neurophysiol, 107*(8), 2072–2082.

Musienko, P., Van den Brand, R., Märzendorfer, O., Roy, R. R., Gerasimenko, Y. P., Edgerton, V. R., & Courtine, G. (2011, June). Controlling specific locomotor behaviors through multidimensional monoaminergic modulation of spinal circuitries. *The Journal of neuroscience : the official journal of the Society for Neuroscience, 31*(25), 9264–9278.

Nadeau, S., Jacquemin, G., Fournier, C., Lamarre, Y., & Rossignol, S. (2010, May). Spontaneous motor rhythms of the back and legs in a patient with a complete spinal cord transection. *Neurorehabilitation and neural repair, 24*(4), 377–383.

Nas, K., Yazmalar, L., Şah, V., Aydın, A., & Öneş, K. (2015, January). Rehabilitation of spinal cord injuries. *World journal of orthopedics, 6*(1), 8–16.

Nash, M. S., Jacobs, P. L., Montalvo, B. M., Klose, K. J., Guest, R. S., & Needham-Shropshire, B. M. (1997). Evaluation of a training program for persons with SCI paraplegia using the Parastep®1 ambulation system: Part 5. Lower extremity blood flow and hyperemic responses to occlusion are augmented by ambulation training. *Archives of Physical Medicine and Rehabilitation, 78*(8), 808–814.

Nott, C. R., Zajac, F. E., Neptune, R. R., & Kautz, S. A. (2010, September). All joint moments significantly contribute to trunk angular acceleration. *Journal of biomechanics, 43*(13), 2648–2652.

Orlovskiĭ, G. N., Deliagina, T. G., & Grillner, S. (1999). *Neuronal Control of Locomotion.* Oxford University Press.

Orlovskii, G. N., & Fel'dman, A. G. (1973). Role of afferent activity in the generation of stepping movements. *Neurophysiology, 4*(4), 304–310.

Orsal, D., Cabelguen, J. M., & Perret, C. (1990, November). Interlimb coordination during fictive locomotion in the thalamic cat. *Experimental brain research, 82*(3), 536–546.

O'Shea, T. M., Burda, J. E., & Sofroniew, M. V. (2017, September). Cell biology of spinal cord injury and repair. *The Journal of clinical investigation, 127*(9), 3259–3270.

Park, S.-W., Wolf, S. L., Blanton, S., Winstein, C., & Nichols-Larsen, D. S. (2008, September). The EXCITE Trial: Predicting a clinically meaningful motor activity log outcome. *Neurorehabilitation and neural repair, 22*(5), 486–493.

Pearson, K. G. (1993). Common Principles of Motor Control in Vertebrates and Invertebrates. *Annual review of neuroscience, 16*(1), 265–297.

Pearson, K. G. (2008, January). Role of sensory feedback in the control of stance duration in walking cats. *Brain Research Reviews, 57*(1), 222–227.

Pierrot-Deseilligny, E. (1989, January). Chapter 25 Peripheral and descending control of neurones mediating non-monosynaptic Ia excitation to motoneurones: a presumed

propriospinal system in man. *Progress in brain research*, *80*, 305–314.

Pratt, C. A., & Jordan, L. M. (1987, January). Ia inhibitory interneurons and Renshaw cells as contributors to the spinal mechanisms of fictive locomotion. *Journal of Neurophysiology*, *57*(1), 56–71.

Prochazka, A. (1996). Proprioceptive feedback and movement regulation. *Handbook of physiology*, *76*, 125.

Prochazka, A. (1999). Quantifying proprioception. *Progress in brain research*, *123*, 133–142.

Prochazka, A. (2015, June). Sensory control of normal movement and of movement aided by neural prostheses. *Journal of Anatomy*, *227*(2), 167–177.

Prochazka, A., & Gorassini, M. (1998a, February). Ensemble firing of muscle afferents recorded during normal locomotion in cats. *The Journal of physiology*, *507 (Pt 1)*, 293–304.

Prochazka, A., & Gorassini, M. (1998b, February). Models of ensemble firing of muscle spindle afferents recorded during normal locomotion in cats. *The Journal of physiology*, *507 (Pt 1)*, 277–291.

Prochazka, A., Sontag, K. H., & Wand, P. (1978). Motor reactions to perturbations of gait: proprioceptive and somesthetic involvement. *Neuroscience letters*, *7*(1), 35–39.

Proske, U., & Gandevia, S. C. (2012, October). The proprioceptive senses: their roles in signaling body shape, body position and movement, and muscle force. *Physiological reviews*, *92*(4), 1651–1697.

Quevedo, J., Fedirchuk, B., Gosgnach, S., & McCrea, D. A. (2000, June). Group I disynaptic excitation of cat hindlimb flexor and bifunctional motoneurones during fictive locomotion. *The Journal of physiology*, *525*(2), 549–564.

Quinlan, K. A., & Kiehn, O. (2007, June). Segmental, synaptic actions of commissural interneurons in the mouse spinal cord. *The Journal of neuroscience : the official journal of the Society for Neuroscience*, *27*(24), 6521–6530.

Rattay, F. (1986, October). Analysis of models for external stimulation of axons. *Biomedical Engineering, IEEE Transactions on*, *33*(10), 974–977.

Rattay, F., Minassian, K., & Dimitrijevic, M. R. (2000, August). Epidural electrical stimulation of posterior structures of the human lumbosacral cord: 2. quantitative analysis by computer modeling. *Spinal Cord*, *38*(8), 473–489.

Restuccia, D. (2000, July). Somatosensory evoked potentials after multisegmental lower limb stimulation in focal lesions of the lumbosacral spinal cord. *Journal of Neurology, Neurosurgery & Psychiatry*, *69*(1), 91–95.

Rho, M. J., Lavoie, S., & Drew, T. (1999, May). Effects of red nucleus microstimulation on the locomotor pattern and timing in the intact cat: a comparison with the motor cortex. *Journal of Neurophysiology*, *81*(5), 2297–2315.

Riener, R., Lünenburger, L., & Colombo, G. (2006, August). Human-centered robotics applied to gait training and assessment. *Journal of rehabilitation research and development*, *43*(5), 679–694.

Robinson, G. A., & Goldberger, M. E. (1985, November). Interfering with inhibition may improve motor function. *Brain research*, *346*(2), 400–403.

Roll, J.-P., Albert, F., Ribot-Ciscar, E., & Bergenheim, M. (2004, August). "Proprioceptive

signature" of cursive writing in humans: a multi-population coding. *Experimental brain research*, *157*(3), 359–368.

Rossignol, S., Bélanger, M., Chau, C., Giroux, N., Brustein, E., Bouyer, L., . . . Reader, T. A. (2000). The Spinal Cat. In *Neurobiology of spinal cord injury* (pp. 57–87). Totowa, NJ: Humana Press.

Rossignol, S., Dubuc, R., & Gossard, J.-P. (2006, January). Dynamic sensorimotor interactions in locomotion. *Physiological reviews*, *86*(1), 89–154.

Rossignol, S., & Frigon, A. (2011, July). Recovery of Locomotion After Spinal Cord Injury: Some Facts and Mechanisms. *Annual review of neuroscience*, *34*(1), 413–440.

Rybak, I. A., Stecina, K., Shevtsova, N. A., & McCrea, D. A. (2006, December). Modelling spinal circuitry involved in locomotor pattern generation: insights from the effects of afferent stimulation. *The Journal of physiology*, *577*(Pt 2), 641–658.

Saal, H. P., & Bensmaia, S. J. (2015, December). Biomimetic approaches to bionic touch through a peripheral nerve interface. *Neuropsychologia*, *79*(Pt B), 344–353.

Sanes, J. N., Mauritz, K. H., Dalakas, M. C., & Evarts, E. V. (1985). Motor control in humans with large-fiber sensory neuropathy. *Human neurobiology*, *4*(2), 101–114.

Sartori, M., Gizzi, L., Lloyd, D. G., & Farina, D. (2013). A musculoskeletal model of human locomotion driven by a low dimensional set of impulsive excitation primitives. *Frontiers in computational neuroscience*, *7*.

Sato, N., Sakata, H., Tanaka, Y. L., & Taira, M. (2010, April). Context-dependent place-selective responses of the neurons in the medial parietal region of macaque monkeys. *Cerebral cortex (New York, N.Y. : 1991)*, *20*(4), 846–858.

Sayenko, D. G., Angeli, C., Harkema, S. J., Edgerton, V. R., & Gerasimenko, Y. P. (2014, March). Neuromodulation of evoked muscle potentials induced by epidural spinal-cord stimulation in paralyzed individuals. *J Neurophysiol*, *111*(5), 1088–1099.

Schindler-Ivens, S., & Shields, R. K. (2000, July). Low frequency depression of H-reflexes in humans with acute and chronic spinal-cord injury. *Experimental brain research*, *133*(2), 233–241.

Schomburg, E. D., Petersen, N., Barajon, I., & Hultborn, H. (1998, September). Flexor reflex afferents reset the step cycle during fictive locomotion in the cat. *Experimental brain research*, *122*(3), 339–350.

Scott, J. G., & Mendell, L. M. (1976, July). Individual EPSPs produced by single triceps surae Ia afferent fibers in homonymous and heteronymous motoneurons. *Journal of Neurophysiology*, *39*(4), 679–692.

Segev, I., Fleshman, J. W., & Burke, R. E. (1990, August). Computer simulation of group Ia EPSPs using morphologically realistic models of cat alpha-motoneurons. *Journal of Neurophysiology*, *64*(2), 648–660.

Sherrington, C. S. (1910, April). Flexion-reflex of the limb, crossed extension-reflex, and reflex stepping and standing. *The Journal of physiology*, *40*(1-2), 28–121.

Shevtsova, N. A., Talpalar, A. E., Markin, S. N., Harris-Warrick, R. M., Kiehn, O., & Rybak, I. A. (2015, May). Organization of left-right coordination of neuronal activity in the mammalian spinal cord: Insights from computational modelling. *The Journal of physiology*,

593(11), 2403–2426.

Shik, M. L., & Orlovsky, G. N. (1976). Neurophysiology of locomotor automatism. *Physiological reviews*, *56*(3), 465–501.

Shik, M. L., Severin, F. V., & Orlovsky, G. N. (1969, May). Control of walking and running by means of electrical stimulation of the mesencephalon. *Electroencephalography and Clinical Neurophysiology*, *26*(5), 549.

Sinkjær, T., Andersen, J. B., Ladouceur, M., Christensen, L. O. D., & Nielsen, J. B. (2004, August). Major role for sensory feedback in soleus EMG activity in the stance phase of walking in man. *The Journal of physiology*, *523*(3), 817–827.

Sinnamon, H. M. (1993). Preoptic and hypothalamic neurons and the initiation of locomotion in the anesthetized rat. *Progress in neurobiology*, *41*(3), 323–344.

Sławińska, U., Majczyński, H., Dai, Y., & Jordan, L. M. (2012, March). The upright posture improves plantar stepping and alters responses to serotonergic drugs in spinal rats. *The Journal of physiology*, *590*(7), 1721–1736.

Sławińska, U., Miazga, K., Cabaj, A. M., Leszczyńska, A. N., Majczyński, H., Nagy, J. I., & Jordan, L. M. (2013, September). Grafting of fetal brainstem 5-HT neurons into the sublesional spinal cord of paraplegic rats restores coordinated hindlimb locomotion. *Experimental neurology*, *247*, 572–581.

Song, S., & Geyer, H. (2015, August). A neural circuitry that emphasizes spinal feedback generates diverse behaviours of human locomotion. *The Journal of physiology*, *593*(16), 3493–3511.

Stienen, A. H. A., Schouten, A. C., Schuurmans, J., & van der Helm, F. C. T. (2007, May). Analysis of reflex modulation with a biologically realistic neural network. *Journal of Computational Neuroscience*, *23*(3), 333–348.

Su, C. F., Haghighi, S. S., Oro, J. J., & Gaines, R. W. (1992, May). "Backfiring" in spinal cord monitoring. High thoracic spinal cord stimulation evokes sciatic response by antidromic sensory pathway conduction, not motor tract conduction. *Spine*, *17*(5), 504–508.

Takakusaki, K. (2013, September). Neurophysiology of gait: from the spinal cord to the frontal lobe. *Movement Disorders*, *28*(11), 1483–1491.

Takakusaki, K., Chiba, R., Nozu, T., & Okumura, T. (2016, July). Brainstem control of locomotion and muscle tone with special reference to the role of the mesopontine tegmentum and medullary reticulospinal systems. *Journal of neural transmission (Vienna, Austria : 1996)*, *123*(7), 695–729.

Takakusaki, K., Habaguchi, T., Saitoh, K., & Kohyama, J. (2004). Changes in the excitability of hindlimb motoneurons during muscular atonia induced by stimulating the pedunculo-pontine tegmental nucleus in cats. *Neuroscience*, *124*(2), 467–480.

Takakusaki, K., Saitoh, K., Harada, H., & Kashiwayanagi, M. (2004, October). Role of basal ganglia-brainstem pathways in the control of motor behaviors. *Neuroscience Research*, *50*(2), 137–151.

Takakusaki, K., Saitoh, K., Nonaka, S., Okumura, T., Miyokawa, N., & Koyama, Y. (2006, June). Neurobiological basis of state-dependent control of motor behaviors. *Sleep and Biological Rhythms*, *4*(2), 87–104.

Takeoka, A., Vollenweider, I., Courtine, G., & Arber, S. (2014, December). Muscle Spindle Feedback Directs Locomotor Recovery and Circuit Reorganization after Spinal Cord Injury. *Cell*, *159*(7), 1626–1639.

Talpalar, A. E., Bouvier, J., Borgius, L., Fortin, G., Pierani, A., & Kiehn, O. (2013, July). Dual-mode operation of neuronal networks involved in left-right alternation. *Nature*, *500*(7460), 85–88.

Talpalar, A. E., Endo, T., Löw, P., Borgius, L., Hägglund, M., Dougherty, K. J., ... Kiehn, O. (2011, September). Identification of Minimal Neuronal Networks Involved in Flexor-Extensor Alternation in the Mammalian Spinal Cord. *Neuron*, *71*(6), 1071–1084.

Thorstensson, A., Nilsson, J., Carlson, H., & Zomlefer, M. R. (1984, May). Trunk movements in human locomotion. *Acta physiologica Scandinavica*, *121*(1), 9–22.

Tillakaratne, N. J. K., Mouria, M., Ziv, N. B., Roy, R. R., Edgerton, V. R., & Tobin, A. J. (2000). Increased expression of glutamate decarboxylase (GAD67) in feline lumbar spinal cord after complete thoracic spinal cord transection. *Journal of Neuroscience Research*, *60*(2), 219.

Tripodi, M., Stepien, A. E., & Arber, S. (2011, October). Motor antagonism exposed by spatial segregation and timing of neurogenesis. *Nature Publishing Group*, *479*(7371), 61–66.

Tuthill, J. C., & Azim, E. (2018, March). Proprioception. *Current Biology*, *28*(5), R194–R203.

Vallbo, A. B., & al Falahe, N. A. (1990, February). Human muscle spindle response in a motor learning task. *The Journal of physiology*, *421*(1), 553–568.

Vallery, H., Lutz, P., von Zitzewitz, J., Rauter, G., Fritschi, M., Everarts, C., ... Bolliger, M. (2013, June). Multidirectional transparent support for overground gait training. *IEEE ... International Conference on Rehabilitation Robotics : [proceedings]*, *2013*, 6650512–7.

Van den Brand, R., Heutschi, J., Barraud, Q., DiGiovanna, J., Bartholdi, K., Huerlimann, M., ... Courtine, G. (2012, May). Restoring Voluntary Control of Locomotion after Paralyzing Spinal Cord Injury. *Science*, *336*(6085), 1182–1185.

Veneman, J. F., Menger, J., van Asseldonk, E. H. F., van der Helm, F. C. T., & van der Kooij, H. (2008, July). Fixating the pelvis in the horizontal plane affects gait characteristics. *Gait & Posture*, *28*(1), 157–163.

Viala, G., & Buser, P. (1969, July). Activités locomotrices rythmiques stéréotypées chez le lapin sous anesthésie légère. *Experimental brain research*, *8*(4), 346–363.

Viala, G., & Buser, P. (1974, November). Inhibition des activités spinales à caractère locomoteur par une modalité particulière de stimulation somatique chez le lapin. *Experimental brain research*, *21*(3).

Wagner, F. B., Mignardot, J.-B., Le Goff-Mignardot, C. G., Demesmaeker, R., Komi, S., Capogrosso, M., ... Courtine, G. (2018, November). Targeted neurotechnology restores walking in humans with spinal cord injury. *Nature Publishing Group*, *563*(7729), 65–71.

Wallen, P., Ekeberg, O., Lansner, A., Brodin, L., Traven, H., & Grillner, S. (1992, December). A computer-based model for realistic simulations of neural networks. II. The segmental network generating locomotor rhythmicity in the lamprey. *Journal of Neurophysiology*, *68*(6), 1939–1950.

Waltz, J. M., Reynolds, L. O., & Riklan, M. (1981). Multi-Lead Spinal Cord Stimulation for

Control of Motor Disorders. *Stereotactic and Functional Neurosurgery*, *44*(4), 244–257.

Wenger, N., Moraud, E. M., Gandar, J., Musienko, P., Capogrosso, M., Baud, L., ... Courtine, G. (2016, January). Spatiotemporal neuromodulation therapies engaging muscle synergies improve motor control after spinal cord injury. *Nature Medicine*, *22*(2), 138–145.

Wenger, N., Moraud, E. M., Raspopovic, S., Bonizzato, M., DiGiovanna, J., Musienko, P., ... Courtine, G. (2014, September). Closed-loop neuromodulation of spinal sensorimotor circuits controls refined locomotion after complete spinal cord injury. *Science Translational Medicine*, *6*(255), 255ra133–255ra133.

Wernig, A., & Müller, S. (1992, April). Laufband locomotion with body weight support improved walking in persons with severe spinal cord injuries. *Spinal Cord*, *30*(4), 229–238.

Wernig, A., Müller, S., Nanassy, A., & Cagol, E. (1995, April). Laufband Therapy Based on'Rules of Spinal Locomotion'is Effective in Spinal Cord Injured Persons. *European Journal of Neuroscience*, *7*(4), 823–829.

Wirz, M., Colombo, G., & Dietz, V. (2001, July). Long term effects of locomotor training in spinal humans. *Journal of Neurology, Neurosurgery & Psychiatry*, *71*(1), 93–96.

Wojtusch, J., & von Stryk, O. (n.d.). HuMoD - A versatile and open database for the investigation, modeling and simulation of human motion dynamics on actuation level. In *2015 ieee-ras 15th international conference on humanoid robots (humanoids)* (pp. 74–79). IEEE.

Wyndaele, M., & Wyndaele, J.-J. (2006, September). Incidence, prevalence and epidemiology of spinal cord injury: what learns a worldwide literature survey? *Spinal Cord*, *44*(9), 523–529.

Yang, J. F., & Gorassini, M. (2006, October). Spinal and brain control of human walking: implications for retraining of walking. *The Neuroscientist : a review journal bringing neurobiology, neurology and psychiatry*, *12*(5), 379–389.

Zajac, F. E., Neptune, R. R., & Kautz, S. A. (2003). Biomechanics and muscle coordination of human walking: Part II: Lessons from dynamical simulations and clinical implications. *Gait & Posture*, *17*(1), 1–17.

Zhang, J., Lanuza, G. M., Britz, O., Wang, Z., Siembab, V. C., Zhang, Y., ... Goulding, M. (2014, April). V1 and v2b interneurons secure the alternating flexor-extensor motor activity mice require for limbed locomotion. *Neuron*, *82*(1), 138–150.

Zhang, T. C., Janik, J. J., & Grill, W. M. (2014, June). Mechanisms and models of spinal cord stimulation for the treatment of neuropathic pain. *Brain research*, *1569*, 19–31.

Zhang, Y., Narayan, S., Geiman, E., Lanuza, G. M., Velasquez, T., Shanks, B., ... Goulding, M. (2008, October). V3 spinal neurons establish a robust and balanced locomotor rhythm during walking. *Neuron*, *60*(1), 84–96.

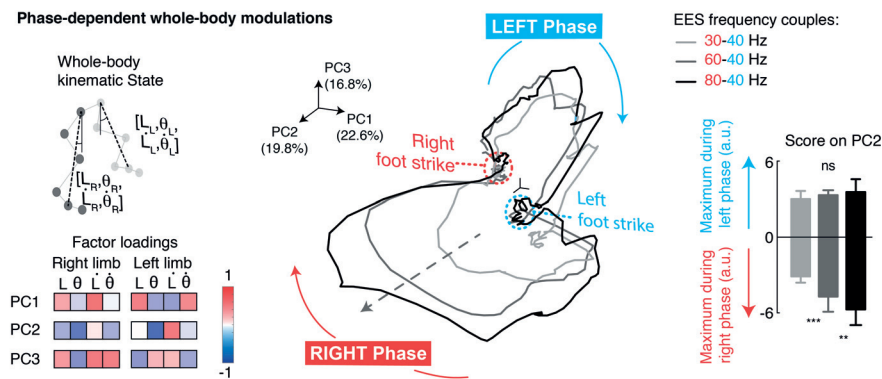# A Appendix

A.1 Supplementary figures of Chapter 2

Figure A.1 | Phase-specific EES promotes independent modulation of left versus right hindlimb movements during locomotion in rats with complete SCI. The biomechanical state of both hindlimbs was captured in an 8-Dimensional vector that includes left and right hindlimb angle (θ_R and θ_L) and length (L_L and L_R), and their respective velocities. A principal component (PC) analysis was applied on the continuous time-series of this vector during locomotion under the different pairs of EES frequencies. The resulting PC trajectories are represented in the new space created by PC1-3. Changes in EES frequencies during the right stance phase only affected PC trajectories during this phase. Color-coded factor loadings are shown to highlight the specific contribution of each hindlimb variable to PC1-3. Bar plot reports the mean score (±SEM, n = 4 rats) on PC2, which captured phase-specific modulation of hindlimb movements (a.u., arbitrary units). ***, $p < 0.001$; **, $p < 0.01$.
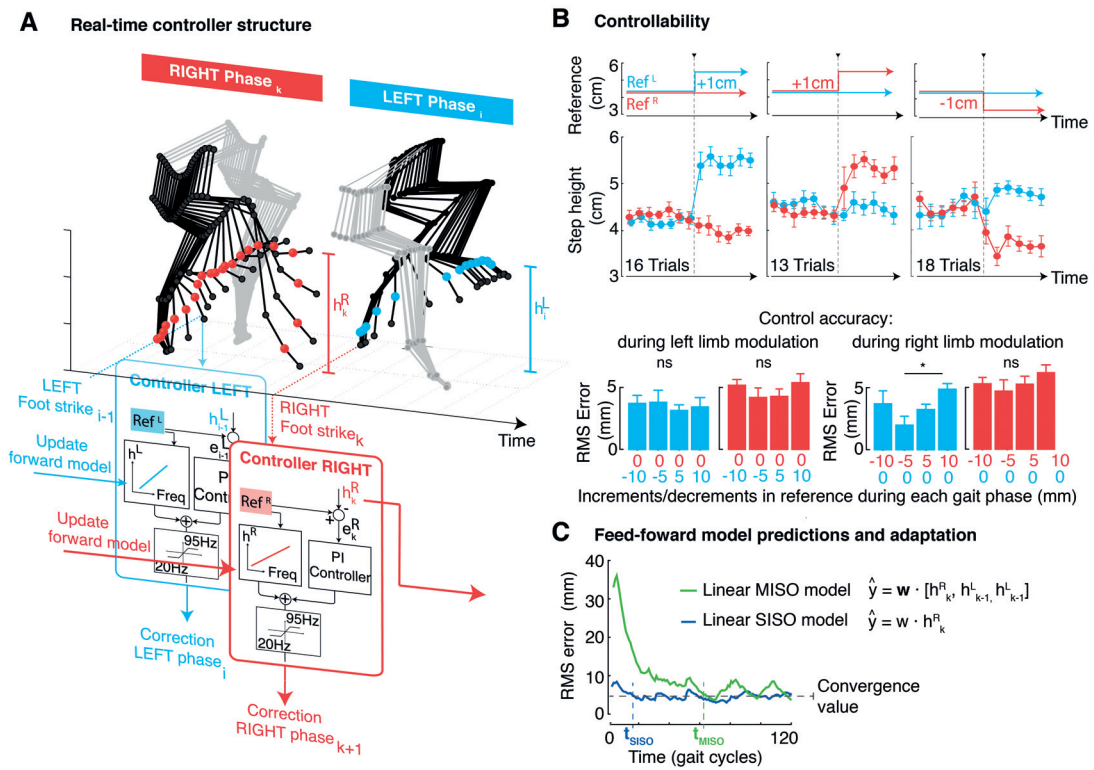
Figure A.2 | Control structure and controllability. A, The control structure is composed of two independent control loops operating in parallel. Each controller monitors the maximum step height of one hindlimb (h^R and h^L, for the right and left hindlimb respectively). Each controller combines a proportional-integral (PI) feedback loop and a feed-forward predictive model, which calculate corrections of EES frequency (f_{i+1}) and apply them at the next gait-phase. The predictive forward model is built from the linear relationship between EES frequency and step height of the monitored hindlimb. This relationship is updated at each iteration through an adaptive Least Mean Squares (LMS) algorithm. A saturating function constraints EES within the functional range of frequencies. **B**, Successive step heights and concomitant EES frequencies during sequences of reference band changes during locomotion of the same rat with complete SCI. Bar plots report the mean ($\pm$ SEM, n = 20-30 trials) RMS values quantifying errors between actual and desired step heights across various sequences during which increments or decrements of desired step heights are implemented in the controller, as indicated along the x-axis. **C**, Comparison of RMS error for feed-forward predictions resulting from the single-input single-output (SISO) linear relationship between frequency and step height, and more complex multiple input single output (MISO) models that account for the step height of the contralateral hindlimb and for previous occurrences. Convergence times are significantly larger with MISO models due to higher dimensionalities, but performances are not improved after convergence.
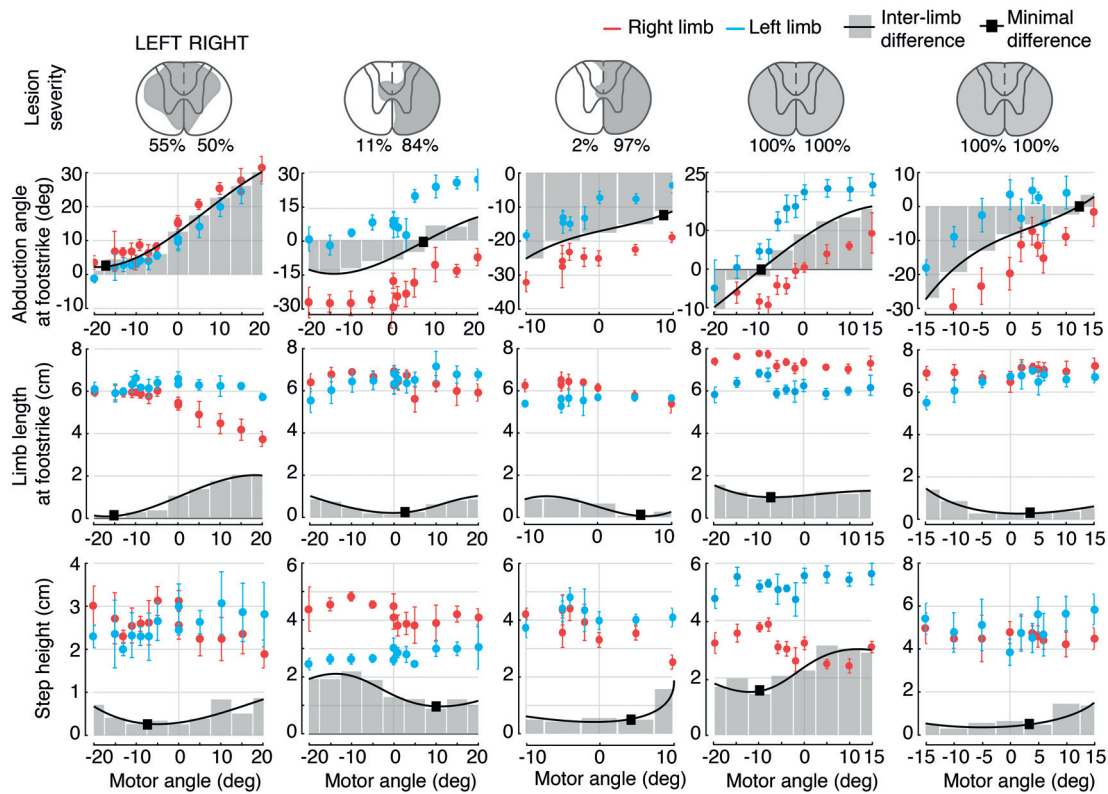
A.2   Supplementary figures of Chapter 3

Figure A.3 | Trunk postural adjustments modulate stepping patterns across animals with different lesion severities. A, Reconstruction of damaged tissue (shaded areas, including percent) on each hemicord for all animals, and mapping of changes in bilateral locomotor features for each rat for their entire input space. The black line represents the interpolated difference between the right and left limbs. Black squares indicate the minimal difference values across the input space.

EMANUELE FORMENTO

Avenue de Cour 11
1007 Lausanne, Switzerland
emanuele.formento@gmail.com
+41 788733892

PUBLICATIONS   LinkedIn   GitHub

STRENGTHS

▸ Advanced knowledge in computational modeling, data analysis, machine learning, and neural engineering.
▸ Excellent problem solving and communication skills.

EDUCATION

2014 - Present	**PhD in Electrical Engineering** with **award-winning** and **high-impact** publications in top-rated journals, École Polytechnique Fédérale de Lausanne (EPFL), Switzerland.
2012 - 2014	**Master's degree in Bioengineering** with minor in **Neuroprosthetics** and **award of Excellence**, EPFL, Switzerland.
2009 - 2012	**Bachelor's degree in Biomedical Engineering,** Polytechnic University of Turin, Italy.
2004 - 2009	**Scientific High School Degree,** Liceo Gino Segrè, Italy.

ACADEMIC EXPERIENCES

2014 - Present	**PhD research**, Prof. Micera and Prof. Courtine labs, EPFL, Switzerland. Used multiple **computational modeling** techniques (e.g., spiking neural networks and musculoskeletal modeling) and experimental procedures to study the mechanisms of electrical spinal cord stimulation therapies for restoring walking after paralysis. **Designed and patented** novel stimulation strategies that optimize the efficacy of these therapies. **Collaborated** with researchers across Europe in the development of the Human Brain Project neurorobotic simulation platform.
2014 - Present	**Teaching assistant**, EPFL, Switzerland. Prepared and **lectured** classes in **modeling for neuroengineering**, managed and organized exercise sessions and exams for various courses, and **supervised** several students for semester and master's thesis projects.
2014 - Present	**Scientific articles reviewer**, EPFL, Switzerland. Reviewed scientific articles for several journals and conferences (e.g., Journal of Neuroengineering and Rehabilitation, International Conference on Intelligent Robots and Systems, and International Conference on Biomedical Robotics and Biomechatronics).
2013	**Master thesis**, Prof. Micera lab, EPFL, Switzerland. Developed advanced myoelectric controllers of hand prosthesis based on multiple **machine learning** techniques, including artificial neural networks and linear discriminant analysis classifiers.

PROFESSIONAL EXPERIENCES

2013	**Second Sight**, 2-months internship, Lausanne, Switzerland. Developed a Matlab program that integrates an eye tracker into the Argus II Retinal Prosthesis System.
2012	**Laboratori Biomicron**, 3-months internship, Turin, Italy. Characterized a bioengineered polymeric device with barrier properties, for oral surgery.

EXTRACURRICULAR EXPERIENCES

2018	**HackaHealth**, 2-days hackathon, Geneva, Switzerland. Participated to a hackathon aiming at engineering personalized solutions for people with motor disabilities. **Led** a team of 5 people to develop a myoelectric controller of a robotic orthosis under a tight time constraint.
2013	**Interdisciplinary robot competition**, 6-months project, EPFL, Switzerland. Designed, developed and programmed an autonomous robot capable of collecting and sorting garbage spread in a complex environment, with a team of 3 students and a limited budget.
2007	**Student exchange program**, 3-months experience abroad, Mount Maunganui College, New Zealand.
2005 - 2012	**Competitive rowing and climbing** with several **awards** at a regional level, Turin, Italy.

TECHNICAL SKILLS

- **Advanced knowledge in modeling** of spiking neural networks, musculoskeletal systems, and of the effect of electrical stimulation on the nervous system**.**

- **5 years of experience in data science** applied to neural and kinematic datasets, with expertise in features engineering, classification and regression, supervised and unsupervised learning, data visualization, and statistical analysis.

- **Excellent programming skills** in Python, Matlab, and C++. Experienced with Git and parallel computing.

- **5 years of experience in biomedical research** with strong skills in experimental design, electrical stimulation, biosignal acquisition and processing, and electronics prototyping.

PERSONAL SKILLS

- **Problem-solving** and **creative thinking**.

- **Oral and written communication**: presented research at several conferences and outreach events, and published articles in prestigious peer-reviewed journals.

LANGUAGES

- **Italian** (Native)

- **English** (Full professional proficiency)

- **French** (Professional working proficiency)

LIST OF PUBLICATIONS & PATENTS

Journal papers

- **E. Formento**, K. Minassian, F. Wagner, JB. Mignardot, C.G. Le Goff, A. Rowald, J. Bloch, S. Micera*, M. Capogrosso* and G. Courtine*, "Electrical spinal cord stimulation must preserve proprioception to enable locomotion in humans with spinal cord injury", **Nature Neuroscience**, 2018.

- E.M. Moraud*, M. Capogrosso*, **E. Formento**, N. Wenger, J. DiGiovanna, G. Courtine[†], S. Micera[†], "Mechanisms underlying the neuromodulation of spinal circuits for correcting gait and balance deficits after spinal cord injury", **Neuron**, 2016. Publication winning the NCCR "**Best Postodoc Paper Award**".

- E.M. Moraud, J.V. Zitzewitz, J. Miehlbradt, S. Wurth, **E. Formento**, J. DiGiovanna, M. Capogrosso, G. Courtine, and S. Micera, "Closed-loop control of trunk posture improves locomotion through the regulation of leg proprioceptive feedback after spinal cord injury", **Scientific Reports**, Nature Publishing Group, 2018.

Patents

- **E. Formento**, M. Capogrosso, S. Micera, G. Courtine, K. Minassian "A sensory information compliant spinal cord stimulation system for the rehabilitation of motor functions", **European patent**, priority number EP20160206606.

Conferences

- **E. Formento***, M. Capogrosso*, K. Minassian, F. B. Wagner, J. B. Mignardot, C. G. M. Le Goff, T. Milekovic, E. Bezard, J. Bloch, S. Micera, G. Courtine, "Dimensions matter: Why do the spinal cords of humans and rodents respond differently to epidural electrical stimulation", **Neuroscience** 2017.

- K. Z. Zhuang, N. Sommer, **E. Formento**, E. D'Anna, Billard, A., Micera, S., "Grasp smarter, not harder: proportional control of an electromyographic prosthesis with a touch of automation", **Neuroscience** 2017.

- **E. Formento***, M. Capogrosso*, E.M. Moraud, G. Courtine[†], S. Micera[†], "Mechanisms underlying the modulation of motor patterns during epidural electrical stimulation of the lumbar spinal cord", **Neural Control of Movement Conference**, 2016.

- **E. Formento***, M. Capogrosso*, E.M. Moraud, M. Caban, G. Courtine, S. Micera, "A model of spinal sensorimotor circuits recruited by epidural stimulation of the spinal cord", **Cosyne Conference**, 2015.

*,[†], Equal contribution.